

**Crystallographic studies on diheme cytochrome *c*  
enzymes**

Dissertation  
zur Erlangung des Doktorgrades  
der Mathematisch-Naturwissenschaftlichen Fakultäten  
der Georg-August-Universität zu Göttingen

vorgelegt von  
Maren Hoffmann  
aus Göttingen

Göttingen 2007

D7

Referent:

Prof. Dr. Oliver Einsle

Korreferent:

Prof. Dr. Ralf Ficner

Tag der mündlichen Prüfung:

04.05.2007

## Table of contents

<b>1</b>	<b>Zusammenfassung .....</b>	<b>1</b>
<b>2</b>	<b>Summary.....</b>	<b>3</b>
<b>3</b>	<b>Introduction.....</b>	<b>5</b>
3.1	<i>Dissimilatory Metal-Reducing Bacteria .....</i>	5
3.2	<i>Iron as Electron Acceptor in Geobacter sulfurreducens .....</i>	7
3.3	<i>Alternative Electron Acceptors.....</i>	8
3.4	<i>Electron Transfer in DMRB.....</i>	9
3.5	<i>Cytochromes .....</i>	12
3.5.1	The Porphyrin Cofactor .....	12
3.5.2	C-Type Cytochromes.....	13
3.5.3	C-Type Cytochrome Maturation.....	14
3.5.3.1	System I .....	14
3.5.3.2	System II.....	16
3.5.3.3	System III.....	16
3.6	<i>Peroxidases.....</i>	16
3.6.1	Eukaryotic Peroxidases.....	17
3.6.2	Bacterial Peroxidases.....	18
3.6.2.1	Structure of Cytochrome <i>c</i> Peroxidases.....	19
3.6.2.2	Reaction Mechanism.....	20
3.6.2.3	IN and OUT Conformation.....	20
3.6.2.4	Electron Transfer within the Cytochrome <i>c</i> Peroxidases.....	21
3.6.3	Other Diheme Cytochrome <i>c</i> Enzymes .....	22
3.7	<i>The Rubber Oxygenase RoxA .....</i>	22
3.8	<i>Goals of this Study.....</i>	25
<b>4</b>	<b>Material and Methods .....</b>	<b>26</b>
4.1	<i>Material .....</i>	26
4.1.1	Chemicals.....	26
4.1.2	DNA and Protein Molecular Weight Marker .....	26
4.1.3	Enzymes and Proteins.....	26
4.1.4	Bacterial Strains.....	26
4.1.4.1	<i>Escherichia coli .....</i>	26
4.1.4.2	<i>Geobacter sulfurreducens.....</i>	27
4.1.5	DNA-Oligonucleotides .....	27

---

4.1.6	Plasmids .....	27
4.1.6.1	pEC86 .....	27
4.1.6.2	pETSN-22 .....	28
4.2	<i>Methods</i> .....	29
4.2.1	Microbiological Methods.....	29
4.2.1.1	Cultivation of <i>Escherichia coli</i> .....	29
4.2.1.2	Cultivation of <i>Geobacter sulfurreducens</i> .....	29
4.2.1.3	Production and Transformation of Competent <i>E. coli</i> Cells.....	30
4.2.1.4	Cultivation of <i>Geobacter sulfurreducens</i> in Soft Agar Tubes.....	31
4.2.1.5	Production of <i>Geobacter sulfurreducens</i> DMSO Stocks.....	31
4.2.2	Molecular Biological Techniques.....	32
4.2.2.1	Polymerase Chain Reaction .....	32
4.2.2.2	DNA Isolation from Agarose Gels & Purification of PCR Products .	32
4.2.2.3	Isolation of Plasmid DNA from Bacteria .....	32
4.2.2.4	Isolation of Genomic DNA from <i>Geobacter sulfurreducens</i> .....	33
4.2.2.5	DNA Restriction Digestion.....	33
4.2.2.6	DNA Ligation .....	33
4.2.2.7	DNA Sequencing .....	34
4.2.2.8	Agarose Gel Electrophoresis .....	34
4.2.3	Protein Biochemical Methods.....	35
4.2.3.1	Cell Disruption.....	35
4.2.3.2	Affinity Chromatography .....	35
4.2.3.3	Size Exclusion Chromatography .....	36
4.2.3.4	SDS-PAGE .....	36
4.2.3.5	Heme Staining.....	37
4.2.4	Protein Concentration Determination.....	37
4.2.5	Spectroscopic Methods .....	37
4.2.5.1	Electron Excitation Spectroscopy.....	37
4.2.5.2	Activity Assay.....	38
4.2.6	Crystallographic Methods.....	39
4.2.6.1	Crystallization.....	39
4.2.6.2	Cryo-Cooling .....	40
4.2.6.3	Data Collection .....	40
4.2.6.4	Structure Determination.....	40
4.2.6.5	Phase Determination.....	42
4.2.6.5.1	Molecular Replacement .....	42
4.2.6.5.2	MAD .....	43
4.2.6.5.3	Isomorphous Replacement.....	45
4.2.6.6	Graphical Representation.....	45
<b>5</b>	<b>Results</b> .....	<b>46</b>
5.1	<i>Purification of the Recombinant Peroxidases from G. sulfurreducens</i> .....	46
5.1.1	Purification of CcpA .....	47

---

5.1.2	Purification of MacA .....	48
5.1.3	Representative Purification of CcpA and MacA .....	49
5.2	<i>Electron Excitation Spectra</i> .....	49
5.3	<i>Peroxidase Activity Assay</i> .....	51
5.4	<i>Sequence Analysis</i> .....	53
5.5	<i>Crystallization and Structure Determination</i> .....	54
5.5.1	Crystallization of CcpA and Data Collection .....	54
5.5.2	Structure Determination of CcpA and Refinement .....	56
5.5.3	Structure Analysis of CcpA .....	58
5.5.4	Crystallization and Data Collection of MacA .....	58
5.5.5	Structure Determination of MacA and Refinement .....	60
5.5.6	Structure Analysis of MacA .....	61
5.6	<i>Overall Structures: CcpA and MacA</i> .....	63
5.6.1	CcpA .....	63
5.6.1.1	Heme Groups .....	63
5.6.2	MacA .....	65
5.6.2.1	Heme Groups .....	65
5.6.3	Comparison of the Overall Structure to Other Peroxidases .....	67
5.6.4	Crystal Packing and Accessible Surface .....	68
5.6.5	Electrostatic Potential .....	69
5.6.6	Calcium Binding Site .....	71
5.6.7	B-Factor Analysis .....	72
5.7	<i>Structure Determination of RoxA</i> .....	73
5.7.1	Crystallization, Data Collection and Structure Determination of RoxA .....	73
5.7.2	Structure Determination of RoxA and Refinement .....	74
5.7.3	Structure Analysis of RoxA .....	74
5.8	<i>Overall Structure of RoxA</i> .....	76
5.8.1	Heme Groups .....	76
5.8.2	Disulfide Bridges .....	78
5.8.3	Surface Properties .....	79
<b>6</b>	<b>Discussion</b> .....	<b>80</b>
6.1	<i>The Physiological Role of CcpA and MacA in Geobacter sulfurreducens</i> .....	80
6.1.1	Gene Expression of <i>ccpA</i> and <i>macA</i> in the <i>rel<sub>Gsu</sub></i> Mutant .....	81
6.1.2	Gene Expression of <i>ccpA</i> and <i>macA</i> in the <i>rpoS</i> Deletion Mutant .....	81
6.1.3	Genome Regions of <i>ccpA</i> and <i>macA</i> .....	82
6.1.4	Description of the <i>macA</i> Deletion Mutant .....	83
6.1.5	Inspection of the <i>omcB</i> Deletion Mutant .....	84
6.1.6	Implications for the Function of CcpA and MacA .....	85
6.2	<i>Bacterial Cytochrome c Peroxidases</i> .....	85

Abbreviations	VIII
6.2.1 Dimer Formation.....	85
6.2.2 Electron Excitation Spectra .....	87
6.2.3 The Calcium Binding Site.....	87
6.2.4 Enzyme Activity .....	88
6.2.5 Catalytic Reaction Mechanism of Cytochrome <i>c</i> Peroxidases .....	90
6.2.6 Electron Transfer in Cytochrome <i>c</i> Peroxidases.....	93
6.3 <i>RoxA</i> .....	95
<b>7 Danksagung .....</b>	<b>100</b>
<b>8 Abbreviations .....</b>	<b>101</b>
<b>9 References.....</b>	<b>103</b>
<b>10 Curriculum vitae.....</b>	<b>116</b>

# 1 Zusammenfassung

Abhängig von ihrer Umwelt und ihrem physiologischen Zustand bilden Bakterien unterschiedliche Elektronentransportketten aus. Elektronentransportsysteme in der inneren Membran übertragen Elektronen von verschiedenen Elektronendonoren wie NADH, organischen Molekülen oder Wasserstoff an lösliche Elektronenakzeptoren wie z.B. Sauerstoff, Nitrat oder Sulfat. Da *Geobacter*-Arten zu den vorherrschenden Mikroorganismen in vielen Bodenhabitaten gehören, wo die dissimilatorische Metallreduktion den dominierenden Stoffwechselprozess darstellt, ist der Elektronentransport innerhalb der Bakterien zu den unlöslichen Eisen(III)oxiden besonders interessant. Ziel der vorliegenden Arbeit war, die Funktion der periplasmatischen *c*-Typ Cytochrome CcpA und MacA des  $\delta$ -Proteobakteriums *Geobacter sulfurreducens* aufzuklären und beide Proteine biochemisch wie auch strukturell zu charakterisieren.

Bakterielle Cytochrom *c* Peroxidasen sind eine weit verbreitete Familie von periplasmatischen Enzymen, die Elektronen aus dem zentralen Stoffwechsel erhalten und die Reduktion von Wasserstoffperoxid mit Hilfe des Häm-Kofaktors katalysieren. Die beiden Proteine aus *Geobacter sulfurreducens* wurden im Hinblick auf Peroxidase-Aktivität untersucht, welche auch tatsächlich nachgewiesen werden konnte. Bei CcpA wie auch bei MacA handelt es sich also um Cytochrom *c* Peroxidasen, deren physiologischer Elektronendonator allerdings noch unbekannt ist. Eine direkte Beteiligung von CcpA und MacA am Elektronentransport zu unlöslichem Eisen wird angenommen (Butler *et al.*, 2004), konnte aber bislang nicht eindeutig nachgewiesen werden und erscheint auf der Basis der Ergebnisse der vorliegenden Arbeit eher unwahrscheinlich.

Da die Struktur der homologen Cytochrom *c* Peroxidase aus dem Organismus *Pseudomonas aeruginosa* gelöst ist (Fülöp *et al.*, 1995), war es möglich, die Kristallstrukturen von CcpA und MacA durch Molekularen Ersatz zu bestimmen. CcpA und MacA bilden Dimere und besitzen jeweils zwei Hämgruppen pro Monomer, wobei sich die Hämgruppen in zwei verschiedenen Domänen befinden. Im hydrophoben Interface zwischen den beiden Domänen befindet sich ein Calciumion, das

wahrscheinlich der Stabilisierung der Reste, die am Elektronentransfer zwischen den beiden Hämgruppen beteiligt sind, dient. Die Strukturen von CcpA und MacA sind den Strukturen der schon bekannten Cytochrom *c* Peroxidasen sehr ähnlich. Der Vergleich zeigt weiterhin, dass der Hauptunterschied zu den schon bekannten Cytochrom *c* Peroxidasen aus anderen Organismen hauptsächlich vom Austausch geladener Reste an der Oberfläche herrührt, wodurch die Proteine aus *Geobacter sulfurreducens* deutlich basischer sind.

Das als „rubber oxygenase“ bezeichnete Protein RoxA aus *Xanthomonas* sp. Stamm 35Y ist ein 74.1 kDa großes, Dihäm-Cytochrom *c*, das *in vitro* zur Spaltung von Kautschuk in der Lage ist. Die Struktur von RoxA wurde durch *Multiwavelength Anomalous Dispersion*-Phasierung (MAD) gelöst und bis zu einer Auflösung von 1.8 Å verfeinert. In den Datenbanken wurden keine Strukturen gefunden, die eine signifikante Ähnlichkeit zu der Gesamtstruktur von RoxA zeigen. Allerdings weist der Bereich, in dem sich die beiden Hämgruppen befinden, strukturelle Homologien zu bakteriellen Dihäm-Cytochrom *c* Peroxidasen auf. Die beiden Hämgruppen sind annähernd senkrecht zueinander angeordnet, wobei die beiden Eisenatome 21.5 Å voneinander entfernt sind. Aminosäurereste, denen eine essentielle Rolle im Elektronentransfer zwischen den Hämgruppen nachgesagt wird, sind in der Struktur von RoxA vorhanden.



## 2 Summary

Bacteria express various electron transport chains depending on their environment and their physiological state. Membrane electron transport systems carry electrons from a number of different electron donors such as NADH, organic molecules or hydrogen to a variety of soluble electron acceptors, e.g. oxygen, nitrate or sulfate. As members of the *Geobacteraceae* are the predominant microorganisms in a variety of subsurface environments in which dissimilatory metal reduction is an important process, the electron transfer chain to insoluble Fe(III) oxides is of special interest. The purpose of the present work was to elucidate the function of the periplasmic diheme cytochromes *c* CcpA and MacA from the  $\delta$ -proteobacterium *Geobacter sulfurreducens* and to biochemically and structurally characterize both proteins.

Bacterial diheme cytochrome *c* peroxidases are a widespread family of periplasmic enzymes that receive electrons from the central metabolism and catalyze the reduction of hydrogen peroxide by means of the heme cofactor. Both proteins from *Geobacter sulfurreducens* were analyzed with regard to peroxidase activity which could be detected. However, the physiological electron donor is still unknown. A direct participation of MacA and CcpA in electron transport to insoluble iron in *Geobacter sulfurreducens* is proposed (Butler *et al.*, 2004), but it could not be proven unambiguously and seems, in the light of the results of the present work, rather unlikely. As the structure of the homologous cytochrome *c* peroxidase of *Pseudomonas aeruginosa* has been solved (Fülöp *et al.*, 1995), it was possible to determine the crystal structures of CcpA and MacA by molecular replacement. CcpA and MacA are dimeric enzymes with one heme group located in each domain of the monomer. In the hydrophobic interface in between the two domains, one calcium ion could be identified that serves probably the stabilization of the residues participating in electron transfer between the two heme groups. Both structures are very similar to known cytochrome *c* peroxidases. Comparison of CcpA and MacA to known cytochrome *c* peroxidases reveals that the divergence is due to substitutions of charged residues on the surface, resulting in a significantly more basic protein.

The rubber oxygenase RoxA from *Xanthomonas* sp. strain 35Y is a 74.1 kDa diheme cytochrome *c* enzyme that has the ability to degrade rubber latex *in vitro*. The structure of RoxA had been determined by *multiwavelength anomalous dispersion* at the K-edge of iron and was refined to a resolution of 1.8 Å. No significant similarity to the overall structure of any known protein was found. However, the structural region comprising both heme groups shows structural homologies to bacterial diheme cytochrome *c* peroxidases. The two heme groups of RoxA are roughly perpendicular to each other and they are separated by an iron-iron distance of 21.5 Å. Residues proposed to be essential for electron transfer in between the heme groups in cytochrome *c* peroxidases are also present in RoxA.

## 3 Introduction

### 3.1 Dissimilatory Metal-Reducing Bacteria

Iron is one of the most abundant metals on earth. In soils and sediments, high amounts of ferric iron ( $\text{Fe}^{3+}$ ) oxides can be found in the forms of hematite ( $\alpha\text{-Fe}_2\text{O}_3$ ), magnetite ( $\text{Fe}_3\text{O}_4$ ), goethite ( $\alpha\text{-FeOOH}$ ) and ferrihydrite ( $\text{Fe}_5\text{HO}_8 \cdot 4\text{H}_2\text{O}$ ) (Kappler and Straub, 2005). Pyrite ( $\text{FeS}_2$ ), siderite ( $\text{FeCO}_3$ ) and vivanite ( $\text{Fe}_3(\text{PO}_4)_2$ ) belong to important ferrous iron ( $\text{Fe}^{2+}$ ) minerals. Thus, in anoxic soils and freshwater sediments, iron represents an important electron acceptor and donor in both of its oxidation states. Several groups of prokaryotes can use iron as substrate to generate energy. Microorganisms such as *Rhodobacter ferrooxidans* (Kappler and Straub, 2005) catalyze the oxidation of ferrous iron under anoxic conditions. Dissimilatory metal-reducing bacteria (DMRB) residing in groundwater, sediments and soils use ferric iron as electron acceptor. By coupling the oxidation of organic compounds or molecular hydrogen (Coppi *et al.*, 2004) to the reduction of different extracellular electron acceptors such as Fe(III), Mn(IV) and U(IV) (Lovley, 1993), they generate energy for their growth. The prominent physiological feature of the *Geobacter* species is their ability to oxidize organic electron donors completely to carbon dioxide. *Geobacter metallireducens* and other *Geobacteraceae* are even able to oxidize aromatic hydrocarbons to  $\text{CO}_2$  and transfer the electrons to Fe(III) (Kane *et al.*, 2002).

From a variety of bacterial and archaeal families it is known, that they reduce Fe(III) dissimilatorily (Lovley *et al.*, 2004). Species like *Shewanella oneidensis* (DiChristina *et al.*, 1988), *Desulfuromonas acetoxidans* (Roden and Lovley, 1993), *Geobacter metallireducens* (Lovley *et al.*, 1993) and *Geobacter sulfurreducens* (Caccavo *et al.*, 1994) are examples of dissimilatory metal-reducing bacteria. The widespread appearance of iron-reducing bacteria also correlates with the availability of Fe(III). Many sediments and soils contain ferric iron minerals in the range of 50-200 mmol per kg wet weight. Ferric iron is therefore an important electron donor even if it is insoluble at neutral pH (Lovley *et al.*, 2004; Kappler and Straub, 2005). On the other hand, the dissimilatory metal-reducing bacteria in general occupy a central position in the global

biogeochemical cycles of metals and serve as catalysts in a variety of important environmental processes, such as the production of minerals (biomineralization), the oxidation of metals (biocorrosion) and the degradation, detoxification and immobilization of contaminations and pollutants (bioremediation).

The process of iron reduction was investigated especially for the species *Geobacter* and *Shewanella*, which belong to the  $\delta$ - and  $\gamma$ -proteobacteria, respectively. The metabolism of *Geobacter* species is of particular interest, as they are widely distributed in diverse anoxic soils and sediments and they are often the most abundant microorganisms (Coates *et al.*, 1996; Lovley *et al.*, 2004), where the microbial reduction of Fe(III) is an important process. Due to the high abundance of Fe(III) and Mn(IV) in these environments, the reduction of iron and manganese is responsible for the anaerobic oxidation of considerable amounts of organic carbon in the form of e.g. acetate.



**Figure 1:** left: Transmission electron micrograph of *Geobacter sulfurreducens* cells grown with soluble Fe(III) citrate, scale bar 0.5  $\mu\text{m}$ . (Reguera *et al.*, 2005). Right: Colonies of *Geobacter sulfurreducens* from a dilution series.

The  $\delta$ -proteobacterium *Geobacter sulfurreducens* was one of the first dissimilatory metal-reducing bacteria with a completely sequenced genome (Methé *et al.*, 2003). The *G. sulfurreducens* genome comprises 3.81 Mb with 3,466 predicted protein encoding genes (Methé *et al.*, 2003). The importance of electron transport is highlighted by the unusually large number of genes for *c*-type cytochromes (see 3.5), 111 altogether and 73 of which contain two or more heme groups. Comparison to the other metal ion-reducing bacteria *Shewanella oneidensis* (a  $\gamma$ -proteobacterium) and *Desulfovibrio vulgaris* (a  $\delta$ -proteobacterium) revealed that some *c*-type cytochromes are common in these three species, but that 43 are unique to *G. sulfurreducens* (Methé *et al.*, 2003).

Genes predicted to code for proteins that are involved in response to oxidative stress such as catalase, superoxide dismutase and cytochrome *c* peroxidases are present in the genome of *Geobacter sulfurreducens* as well as genes for flagella and pili production.

Even genes appearing to encode a terminal cytochrome *c* oxidase were found indicating that *G. sulfurreducens* has the ability to use oxygen as terminal electron acceptor (Lin *et al.*, 2004). The availability of the genome sequence provided new insights into the function of the DMRB and especially into the physiology of *Geobacter sulfurreducens* that was previously thought to be nonmotile and strict anaerob.

### 3.2 Iron as Electron Acceptor in *Geobacter sulfurreducens*

Every cell faces the problem of energy generation in order to survive. In this context, electron transfer reactions are of fundamental importance. However, in contrast to the microorganisms that reduce final electron acceptors in form of free diffusing gas or soluble substrates, DMRB are faced with an exceptional challenge: They respire anaerobically with terminal electron acceptors that are as Fe(III) oxide highly insoluble at pH values above 4. Consequently, the oxides cannot diffuse into the cell or be uptaken, while Fe(III) present one of the most important electron acceptor in anaerobic environments. In theory, the order in which electron acceptors are utilized is determined by the redox potential. At low pH,  $\text{Fe}^{3+}/\text{Fe}^{2+}$  has a redox potential ( $E_0' = +0.76\text{ V}$ ) comparable to oxygen making the reduction of Fe(III) an energetically favorable reaction. However, the energy associated with the reduction of Fe(III) at circumneutral pH is less energetically favorable as the redox potential is less positive ( $E_0' = +0.2\text{ V}$ ) (Madigan *et al.*, 2002).

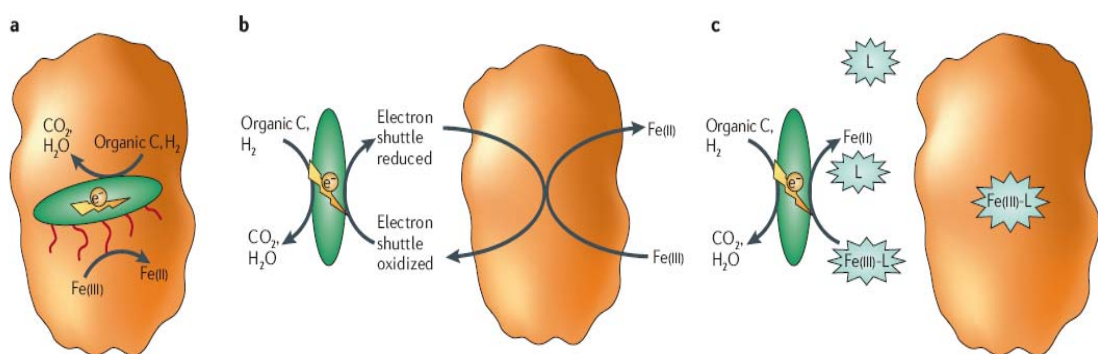


**Figure 2:** Different strategies of electron transport to insoluble Fe(III) oxides (Weber *et al.*, 2006). (a) In *Geobacter* species, direct contact to the insoluble Fe(III) oxides is required. The extracellular pili are proposed to act as electrical conductors. (b) Low molecular electron shuttles carry electrons to the insoluble iron. (c) The secretion of  $\text{Fe}^{3+}$  chelators by microorganisms such as *Geothrix* sp. aids in the dissolution of Fe(III) oxides and provides more readily available Fe(III).

DMRB can also reduce U(VI) or Tc(VII), that exist as soluble substrates but are reduced to insoluble end products.

To circumvent the physiological problem associated with the insolubility of the substrate or end products of the metabolism, diverse strategies were developed by different metal-reducing species (see figure 2) (DiChristina, 2005).

In contrast to *Geobacter* species, *Shewanella* species have resolved the problem by excreting low molecular electron shuttles, carrying electrons from the cell to insoluble iron that is subsequently reduced abiotically (Newman and Kolter, 2000). An alternative solution to reduce insoluble Fe(III) without making direct contact to the insoluble Fe(III) oxides is the production and secretion of siderophores, a common tool of various bacteria and fungi to enhance iron solubility under iron-limiting conditions (Butler, 1998; Kraemer *et al.*, 2005). Siderophores are low molecular weight Fe<sup>3+</sup> chelating compounds with high specificity and affinity for iron. The dissolved ferric siderophore complexes are then recognized and can be transported across the cell membrane.

Another possibility to respire insoluble iron is a terminal reductase located in the outer membrane that takes electrons from the central metabolism in the cytoplasm and transfers them by direct contact to the insoluble iron minerals. C-type cytochromes are a part of the electron transport chain to the extracellular iron reductase in *G. sulfurreducens* (DiChristina, 2005). Additionally, the production of so-called nanowires has been reported to facilitate electron transfer to the Fe(III) oxide surface. These extracellular pili act as electrical conductor, but they are not necessarily required for the attachment to the iron mineral surface (Reguera *et al.*, 2005). In case of *Geobacter metallireducens*, it was shown that pili help in accessing insoluble Fe(III) by chemotaxis (Childers *et al.*, 2002).

### 3.3 Alternative Electron Acceptors

*Geobacter sulfurreducens* uses also elemental sulfur, Co(III)-EDTA or malate as electron acceptors (Caccavo *et al.*, 1994). Like most Fe(III)-reducing bacteria, *G. sulfurreducens* reduces as well Mn(VI) and other metals. Toxic metals or metalloids often occur in their soluble form in the groundwater and thus are mobile. However, under anoxic conditions microorganisms such as *Geobacteraceae* are able to reduce them to insoluble end products that precipitate and can be removed from the

groundwater (Lovley, 2001; Lovley, 2002). Especially the ability to reduce uranium makes *Geobacter sulfurreducens* an interesting tool for bioremediation.

Growth on fumarate results in a threefold higher cell yield compared to Fe(III) citrate as electron acceptor (Esteve-Núñez *et al.*, 2004), meaning that the reduction of fumarate provides more energy than reduction of Fe(III) citrate. However, it was shown that, as long as Fe(III) was present in the culture, the levels of mRNA for fumarate reductase were significantly lower under acetate-limiting conditions such that the fumarate reduction was inhibited and the utilization of fumarate as an electron donor was favored (Esteve-Núñez *et al.*, 2004).

*Geobacteraceae* can also use graphite electrodes as sole electron acceptors for anaerobic respiration. There, electron donors like acetate are completely oxidized to CO<sub>2</sub>. The rates of electron transport can be compared to those of electron transport to Fe(III) citrate (0.21 to 1.2 μmol electrons/ mg of protein/ min in comparison to 1-3 μmol electrons/ mg of protein/ min during transfer to soluble Fe(III) citrate) (Bond and Lovley, 2003). This was the first report of microbial electricity production. The experiments showed, on the one hand, that electrode reduction supported growth of the bacteria and, on the other hand, that *Geobacter sulfurreducens* is capable of producing electric current when attached to electrodes.

Previously, *Geobacter* sp. have been classified as strict anaerobes. However, in the genome of *Geobacter sulfurreducens* homologs of catalase, superoxide dismutase, rubrerythrin, peroxidases and cytochrome *c* oxidase were identified (Methé *et al.*, 2003). These enzymes provide the possibility of scavenging oxygen radicals and therefore allow for exposure to oxygen or even to utilize oxygen as terminal electron acceptor. Growth experiments revealed that *G. sulfurreducens* can grow at least for 24 h with oxygen as single electron source (Lin *et al.*, 2004). This suggests that the organism may be able to survive at the anoxic-oxic interface.

### 3.4 Electron Transfer in DMRB

The electron transfer chain to insoluble Fe(III) oxides in *Geobacter* species is of special interest, as insoluble Fe(III) oxides are the primary source of Fe(III) for the dissimilatory iron reduction. In contrast to classical respiratory metabolism, this pathway of iron reduction ends in an electron transfer system localized in the outer

membrane, where it is in direct contact to insoluble iron minerals. Hence, two membranes need to be crossed.

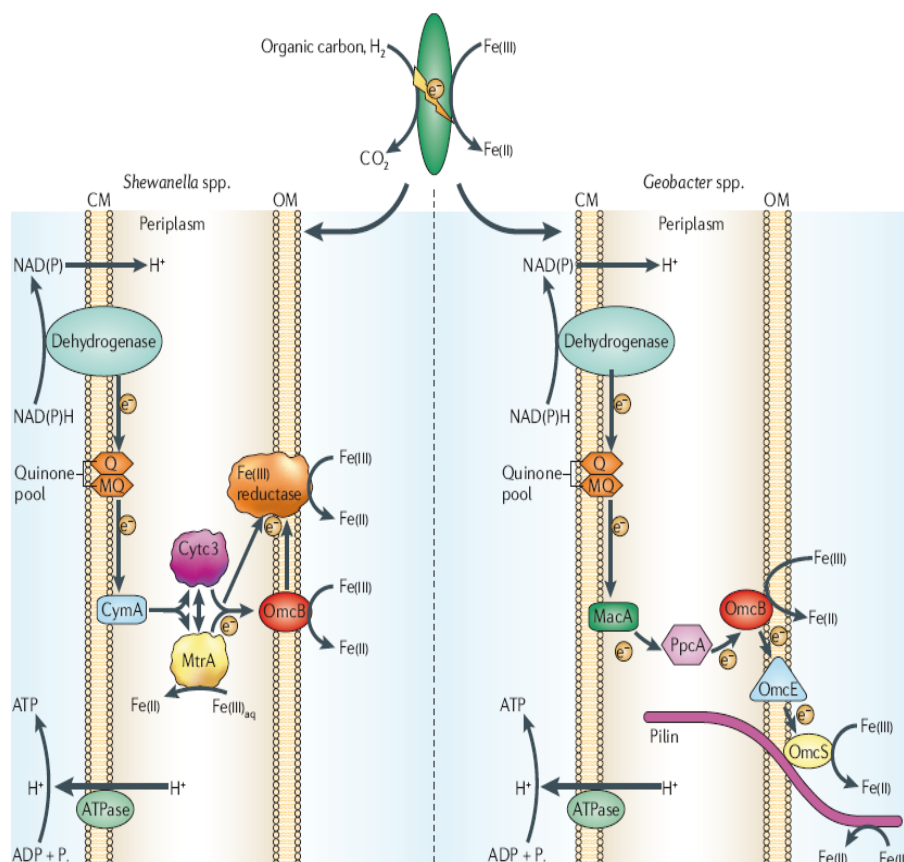


**Figure 3:** Model of the electron transport chain involved in dissimilatory Fe(III) reduction by *Shewanella* and *Geobacter* species (Weber *et al.*, 2006). The description of the electron transfer proteins is found in the text. CM, cytoplasmic membrane; OM, outer membrane; Q, quinone; MQ, menaquinone.

Electron transfer has been most investigated in *Geobacter* and *Shewanella* species. In both cases, electron transport proteins and quinones in the inner membrane are considered to transfer electrons to electron transport proteins in the periplasm. Subsequently, *c*-type cytochromes act as carriers transferring electrons to a reductase localized in the outer membrane. Due to the identification of *c*-type cytochromes proposed to be involved in electron transport to insoluble iron (Leang *et al.*, 2003; Lloyd *et al.*, 2003; Butler *et al.*, 2004), different models for the dissimilatory iron reduction have been developed (see figure 3) (Weber *et al.*, 2006) and need to be verified.

In *Shewanella* species, electrons are transferred from menaquinone to the membrane-bound tetraheme *c*-type cytochrome CymA and subsequently to further electron carriers in the periplasm. The tetraheme *c*-type cytochrome Cyt *c*<sub>3</sub> and the decaheme



cytochrome MtrA are considered to be the electron carriers to an outer membrane protein (Gordon *et al.*, 2000; Pitts *et al.*, 2003). OmcB is an outer membrane *c*-type cytochrome that can reduce extracellular Fe(III) directly (Myers and Myers, 2002). However, some Fe(III) reduction still occurs in the *omcB* mutant indicating that Fe(III) reduction is not exclusively dependent on OmcB (Myers and Myers, 2002; Weber *et al.*, 2006).

The large number of *c*-type cytochromes in *Geobacter sulfurreducens* reflects the complex electron transport systems that lead to a huge variability in utilizing different electron acceptors, giving rise to the assumption that various alternative electron transfer chains to the outer membrane may exist (Leang *et al.*, 2005).

In the currently proposed model for *Geobacter sulfurreducens*, the diheme cytochrome MacA is considered to be the primary acceptor for the electrons derived from menaquinone in the inner membrane (Weber *et al.*, 2006). Subsequently, electrons are transferred to periplasmic *c*-type cytochromes such as PpcA, a 9.6 kDa periplasmic triheme cytochrome *c* (Lloyd *et al.*, 2003).

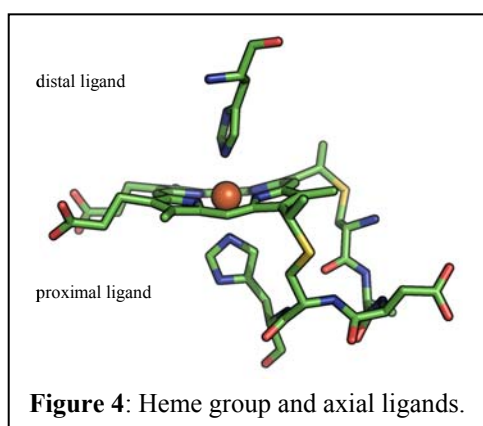
Obviously, multiheme *c*-type cytochromes in the outer membrane are key players in the reduction of metal ions. Gene expression and functional studies revealed that the 85.5 kDa dodecaheme cytochrome OmcB is required for optimal Fe(III) reduction (Leang *et al.*, 2003). The rate of Fe(III) reduction in an *omcB* deletion mutant was significantly impaired and was only 3-6% of that of the wild type. However, the mutant adapted to growth on soluble Fe(III) but not on insoluble Fe(III) (Leang *et al.*, 2005). At least two further outer membrane *c*-type cytochromes, OmcE and OmcS (Mehta *et al.*, 2005), have been reported to be required for the electron transfer to solid Fe(III) oxides. Not only cytochromes are involved in this electron transfer chain. When respiring Fe(III) oxides, *Geobacter sulfurreducens* produces pili. It was shown that these cell appendages not only serve for the attachment of the cells to the ferric iron but they are also conductive and active in transfer of electrons to the iron oxides (Reguera *et al.*, 2005).

In spite of all recent progress, the mechanism DMRB apply to reduce metals like ferric iron or manganese oxides remains unclear and further investigations are warranted.

## 3.5 Cytochromes

### 3.5.1 The Porphyrin Cofactor

Members of the  $\alpha$ -proteobacteria condense the heme precursor molecule  $\delta$ -aminolevulinic acid from glycine and succinyl-coenzymeA, whereas most of the bacteria including *Escherichia coli* use the C<sub>5</sub> pathway (Jahn *et al.*, 1991; Thöny-Meyer, 1997). Several subsequent reactions are necessary to make protoporphyrin IX (Daily, 1997). The final incorporation of the ferrous iron is catalyzed by the enzyme ferrochelatase.



The four pyrrole nitrogen atoms of the heme group are strong chelators for metal ions such as ferric or ferrous iron. In addition, iron is ligated by one or two axial, protein-derived ligands. Heme iron occurs in 5- or 6-coordinated state with ligands in the form of histidine N<sup>ε</sup> or - more rarely - N<sup>δ</sup>, cysteine S<sup>γ</sup>, methionine S<sup>δ</sup>, tyrosine O<sup>η</sup> and lysine N<sup>ζ</sup> side chains or terminal amino

groups provided by the peptide chain (Fita and Rossmann, 1985; Sundaramoorthy *et al.*, 1995; Einsle *et al.*, 2000). The distal ligand is positioned distantly in the primary sequence from the CXXCH motif. Furthermore, non-protein ligands may be bound that in most cases are related to the function of the protein, such as oxygen in hemoglobin or substrates and reaction intermediates in many enzymes.

The heme cofactor is redox-active and can be in the reduced (Fe<sup>2+</sup>) or oxidized (Fe<sup>3+</sup>) state. Therefore, these proteins are part of one-electron transfer reactions. Their redox potential determines the direction of electron transfer and usually falls into the range of -400 - +400 mV (Moore and Pettigrew, 1990). The redox potential is strongly dependent on the axial ligands. Methionine sulfur is a good electron acceptor and favors the relatively electron-rich reduced state resulting in a more positive redox potential compared to bis-histidinyll coordinated heme groups (Moore and Pettigrew, 1990).

The heme group is a conjugated system leading to prominent spectroscopic features. The most important transitions are the alpha, beta and Soret bands. This characteristic absorption pattern which is due to charge transfer and  $\pi$  to  $\pi^*$  transitions within the

pyrrole ring and the different oxidation states of the iron can be used to gain informations about the protein by electron excitation spectroscopy, an efficient analytical tool in the research of *c*-type cytochromes.

### 3.5.2 C-Type Cytochromes

*C*-type cytochromes are a widespread group of proteins that are found in animals, plants and bacteria. Besides the specific heme binding site, they have a second specific property in common. A characteristic N-terminal signal sequence serves for the export from the place of protein synthesis to the appropriate compartment. Bacterial *c*-type cytochromes are soluble or membrane-bound proteins outside the cytoplasm, located in the periplasm or in the inner or outer membrane.

Iron protoporphyrin IX is the cofactor of cytochromes, and it is found in various modifications in nature. Heme proteins serve a wide range of biological functions including the binding of oxygen (hemoglobins), electron transfer reactions and the catalysis of enzymatic reactions, especially of the oxygen metabolism (oxidases, peroxidases, catalases and hydroxylases). The catalytic variability of cytochromes originates from the nature of the protoporphyrin IX substituents as well as from the environment and the axial ligand provided by the surrounding protein (Moore and Pettigrew, 1990).

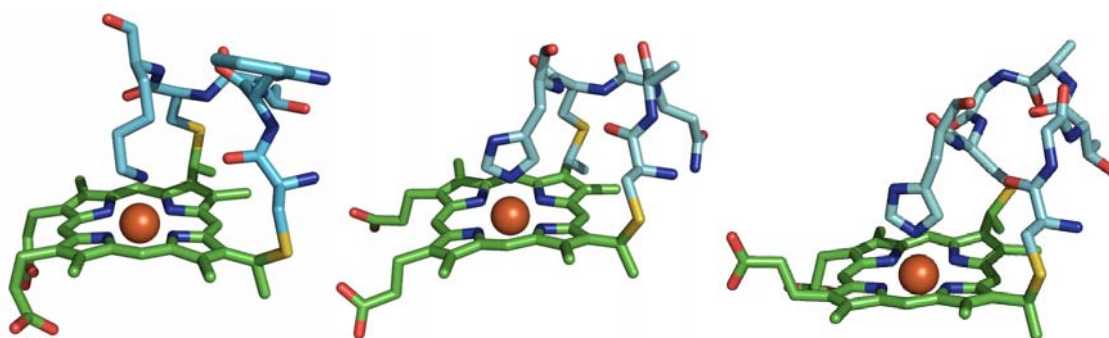


**Figure 5:** left: CXXCK-motif (cytochrome *c* nitrite reductase, pdb accession code 1FS7), mid: CXXCH-motif (cytochrome *c*, pdb accession code 1HRC), right: CXXXXCH-motif (cytochrome *c*<sub>3</sub>, pdb accession code 2CTH)

This work is focussed on heme *c* as it occurs in *c*-type cytochromes. Their characteristic feature is the covalent attachment of the heme group via thioether bonds from the vinyl groups to the cysteine side chains of a conserved binding motif in the protein matrix. The cysteines are most commonly arranged within a CXXCH-motif, but rare exceptions like CXXXXCH-, CXXXXXCH- or CXXCK-motives for the cofactor binding to the

protein are also possible (Bushnell *et al.*, 1990; Einsle *et al.*, 2000). Histidine and lysine, provided by the common heme binding motif, are found as proximal axial ligands. Often, also a sixth ligand exists which is mostly a methionine or a histidine. The number of heme groups per protein chain is variable, from one up to 27, as predicted for a protein in *Geobacter sulfurreducens* (Méthé *et al.*, 2003).

### 3.5.3 C-Type Cytochrome Maturation

C-type cytochrome maturation is a posttranslational process involving the transport of heme, secretion of the polypeptide chain through the membrane and covalent attachment of the heme to the apoprotein. This process converts a linear apoprotein to a three-dimensional holoprotein with one or more covalently bound and structure-giving heme groups (Thöny-Meyer, 1997; Kranz *et al.*, 1998; Barker and Ferguson, 1999). However, the detailed mechanism during which the two thioether bonds between the cysteines of the CXXCH-motif and the vinyl groups of the heme group are formed is still unclear.

The *c*-type cytochrome maturation system comprises several components and differs remarkably within several bacteria and eukaryotic cells. Three systems for the biogenesis of *c*-type cytochromes have been evolved.

#### 3.5.3.1 System I

System I is the most common maturation system for *c*-type cytochromes found e.g. in  $\alpha$ - and  $\gamma$ -proteobacteria, in plant or protozoal mitochondria and in archaea (Kranz *et al.*, 1998).

*E. coli* does not synthesize *c*-type cytochromes under aerobic conditions. However, under anaerobic respiratory conditions, *E. coli* was found to involve system I in the synthesis of *c*-type cytochromes (see figure 6). Five different *c*-type cytochromes can be detected in *E. coli* when nitrate, nitrite or trimethylamine N-oxide (TMAO) are present as terminal electron acceptors (Iobbi-Nivol *et al.*, 1994). This is due to the fact that the expression of genes of the *aeg-46.5* region is induced under anaerobic conditions and in the presence of nitrate, nitrite or TMAO. Further investigations revealed that genes of the cluster *ccmABCDEFGH* present in the *aeg-46.5* region are required for *c*-type cytochrome maturation (Thöny-Meyer *et al.*, 1995). Ccm proteins presumably form a

maturase complex that coordinates the different steps of cytochrome *c* maturation. The key steps occur on the periplasmic side of the cytoplasmic membrane.

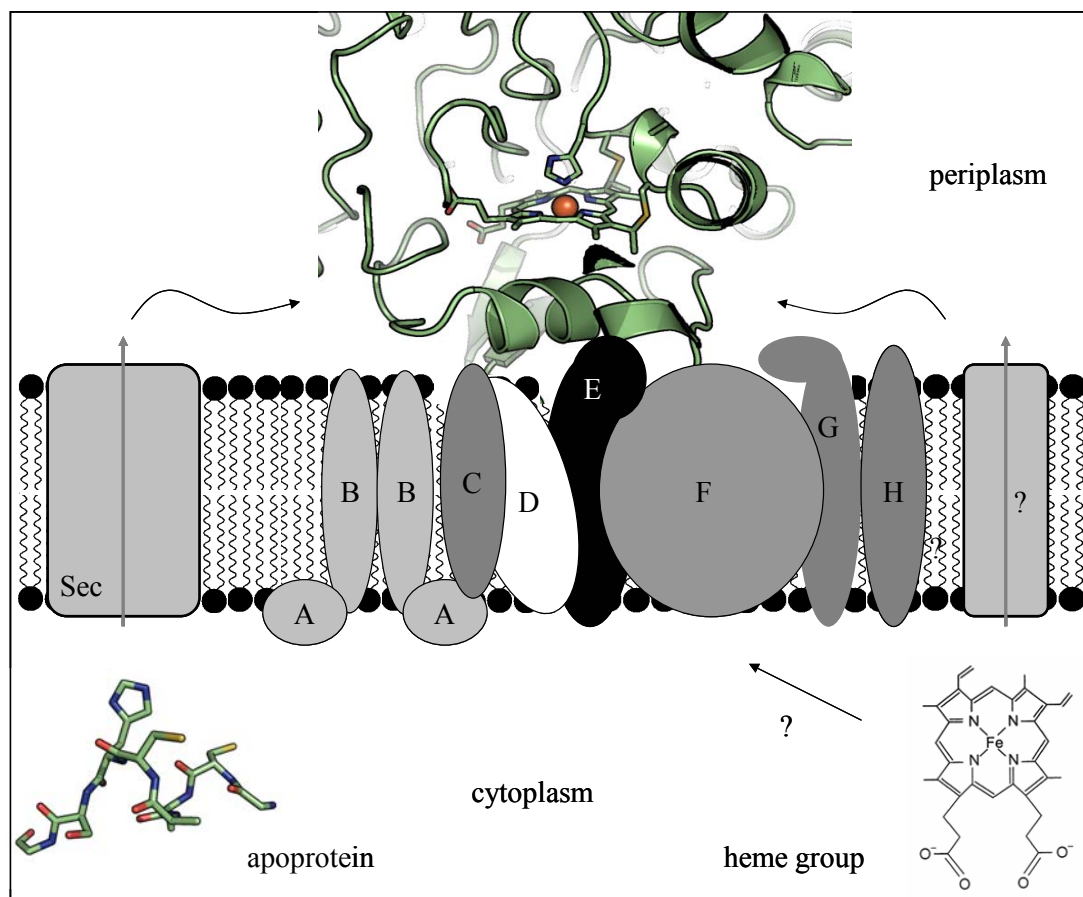


**Figure 6:** System I. C-type cytochrome maturation occurs in the periplasm. The apoprotein is transported via the Sec-dependent pathway into the periplasm; the transport mechanism of the heme group into the periplasm is still unknown. CcmAB: ABC transporter, CcmE: heme chaperone.

The heme group and the apoprotein are synthesized separately in the bacterial cytoplasm. The apoprotein is then translocated via the Sec-dependent pathway (Thöny-Meyer, 2002) across the cytoplasmic membrane. How many and which heme carriers are involved in the transport of the heme group into the periplasm is not known so far. After the translocation, heme is covalently but transiently bound to the heme chaperone CcmE (Schulz and Thöny-Meyer, 2000). The small protein CcmD is implicated in heme delivery to the heme chaperone CcmE (Ahuja and Thöny-Meyer, 2005), forming a ternary complex that consists of CcmCDE. CcmF is involved in the release of heme from the heme chaperone (Thöny-Meyer, 2002). From there on, heme is transferred to the apoprotein. The reduction of the cysteines of the CXXCH-motif prepares the

binding reaction. For this, electrons are transported from a cytoplasmic thioredoxin to the transmembrane protein DsbD and finally on to the reductases CcmG and CcmH.

Biotechnologically, the ccm machinery can also be coerced into producing *c*-type cytochromes in the presence of oxygen. When the *ccmABCDEFGH* genes are expressed from a plasmid, the formation of holocytochrome *c* can be achieved (Arslan *et al.*, 1998; Huston *et al.*, 2007). This method is employed in the present work to express the *c*-type cytochromes of interest.

### 3.5.3.2 System II

System II is found in gram-positive bacteria, chloroplasts as well as in some  $\beta$ -,  $\delta$ - and  $\epsilon$ -proteobacteria. It bears some resemblances to system I with respect to components ensuring the reduction of the cysteines; otherwise both systems are quite different. At least the four proteins CcsA, Ccs1, ResA and CcdA are involved in the assembly of *c*-type cytochromes (Kranz *et al.*, 1998).

*Geobacter sulfurreducens* uses system II (Stevens *et al.*, 2004). Nevertheless, it is possible to heterologously overproduce *c*-type cytochromes from *Geobacter sulfurreducens* in *E. coli* by means of coexpressing system I (see 3.5.3.1) (Lloyd *et al.*, 2003; Heitmann and Einsle, 2005).

### 3.5.3.3 System III

This is the simplest known kind of *c*-type cytochrome maturation machinery and is found e.g. in mitochondria of fungi, vertebrates and invertebrates (Kranz *et al.*, 1998). Two different types of cytochrome *c* lyases representing central components of the *c*-type cytochrome biogenesis system III have been identified. Cytochrome *c* lyase (CCHL) is required for the formation of the two thioether bonds between the heme group and the apocytochrome, and the cytochrome *c*<sub>1</sub> heme lyase (CC<sub>1</sub>HL) is required for the maturation of cytochrome *c*<sub>1</sub>, an integral part of the *bc*<sub>1</sub>-complex.

## 3.6 Peroxidases

Oxidative stress can manifest itself in the generation of toxic oxygen intermediates, including the superoxide anion (O<sub>2</sub><sup>-</sup>), hydrogen peroxide (H<sub>2</sub>O<sub>2</sub>) and the hydroxyl

radical ( $\text{HO}^\bullet$ ), that evolve from the incomplete reduction of oxygen (see figure 7). The reactive oxygen species can cause damage to proteins, DNA and membranes.

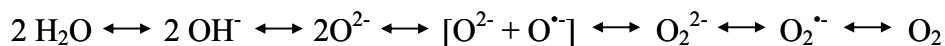


**Figure 7:** Toxic oxygen intermediates of the incomplete reduction of oxygen (Kaim and Schwederski, 2004). Hydrogen peroxide is formed by the protonation of peroxide ( $\text{O}_2^{2-}$ ).

In bacteria, three main classes of enzymes are involved in the removal of hydrogen peroxide from the cell (Atack and Kelly, 2007). Cytoplasmic catalases cleave hydrogen peroxide into water and oxygen whereas glutathione peroxidases catalyze the reduction of  $\text{H}_2\text{O}_2$  in the presence of glutathione. Finally, there are the cytochrome *c* peroxidases catalyzing the reduction of hydrogen peroxide to water which draw electrons from the electron transfer chain. They are a widespread family of extracytoplasmic enzymes catalyzing the conversion of  $\text{H}_2\text{O}_2$  by means of the heme cofactor. Eukaryotes as well as prokaryotes contain cytochrome *c* peroxidases but they differ in mechanism and structure.

### 3.6.1 Eukaryotic Peroxidases

Eukaryotic peroxidases are located in the inter-membrane space of mitochondria. They contain one single *b*-type heme group as active site. The overall reaction is similar to bacterial peroxidases, but the catalytic mechanism is significantly different (Lu, 2006; Atack and Kelly, 2007).

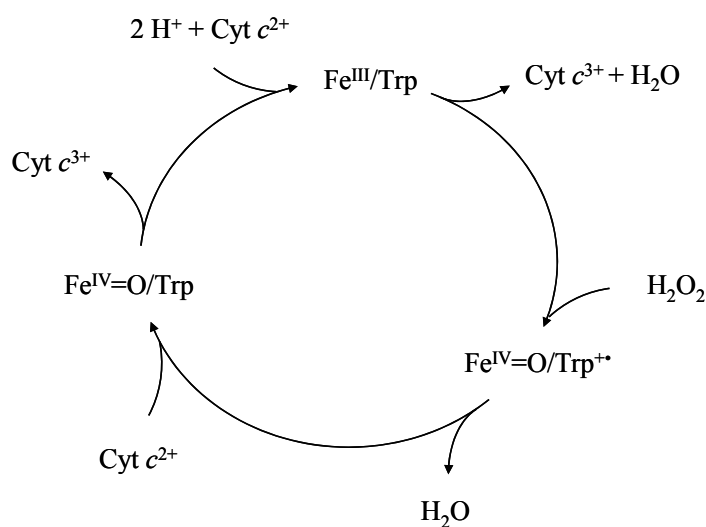


**Figure 8:** Catalytic reaction mechanism of eukaryotic peroxidases.

The reaction generates an oxo-ferryl intermediate of the heme and a cation radical on a nearby tryptophan as the reduction of hydrogen peroxide requires two electrons (Sivaraja *et al.*, 1989). In contrast to eukaryotic peroxidases, the bacterial cytochrome *c* peroxidases (Ccps) incorporate a second heme group avoiding the generation of this radical.

Interestingly, cytochrome *c* peroxidase and manganese peroxidase catalyzing the biodegradation of lignin show a similar heme binding site. The main differences are found in the  $Mn^{II}$  binding site and a conserved aromatic residue near the heme group. In the eukaryotic Ccps there is a tryptophan instead of a phenylalanine. Additionally, many ligands for  $Mn^{II}$  in MnP are missing in CcP (Lu, 2006). These two enzymes are an example for proteins with similar scaffolds but different substrates and thus different catalyzed reactions.

### 3.6.2 Bacterial Peroxidases

Cytochrome *c* peroxidases receive electrons from the central metabolism via cytochrome *c* or in some cases from copper proteins (Pauleta *et al.*, 2004b). They are located in the periplasm where they catalyze the two-electron reduction of hydrogen peroxide to water.

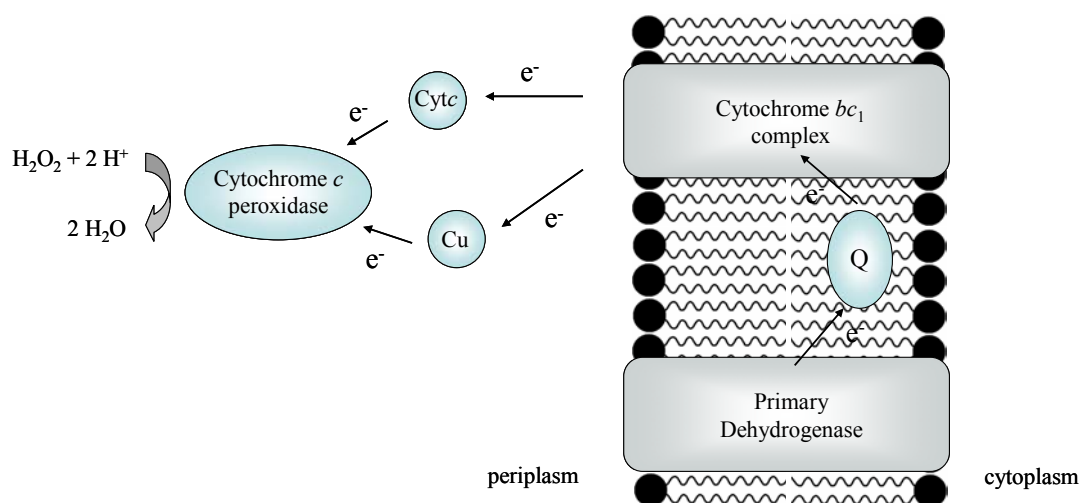


**Figure 9:** Scheme of a typical bacterial electron transport system. In gram-negative bacteria the cytochrome *c* peroxidase is located in the periplasm. Most of the bacteria possess only one peroxidase (Atack and Kelly, 2007). Cytochromes *c* (Cyt*c*) and cupredoxins (Cu) are currently considered to be electron ( $e^-$ ) donors to the peroxidase. Q: quinone pool



Bacterial cytochrome *c* peroxidases have been isolated from *Methylococcus capsulatus* (Zahn *et al.*, 1997), *Nitrosomonas europaea* (Arciero and Hooper, 1994), *Paracoccus pantotrophus* (Goodhew *et al.*, 1990), *Pseudomonas aeruginosa* (Ellfolk and Soininen, 1970), *Pseudomonas stutzeri* (Villalain *et al.*, 1984) and *Rhodobacter capsulatus* (Hanlon *et al.*, 1992). Depending on the species, molecular weights range from 35-40 kDa (Atack and Kelly, 2007) and they are commonly purified as homodimers (Gilmour *et al.*, 1994; Alves *et al.*, 1999; De Smet *et al.*, 2001). Crystal structures are available from *Pseudomonas aeruginosa* (Fülöp *et al.*, 1995), *Nitrosomonas europaea* (Shimizu *et al.*, 2001), *Paracoccus denitrificans* (Echalier *et al.*, 2004) and *Paracoccus pantotrophus* (Echalier *et al.*, 2006).

In contrast to eukaryotic peroxidases, bacterial CCPs consist of two domains, each with one covalently bound heme group. The high potential (HP) heme acting as the electron transfer center is situated in the C-terminal domain and its heme iron is methionine-histidine coordinated. The midpoint redox potential varies between the bacterial species from +320 mV in *P. aeruginosa* (Ellfolk *et al.*, 1983) to +130 mV in *N. europaea* (Shimizu *et al.*, 2001). The low potential (LP) heme is located in the N-terminal domain and is the site of peroxidase activity. In the oxidized form, the low potential heme is coordinated by two histidine residues and therefore is inactive. Here, the LP site has a midpoint redox potential of -330 mV in *P. aeruginosa* and +70 mV in *N. europaea* (Shimizu *et al.*, 2001).

### 3.6.2.1 Structure of Cytochrome *c* Peroxidases

The two heme groups are roughly perpendicular to each other and are separated by an iron-iron distance of about 21 Å (see figure 10). The shortest distance between the heme groups is approximately 10 Å between their propionate groups.

Both domains are connected by three strands of protein chain. The interface in between is hydrophobic, providing a typical Ca<sup>2+</sup> binding site (Fülöp *et al.*, 1995), where the amide oxygen of an asparagine, the main chain carbonyls of a threonine and a proline and four water molecules are ligating the Ca<sup>2+</sup> ion.

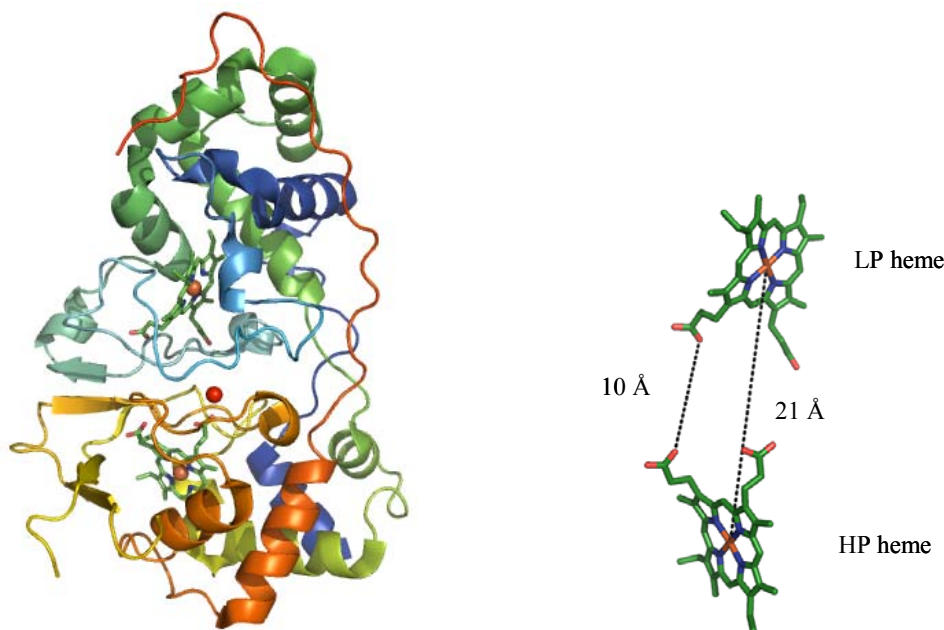


**Figure 10:** The structure of the cytochrome *c* peroxidase of *Pseudomonas aeruginosa* (Fülöp *et al.*, 1995) is the first structure solved of a bacterial cytochrome *c* peroxidase (pdb accession code 1EB7).

### 3.6.2.2 Reaction Mechanism

In its oxidized form, the peroxidase of *Pseudomonas aeruginosa* exhibits the high potential heme Fe<sup>III</sup> in a high spin/ low spin equilibrium (Foote *et al.*, 1984) whereas the iron is ligated by methionine and histidine. The low potential heme is coordinated by two histidines in the oxidized state. Consequently, the N-terminal domain has to undergo a conformational rearrangement to allow access for and binding of hydrogen peroxide. The current model suggests that the reduction of the high potential heme results in the switch of the low potential heme to high spin state. In this mixed valence form, the second histidine ligand of the low potential heme is released from the iron so that H<sub>2</sub>O<sub>2</sub> has access to the active site. One electron is abstracted from the high potential iron and one from the low potential iron with the formation of an oxo-ferryl intermediate. However, the mechanism of hydrogen peroxide reduction in bacterial cytochrome *c* peroxidases is not yet fully understood.

### 3.6.2.3 IN and OUT Conformation

Bacterial Ccps are active in the mixed valence state, where the high potential electron transferring heme is in its reduced state and the low potential peroxidatic heme is in its oxidized state. The only exception known so far represents the peroxidase of

*N. europaea* which is also active in its oxidized state. The flexible loop that is rearranged in the peroxidase of e.g. *P. aeruginosa* or *P. nautica* is here always in the OUT-confirmation, hence the heme is always 5-coordinated and therefore the enzyme is always accessible to substrate (Arciero and Hooper, 1994).

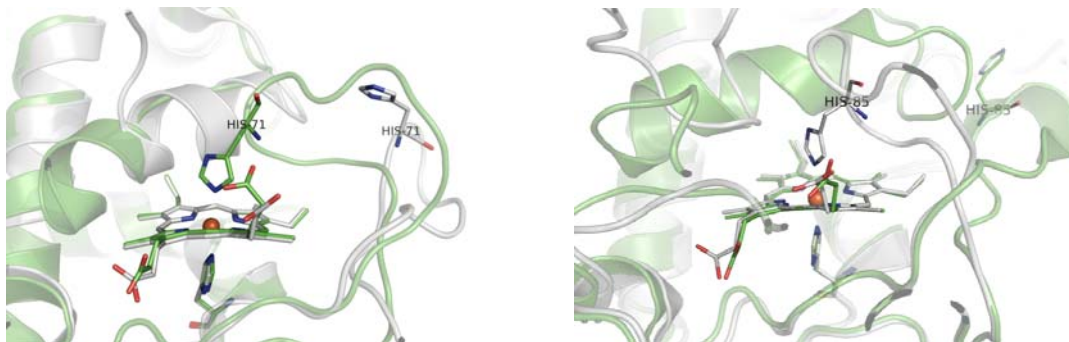


**Figure 11:** left: IN-form (green, pdb accession code 1RZ6) and OUT-form (grey, pdb accession code 1RZ5) of *Pseudomonas nautica*, right: oxidized-form (grey, pdb accession code 2C1U) and mixed-valence form (green, pdb accession code 2C1V) of *Paracoccus pantotrophus*.

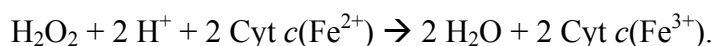
The other peroxidases need to be reduced before they can function as catalysts; only a change in the coordination of the heme iron at the active site allows substrate binding.

Two structures of the peroxidase of *P. nautica* are available due to photoreduction in the X-ray beam (Dias *et al.*, 2004). The IN-form is inactive and contains no calcium. The OUT-form has calcium bound and the loop comprising His71 is flipped out in the photoreduced state (Dias *et al.*, 2004).

### 3.6.2.4 Electron Transfer within the Cytochrome *c* Peroxidases

For the electron transfer to the substrate hydrogen peroxide, it is necessary that electrons derived from an electron donor such as cytochrome *c* or pseudoazurin are first transferred to the HP heme and further on via an electron transport pathway to the active site.

Ccps can accept two electrons from ferrous cytochrome *c* during catalysis according to:



The high potential heme receives electrons from external donors and mediates the transfer to the active site located about 21 Å away from the transferring heme. Currently, the way of the electrons from the electron transfer center to the active site is subject for speculations. It is proposed that the heme propionates and the conserved

Trp94 located in the hydrophobic patch are conduits for the electrons (Dias *et al.*, 2004; De Smet *et al.*, 2006).

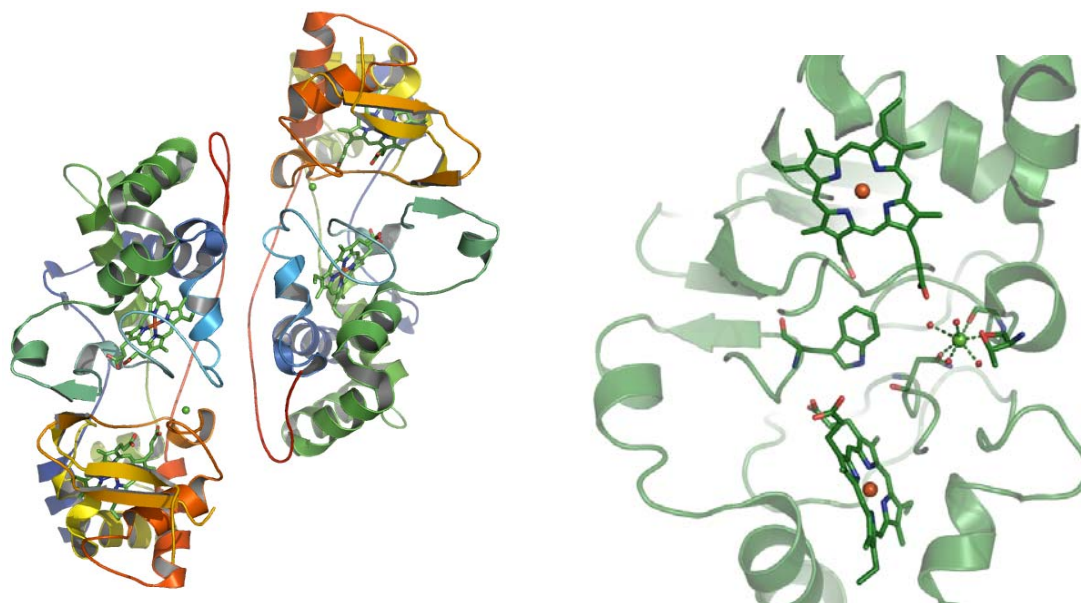


**Figure 12:** One heme group is located in each domain; tryptophan and calcium are located in the hydrophobic interface.

### 3.6.3 Other Diheme Cytochrome *c* Enzymes

Bacterial peroxidases are an example for proteins with similar scaffold performing different functions. MauG proteins are very similar to the bacterial peroxidases considering their sequences, but they show differences with respect to their function. MauG is one of the four proteins responsible for the biosynthesis of the methylamine dehydrogenase (MADH) (Wang *et al.*, 2003), involved in the generation of the tryptophan tryptophylquinone cofactor. The enzyme shows just a low peroxidase activity.

The rubber oxygenase A (RoxA) is a further example. Sequence comparison with cytochrome *c* peroxidases displays a few conserved residues, but for this enzyme no peroxidase activity was detected (Jendrossek and Reinhardt, 2003; Braaz *et al.*, 2004).

## 3.7 The Rubber Oxygenase RoxA

Natural rubber is synthesized by many plants and several fungi. Its main source is the rubber tree (*Hevea brasiliensis*). One of the main components, the biopolymer poly (*cis*-1,4-isoprene) contains many linear isoprene-subunits ( $C_5H_8$ ) and two *trans*-isoprene units at each end (see figure 13) (Eng *et al.*, 1994; Tanaka *et al.*, 1996). Natural rubber

does not accumulate in the environment, consequently there has to be continuous biological degradation. From a variety of bacteria, especially belonging to the actinomycetes, it is known that they exist on natural rubber medium and use rubber as carbon source. *Xanthomonas* sp. strain 35Y is so far the only known gram-negative bacterium degrading natural rubber. It was shown that *Xanthomonas* sp. strain 35Y secretes a rubber-degrading component into the polyisoprene containing medium that leads mainly to the formation of one degradation product, 12-oxo-4,8-dimethyl-trideca-4,8-dien-1-al (ODTD) (Braaz *et al.*, 2004). First indications of an extracellular enzyme that is responsible for the degradation of natural rubber were found by Tsuchii and Takeda (Tsuchii and Takeda, 1990).

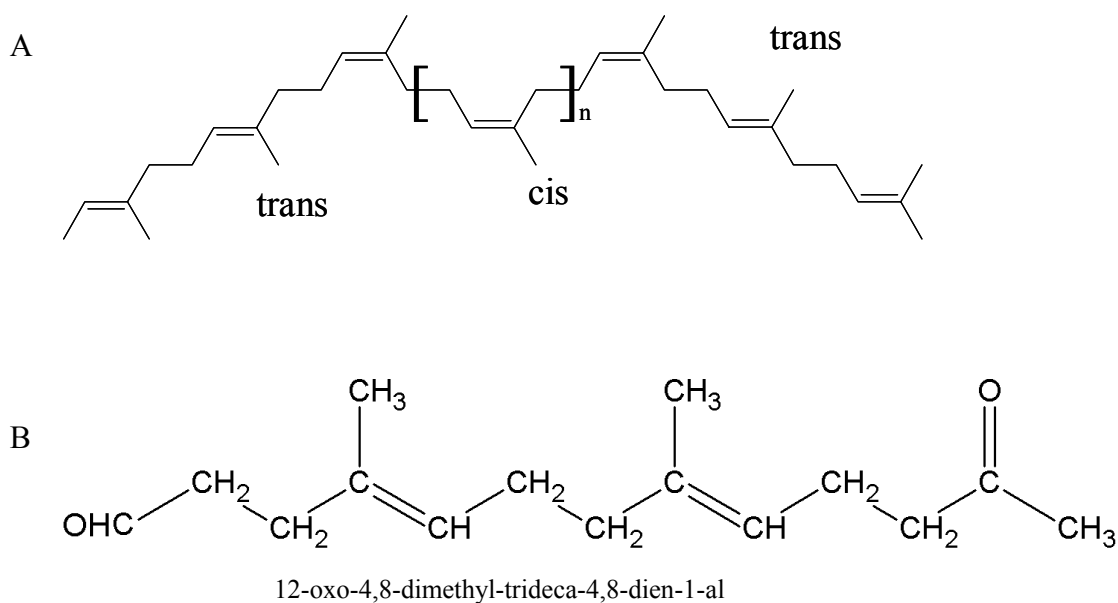


**Figure 13:** Structure of (A) polyisoprene,  $n = 100-10000$ , and (B) ODTD.

The rubber oxygenase A (RoxA) was first purified from medium of rubber-grown *Xanthomonas* sp. strain 35Y and it showed a strong absorbance maximum at 406 nm (Braaz *et al.*, 2004). The amino acid sequence then turned out to comprise two heme binding motifs agreeing with this specific absorbance (Jendrossek and Reinhardt, 2003). RoxA degrades natural rubber *in vitro* as well as synthetically produced poly (*cis*-1,4-isoprene), but it seems to be specific for oligomers and polymers of 1,4-isoprene. Natural rubber as well as synthetically produced poly (*cis*-1,4-isoprene) were cleaved by purified RoxA whereas oligomers from *trans*-1,4-isoprene and aromatic compounds

---

were not degraded by RoxA. By the means of labeling experiments it could be shown that the dioxygen dependent reaction at least incorporates one oxygen atom from O<sub>2</sub> into ODTD (Braaz *et al.*, 2005).

### 3.8 Goals of this Study

One goal of this study was to elucidate the protein structures of components of the dissimilatory metal reduction pathway in DRMB. The cytochrome *c* peroxidase homologs MacA and CcpA from *Geobacter sulfurreducens* were shown to be related to the electron transfer chain to insoluble electron acceptors outside the bacterial cells (Butler *et al.*, 2004; Leang *et al.*, 2005). Additionally, it was found out that MacA is not required for the oxidative stress response and that there is no homolog of cytochrome *c* that usually functions as electron donor to Ccps in the genome of *Geobacter sulfurreducens*. Thus, the question arose whether the structures of MacA and CcpA are similar to classical Ccps and if both enzymes show peroxidase activity.

First, an expression and purification system for the two *c*-type cytochromes needed to be established, as both proteins should be overexpressed heterologously in *E. coli* and purified by affinity chromatography without the use of a possibly heme interacting His-tag. Then, CcpA and MacA should be characterized biochemically and structurally.

Furthermore, the structure of the diheme cytochrome *c* enzyme RoxA from *Xanthomonas sp.* strain 35Y ought to be evaluated and compared to the structures of cytochrome *c* peroxidases. RoxA exhibits conserved residues of the core region of Ccps (Jendrossek and Reinhardt, 2003) leading to the assumption that general properties of electron transfer between the two heme groups within the proteins or parallels between the reaction mechanisms can be pointed out.

## 4 Material and Methods

### 4.1 Material

#### 4.1.1 Chemicals

All standard chemicals were of analytical purity grade (p.a.) and were obtained from the following companies: Applichem (Darmstadt, Germany), Merck (Darmstadt, Germany), Roth (Karlsruhe, Germany) and Sigma-Aldrich (Deisenhofen, Germany).

#### 4.1.2 DNA and Protein Molecular Weight Marker

The GeneRuler (MBI Fermentas, St. Leon-Rot, Germany) served as DNA marker. For sizing of proteins by SDS-PAGE, the unstained protein molecular weight marker from MBI Fermentas was used.

#### 4.1.3 Enzymes and Proteins

Restriction endonucleases, *Pfu* DNA polymerase and T4 DNA ligase were obtained from MBI Fermentas (St. Leon-Rot, Germany).

#### 4.1.4 Bacterial Strains

##### 4.1.4.1 *Escherichia coli*

XL10-Gold (Stratagene, USA):

$Tet^r \Delta(mcrA)183 \Delta(mcrCB-hsdSMR-mrr)173 \text{ endA1 } supE44 \text{ thi-1 } recA1 \text{ gyrA96 } relA1 \text{ lac Hte [F' } proAB \text{ lacI}^q \text{Z}\Delta M15 \text{ Tn10 (Tet}^r \text{) Tn5 (Kan}^r \text{) Amy]}$ .

BL21(DE3) (Novagen, Darmstadt, Germany):

$[F^- \text{ ompT } hsdS_B (r_B^- \text{ m}_B^-) \text{ gal dcm (DE3)}]$



#### 4.1.4.2 *Geobacter sulfurreducens*

The strain *Geobacter sulfurreducens* PCA (DSM 12127) (Caccavo *et al.*, 1994) was obtained from the *German Collection of Microorganisms and Cell Cultures* (DSMZ, Braunschweig, Germany).

#### 4.1.5 DNA-Oligonucleotides

DNA-oligonucleotides were obtained from MWG (Ebersberg, Germany) in HPSF (high purity salt free) quality.

Primers were constructed for the pETSN-22 vector (4.1.6.2). For this, the signal sequences of MacA and CcpA were determined by the SignalP v 3.0 server (Bendtsen *et al.*, 2004) in order to omit the *Geobacter* leader sequences as the pETSN-22 vector provides the OmpA signal sequence from *E. coli*.

CcpA: 2813_f_EcoRI:	5'-CGA ATT CGG CCG ATG AGC TGC AGC AG-3'
2813_r_XhoI:	5'-CCT CGA GTT ACA GTC TGG GGC GCG GTG-3'
MacA: MacA_f_EcoRI:	5'-CCC GAA TTC AAA AGA GGA TGT CAT GAA ACG-3'
MacA_r_XhoI:	5'-AAA CTC GAG TCA GTT GCT GAC CGG CCT G-3'
pETSN-22: pETS-22_f:	5'- AAT TCG AGC TCC GTC GAC AAG CTT GCG GCC GCA C-3'
pETS-22_r:	5'-TCG AGT GCG GCC GCA AGC TTG TCG ACG GAG CTC G-3'

#### 4.1.6 Plasmids

##### 4.1.6.1 pEC86

By means of the pEC86 plasmid (figure 14), the *ccm* (cytochrome *c* maturation) genes are constitutively expressed under the control of a *tet* promoter. This vector is based on the pACYC184 plasmid and contains besides the genes *ccmABCDEFGHIH*, providing the cytochrome *c* maturation machinery, a chloramphenicol resistance marker (Arslan *et al.*, 1998) and was generously provided by Prof. Linda Thöny-Meyer.

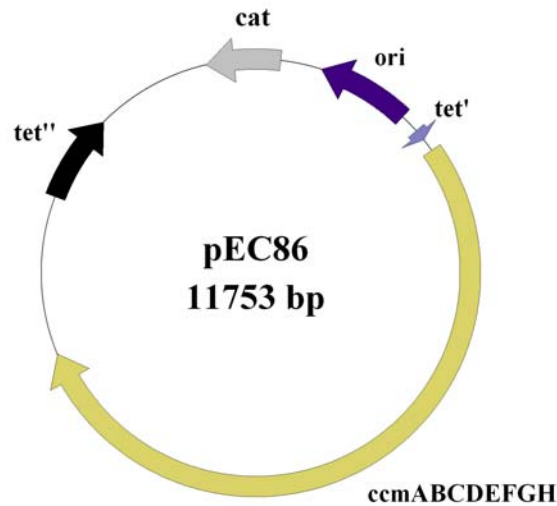


**Figure 14:** Schematic representation of the vector pEC86. Cat: chloramphenicol resistance marker, ori: origin, ccmABCDEFGHI: cytochrome *c* maturation genes, tet': tet promoter, tet'': tetracycline resistance marker

#### 4.1.6.2 pETSN-22

The plasmids used for heterologous expression of the two *c*-type cytochromes from *Geobacter sulfurreducens* are based on the vector pET22b(+) (Novagen, Darmstadt, Germany). However, the pET22b(+) vector was modified by replacing the ribosome binding site and the *pelB* signal sequence with the analogous sequence from the pASK-IBA44 vector (IBA, Göttingen, Germany) using the *XbaI* and *XhoI* restriction sites. Afterwards, the multiple cloning site (mcs) derived from pASK-IBA44 was exchanged for the sequence between *EcoRI* and *XhoI* restriction sites in pET22b(+) using the primers pETS-22\_f/r.



**Figure 15:** Organization of the pETSN-22 cloning site. The genes *ccpA* and *macA* were cloned into the pETSN-22 vector via *EcoRI* and *XhoI* restriction sites resulting in constructs that consist of the sequence of *ccpA* and *macA*, respectively, with preceding OmpA signal sequence and N-terminal *Strep-tagII*.

During secretion of the recombinant proteins into the periplasm, the OmpA leader sequence is cleaved off so that the processed protein starts with an alanine-serine linker.

## 4.2 Methods

### 4.2.1 Microbiological Methods

#### 4.2.1.1 Cultivation of *Escherichia coli*

<b>Luria-Bertani (LB) medium</b>	
1% (w/v) tryptone	
0.5% (w/v) yeast extract	
1% (w/v) sodium chloride	

*Escherichia coli* strains were grown in Luria-Bertani medium. Precultures for DNA isolation or the expression of protein were incubated overnight at 37°C.

The proteins MacA and CcpA were expressed heterologously in *E. coli* BL21(DE3)::pEC86 overnight at 30°C. Therefore, LB medium supplemented with 100 µg/ml ampicillin and 20 µg/ml chloramphenicol for antibiotic resistance selection was inoculated with 1 (v/v) % of inoculum.

#### 4.2.1.2 Cultivation of *Geobacter sulfurreducens*

<b>Modified NBAF medium</b>	
acetate	15 mM
fumarate	40 mM
NH <sub>4</sub> Cl	0.20 g
KH <sub>2</sub> PO <sub>4</sub>	0.42 g
K <sub>2</sub> HPO <sub>4</sub>	0.22 g
KCl	0.38 g
NaHCO <sub>3</sub>	1.80 g
Na <sub>2</sub> CO <sub>3</sub>	0.50 g

<b>Vitamin solution m141</b>	
biotin	2.0 mg
folic acid	2.0 mg
pyridoxine-HCl	10.0 mg
thiamine-HCl • 2 H <sub>2</sub> O	5.0 mg
riboflavin	5.0 mg
nicotinic acid	5.0 mg
D-Ca-pantothenate	5.0 mg
vitamin B <sub>12</sub>	0.1 mg
p-aminobenzoic acid	5.0 mg
lipoic acid	5.0 mg
dH <sub>2</sub> O	1000 ml

<b>Trace element solution m141+</b>	
nitrilotriacetic acid	1.50 g
MgSO <sub>4</sub> • 7 H <sub>2</sub> O	3.00 g
MnSO <sub>4</sub> • 2 H <sub>2</sub> O	0.50 g
NaCl	1.00 g
FeSO <sub>4</sub> • 7 H <sub>2</sub> O	0.10 g
CoSO <sub>4</sub> • 7 H <sub>2</sub> O	0.18 g
CaCl <sub>2</sub> • 2 H <sub>2</sub> O	0.10 g
ZnSO <sub>4</sub> • 7 H <sub>2</sub> O	0.18 g
CuSO <sub>4</sub> • 5 H <sub>2</sub> O	0.01 g
KAl(SO <sub>4</sub> ) <sub>2</sub> • 12 H <sub>2</sub> O	0.02 g
H <sub>3</sub> BO <sub>4</sub>	0.01 g
Na <sub>2</sub> MoO <sub>4</sub> • 2 H <sub>2</sub> O	0.01 g
NiCl <sub>2</sub> • 6 H <sub>2</sub> O	0.025 g
Na <sub>2</sub> SeO <sub>3</sub> • 5 H <sub>2</sub> O	0.50 mg
Na <sub>2</sub> WO <sub>4</sub> • 2 H <sub>2</sub> O	0.40 mg
dH <sub>2</sub> O	1000 ml

Cells of *Geobacter sulfurreducens* were cultivated in modified NBAFYE medium (Coppi *et al.*, 2001).

The modified NBAF medium was supplemented with 1% (v/v) vitamin solution m141 (DSMZ, Braunschweig, Germany), 1% (v/v) trace element solution m141+ (DSMZ) and 0.1% (w/v) yeast extract and autoclaved at 121°C for 20 minutes in a Widdel flask. Afterwards, the medium was cooled down while gassing with inertal gas (80% N<sub>2</sub>, 20% CO<sub>2</sub>) (Airliquide, Germany). Sterile filtered cysteine serving as reductant and sulfur source was added and the pH was adjusted with 6 M HCl to 7.2. The medium was inoculated with 5-10% of its volume or with a DMSO stock (see 4.2.1.5) of *G. sulfurreducens* cells and incubated at 30°C on a roller.

#### 4.2.1.3 Production and Transformation of Competent *E. coli* Cells

<b>TFB-1 buffer:</b> pH 5.8 with acetic acid	<b>TFB-2 buffer:</b> pH 6.5 with 1M NaOH
30 mM potassium acetate pH 7.0	10 mM NaMOPS pH 7.2
50 mM MnCl <sub>2</sub>	75 mM CaCl <sub>2</sub>
10 mM CaCl <sub>2</sub>	10 mM RbCl
100 mM RbCl	15% glycerol
15% glycerol	

500 ml LB medium, supplemented with appropriate antibiotics, were inoculated with a 5 ml preculture to produce chemically competent *E. coli* cells. The cells were grown at 37°C to an optical density of OD<sub>600</sub> = 0.6 before they were pelleted by centrifugation (10 minutes at 4,000 x g and 4°C). Subsequently, the cell pellet was carefully resuspended in 150 ml ice-cold TFB-1 buffer and chilled for 5 minutes on ice. After one further centrifugation, the pellet was dissolved in 5 ml ice-cold TFB-2 buffer and divided into 50 µl aliquots that were frozen in liquid nitrogen and stored at -80°C.

Prior to transformation, the cells were thawed on ice and 20-100 ng of DNA or the ligation mixture were added. After 30 minutes of incubation on ice, cells were subjected to a 37°C heat shock for 10 minutes. Afterwards, cells were chilled on ice for further 10 minutes before addition of 200 µl LB medium without antibiotics. In order to develop the antibiotic resistance, cells were incubated for 30-60 minutes at 37°C and then plated on selective agar or inoculated in a selective medium.

#### 4.2.1.4 Cultivation of *Geobacter sulfurreducens* in Soft Agar Tubes

7.5% (w/v) brain heart infusion agar was boiled in water. Yeast extract and cysteine were added to final concentrations of 0.1% (w/v) and 8 mM, respectively, before 3 ml of this mixture were filled into a hungate tube. Subsequently, the tubes were sealed with aluminium foil and autoclaved. Immediately afterwards, the tubes containing liquid agar were placed in a 60°C water bath. 6 ml of NBAFYE medium were added and after a short cooling time the agar was inoculated with 200 µl pre-culture. Every following tube was inoculated with 1 ml of the preceding tube. Finally, inertal gas (80% N<sub>2</sub>, 20% CO<sub>2</sub>) (Airliquide, Germany) was directed by means of a sterile filter over the agar and the tube was closed air-tight. The bacteria were incubated at 30°C.

#### 4.2.1.5 Production of *Geobacter sulfurreducens* DMSO Stocks

Buffer
1 mM HEPES/ NaOH pH 7
1 mM MgCl <sub>2</sub>
175 mM sucrose

A single colony of *Geobacter sulfurreducens* was taken out of the agar using a Pasteur pipette and then amplified in 5 ml NBAFYE medium. 500 ml NBAFYE medium were inoculated with this preculture and incubated at 30°C to an OD<sub>600</sub> = 0.5. From that point on, the cells were treated with a glas pipette and handled under anaerobic conditions. After one centrifugation step (8 minutes at 3,500 x g, 4°C), the cells were carefully resuspended in 400 ml ice-cold buffer and then spinned down again. This washing step was repeated once. Finally, the pellet was taken in 2 ml buffer + 400 µl (60% DMSO + 40% buffer) and aliquoted. The 100 µl aliquots were frozen in liquid nitrogen and stored at -80°C.

## 4.2.2 Molecular Biological Techniques

### 4.2.2.1 Polymerase Chain Reaction

PCR reaction mixture	
1 X	<i>Pfu</i> buffer
250 $\mu$ M	dNTPs
10% (v/v)	DMSO
8 mM	MgSO <sub>4</sub>
0.2 $\mu$ l	genomic DNA of <i>G. sulfurreducens</i>
0.2 $\mu$ l	<i>Pfu</i> DNA polymerase
1 $\mu$ l	5'-Primer
1 $\mu$ l	3'-Primer
	dH <sub>2</sub> O @ 50 $\mu$ l

The Polymerase chain reaction (PCR) (Mullis and Faloona, 1987; Saiki *et al.*, 1988) is an *in vitro* method for the exponential amplification of any DNA fragment. This technique enables the selective amplification of a short, exactly defined part of a DNA strain out of a complex DNA mixture.

A PCR cycler from Biometra (Göttingen, Germany) was used for DNA amplification. For the amplification of genes from genomic DNA from *Geobacter sulfurreducens*, the highly thermostable *Pfu* DNA polymerase (MBI Fermentas, St. Leon-Rot, Germany) derived from the hyperthermophilic archaeum *Pyrococcus furiosus* was used. The enzyme catalyzes the synthesis of duplex DNA in 5'→3' direction and possesses an additional 3'→5' exonuclease activity correcting nucleotide incorporation errors. In order to reduce non-specific PCR products, an established touch-down PCR protocol was used starting at a high annealing temperature that was subsequently stepwise decreased. The size of the generated PCR product was subsequently verified by means of agarose gel electrophoresis.

### 4.2.2.2 DNA Isolation from Agarose Gels & Purification of PCR Products

For the isolation of DNA fragments from agarose gels, the *QIAquick Gel Extraction* kit (Qiagen, Hilden, Germany) and the *Nucleotrap* kit (Macherey& Nagel, Düren, Germany) were used. Purification of the PCR products was carried out with the *QIAquick PCR purification* kit (Qiagen).

### 4.2.2.3 Isolation of Plasmid DNA from Bacteria

The preparation of plasmid DNA in analytical scale was performed with the *QIAprep Spin Miniprep* kit (Qiagen, Hilden, Germany) or the *Nucleo Spin* kit (Macherey& Nagel, Düren, Germany). Isolation of plasmid DNA in preparative scale

was carried out according to manufacturer's instructions for the *Plasmid Midi* kit (Qiagen).

#### 4.2.2.4 Isolation of Genomic DNA from *Geobacter sulfurreducens*

<b>CTAB/NaCl</b>
10 % (w/v) CTAB (hexadecyl-trimethyl-ammoniumbromide)
0.7 M NaCl

<b>TE-buffer</b>
10 mM Tris pH 8
1 mM EDTA

2 ml of an overnight culture of *Geobacter sulfurreducens* were sedimented by centrifugation. The pellet was resuspended in 567  $\mu$ l TE-buffer, 30  $\mu$ l 10% (w/v) SDS and 3  $\mu$ l Proteinase K (20 mg/ ml) and the mixture was incubated at 37°C for one hour. Then, 100  $\mu$ l 5 M NaCl and 80  $\mu$ l CTAB/ NaCl were added, vortexed and incubated at 65°C for 10 minutes. 700  $\mu$ l of a 24:1 mixture of chloroform/ isoamyl alcohol (Applichem, Darmstadt, Germany) were added. Again, the mixture was vortexed before it was centrifuged 5 minutes at 16,000 x g. The aqueous phase was transferred into a new cup. The chloroform/ isoamyl (24:1) alcohol extraction step (+ 500  $\mu$ l, vortex, 5 minutes at 16,000 x g, fresh cup) was repeated three times. 0.5  $\mu$ l RNase were added prior to the incubation at 37°C for 30 minutes. 500  $\mu$ l ice-cold isopropanol were added and the mixture was incubated one hour at -20°C. The precipitated DNA was pelleted for 20 minutes at 16,000 x g and 4°C. Subsequently, the pellet was washed with 70% ethanol, dried and then dissolved in 50-100  $\mu$ l 10 mM Tris pH 8.

#### 4.2.2.5 DNA Restriction Digestion

The restriction digestion was performed according to manufacturer's instructions (MBI Fermentas, St. Leon-Rot, Germany). Usually, the DNA was incubated one hour at 37°C before the enzymes were inactivated by a heat shock at 65°C for 20 minutes.

#### 4.2.2.6 DNA Ligation


The DNA ligation was carried out with the T4 DNA ligase according to manufacturer's instructions (MBI Fermentas, St. Leon-Rot, Germany). Generally, a fivefold molar excess of insert fragment compared to the vector fragment was applied and the mixture was incubated at 4°C overnight.

#### 4.2.2.7 DNA Sequencing

PCR reaction mixture	
200 ng	DNA
8 pmol	primer
1 $\mu$ l	Seq-mix BigDye <sup>®</sup> Terminator v1.1 (Applied Biosystems)
1 $\mu$ l	10 X sequencing buffer (Applied Biosystems)
	dH <sub>2</sub> O @ 10 $\mu$ l

Amplification of the DNA was carried out using a single primer and the following protocol according to the chain termination method (Sanger *et al.*, 1977):

##### Cycle

Denaturation	94°	2'		
Denaturation	94°	30''		25 x
Primer-hybridisation	50°	30''		
Elongation	60°	2'		

1  $\mu$ l 125 mM EDTA, 1  $\mu$ l 3 M sodium acetate and 50  $\mu$ l 100% ethanol were added before the reaction mixture was chilled on ice for 5 minutes. DNA was spun down by centrifugation (16,000 x g, 4°C, 15 minutes) and then washed with 70  $\mu$ l 70% ethanol. The supernatant after one further centrifugation (16,000 x g, 4°C, 5 minutes) was discarded and the DNA was dried prior to solving in 30  $\mu$ l dH<sub>2</sub>O. Analysis and documentation of the samples was kindly performed with an ABIPrism 3100 DNA Sequencer in the Department of Developmental Biochemistry (University of Göttingen).

#### 4.2.2.8 Agarose Gel Electrophoresis

TAE-buffer	Agarose gel loading buffer
40 mM Tris base	0.25% bromphenol blue
20 mM acetic acid	0.25% xylene cyanol FF
2 mM EDTA	30% glycerol

Agarose forms a matrix meshwork in which larger DNA fragments are more strongly retained than smaller ones, leading to a separation of the sample by size. For this, 1% agarose gels (1% (w/v) agarose in TAE-buffer) were used. The solid gel was placed in the electrophoresis chamber filled with TAE-buffer such that the gel was completely submerged in buffer. Samples were mixed with sample buffer and SYBR Green I (Molecular Probes, Karlsruhe, Germany) was added as fluorescence dye. For the size determination of the resulting DNA bands, a DNA molecular weight marker (MBI Fermentas, St. Leon-Rot, Germany) was used.



Electrophoresis was performed with a field intensity between 5 to 10 V/ cm. Afterwards, the documentation was carried out with the GelDoc 2000 (BioRad, München, Germany).

### 4.2.3 Protein Biochemical Methods

#### 4.2.3.1 Cell Disruption

Lysis buffer
20 mM Tris pH 8
250 mM NaCl
ALP (protease-inhibitor cocktail)

The cells were resuspended in 3 ml lysis buffer per gramm cells. The cell suspension was disrupted by five passages through a microfluidizer S100 (Microfluidics, Newton, USA) and cooled on ice in between the cycles. After centrifugation for 20 minutes at 20,000 x g and then for one hour at 100,000 x g, the supernatant was ready for purification by affinity chromatography.

#### 4.2.3.2 Affinity Chromatography

Loading Buffer	Elution Buffer	Storage Buffer
20 mM Tris pH 8	20 mM Tris pH 8	20 mM Tris pH 8
250 mM NaCl	250 mM NaCl	250 mM NaCl
	2.5 mM desthiobiotin	1 mM HABA (hydroxy-azophenyl-benzoic acid)

All purification steps were performed at 20°C with an Äkta Prime chromatography system (GE Healthcare, München, Germany).

The *Strep*-tag purification system is based on the selective binding of *Strep*-tagII fusion proteins to modified streptavidin (*Strep*-tactin) (Skerra and Schmidt, 2000). The soluble fraction was loaded with a rate of 1 ml/ min to the *Strep*-tactin column equilibrated with loading buffer. Proteins that did not bind to the sepharose were washed from the column with loading buffer. Absorbance at 280 nm was monitored and the bound protein was eluted with elution buffer as soon as the absorbance stayed constant. The eluate was collected in 2 ml fractions. Subsequently, the column was washed with 2 column volumes of elution buffer, 5 column of loading buffer and then with 5 column volumes of storage buffer.

The fractions were analyzed by SDS-PAGE (see 4.2.3.4). Cytochrome-containing fractions were pooled and concentrated by ultrafiltration (30.000 Da cut-off) (Vivaspin, Sartorius, Germany) to a volume of 1-2 ml.

### 4.2.3.3 Size Exclusion Chromatography

<b>Buffer</b>
20 mM Tris pH 8
150 mM NaCl

The separation of the proteins by size was achieved by size exclusion chromatography, whereby the protein was simultaneously rebuffed and separated from impurities and misfolded protein.

The concentrated protein was filtrated with a 0.22  $\mu\text{m}$  centrifugal filter device (Millipore, Schwalbach, Germany) and then loaded at a rate of 1 ml/ min to a pre-equilibrated Superdex 200 26/ 60 column (GE Healthcare, München, Germany). Fractions containing the pure protein were analyzed by SDS-PAGE and afterwards pooled and concentrated by ultrafiltration.

### 4.2.3.4 SDS-PAGE

<b>Resolving gel 12.5%</b>	<b>Volume</b>
30% bis-acrylamid	3.8 ml
1.88 mM Tris pH 8.8	1.8 ml
0.5% SDS	1.8 ml
TEMED	16 $\mu\text{l}$
10% APS	45 $\mu\text{l}$
ddH <sub>2</sub> O	1.6 ml

<b>Stacking gel 5%</b>	<b>Volume</b>
30% bis-acrylamid	0.5 ml
0.625 mM Tris pH 8.8	0.6 ml
0.5% SDS	0.6 ml
TEMED	6 $\mu\text{l}$
10% APS	15 $\mu\text{l}$
ddH <sub>2</sub> O	1.3 ml

<b>Coomassie Staining solution</b>	<b>Destaining solution</b>
10% ethanol 5% acetic acid 0.002% Coomassie (G250:R250 = 4:1)	10% ethanol

<b>5 X loading buffer</b>	<b>1 X running buffer</b>
0.5 M Tris/HCl pH 6.8	25 mM Tris base
40% glycerol	192 mM glycine
8% (w/v) SDS	0.1% (w/v) SDS
0.004% bromphenol blue	

Proteins were separated according to their electrophoretic properties by SDS-PAGE (Laemmli, 1970). This occurs in dependence on the length of the peptide chain or of the molecular weight as well as on protein folding state. The samples were mixed with

sample buffer and boiled for 5 minutes. By using the anionic detergent SDS in the sample buffer, proteins are denatured and obtained a net negative charge proportional to the length of the polypeptide chain, corresponding to their molecular weight. After 5 minutes of centrifugation, the samples were applied to the stacking gel pockets.

SDS gels were prepared with the Hoefer miniVE SDS gel system (GE Healthcare, München, Germany). The separation was carried out at 25 mA for one and at 50 mA for two gels, respectively. By application of an electric field, molecules are separated according to their charge and size, so that the negatively charged proteins migrate across the electric field to the anode.

Subsequently, the gels were incubated in 20 ml Coomassie staining solution for about 30 minutes. After destaining with 10% ethanol, gels were analyzed and documented with a GelDoc 2000 (Biorad, München, Germany).

#### 4.2.3.5 Heme Staining

Staining solution
1.25 mM 3,3',5,5'-tetramethylbenzidine (TMBZ)
30% methanol
250 mM sodium acetate pH 5.0

TMBZ was solved in methanol and then acetate was added. The gel was incubated in this staining solution for 30 minutes before H<sub>2</sub>O<sub>2</sub> from a fresh 30% stock solution was added to a final concentration of 52 mM (Goodhew *et al.*, 1986). The developing color reaction was observed and stopped by washing with 30% 1-propanol and 250 mM sodium acetate pH 5. Documentation of the gel was carried out immediately.

#### 4.2.4 Protein Concentration Determination

Protein concentration was determined by the bicinchoninic acid method (BCA) (Smith *et al.*, 1985).

#### 4.2.5 Spectroscopic Methods

##### 4.2.5.1 Electron Excitation Spectroscopy

Electron excitation spectroscopy uses electromagnetic waves of the ultraviolet (UV) and the visible light. The resulting electron excitation spectra are due to electronic transitions, including charge transfer (ligand-to-metal charge transfer, metal-to-ligand charge transfer and metal-to-metal charge transfer), d to d and  $\pi$  to  $\pi^*$  transitions.

Lambert-Beer's law quantifies the absorbance of radiation from the spectrum according to

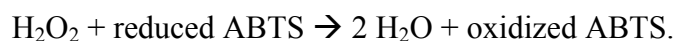
$$E = \varepsilon \cdot c \cdot d,$$

where E is the absorbance, d is the pathlength through the cuvette [cm], c is the concentration of the absorbing compound [ $\text{mol} \cdot \text{l}^{-1}$ ] and  $\varepsilon$  is the molar extinction coefficient [ $\text{l} \cdot \text{mol}^{-1} \cdot \text{cm}^{-1}$ ].

Spectra were recorded using an Ultrospec™ 2100 *pro* spectrophotometer (GE Healthcare, München, Germany).

#### 4.2.5.2 Activity Assay

The peroxidase activity was determined by the  $\text{ABTS}^{\bullet-}/\text{ABTS}^{2-}$  (2,2'-azino-bis(3-ethylbenzthiazoline-6-sulfonic acid)) system (Childs and Bardsley, 1975). ABTS was obtained from Sigma (Deisenhofen, Germany).



The colorless  $\text{ABTS}^{2-}$  anion reduces the peroxidase and becomes the oxidized radical  $\text{ABTS}^{\bullet-}$  ion due to the release of one electron. This  $\text{ABTS}^{\bullet-}$  radical is relatively stable and has an extinction coefficient of  $36 \text{ mM}^{-1} \text{ cm}^{-1}$  at 420 nm (Chen *et al.*, 2002). Reduction of hydrogen peroxide requires two electrons such that two ABTS ions transfer electrons to one  $\text{H}_2\text{O}_2$ .

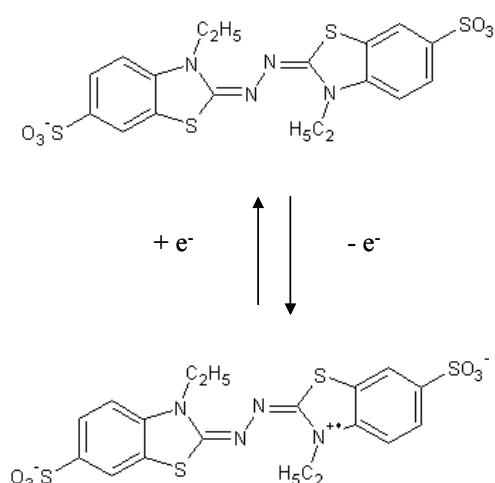


**Figure 16:** ABTS is oxidized by one electron, forming a metastable radical cation; the radical cation then slowly disproportionates into ABTS (initial state) and an azodication

The activity was assayed under anaerobic conditions. Therefore all solutions were degassed prior to the measurement in an anaerobic cuvette. The enzymes were reduced by the addition of  $10 \mu\text{M}$  sodium dithionite ( $\text{Na}_2\text{S}_2\text{O}_4$ ) to the protein solution.

Reaction mixture
10 mM potassium phosphate buffer pH 7.1
2.925 mM ABTS
x $\mu\text{M}$ $\text{H}_2\text{O}_2$
enzyme

The increase of absorbance was followed photometrically at 420 nm upon addition of enzyme or hydrogen peroxide.

The  $\text{H}_2\text{O}_2$  concentration was verified photometrically by its extinction coefficient at 240 nm ( $\epsilon_{240} = 39.4 \text{ M}^{-1}\text{cm}^{-1}$ ) (Nelson and Kiesow, 1972).

## 4.2.6 Crystallographic Methods

### 4.2.6.1 Crystallization

The aim of a crystallization experiment is the reproducible growth of ordered crystals that are used for X-ray diffraction experiments in order to determine the electron density and consequently the 3-dimensional structure of the molecule.

Proteins were crystallized by vapour diffusion using *sitting drop* Cryschem crystallization plates (Hampton Research, USA) sealed with Crystal Clear Tape. This method allows the equilibration of a drop containing a defined mixture of protein and precipitant via gas phase against the reservoir solution.

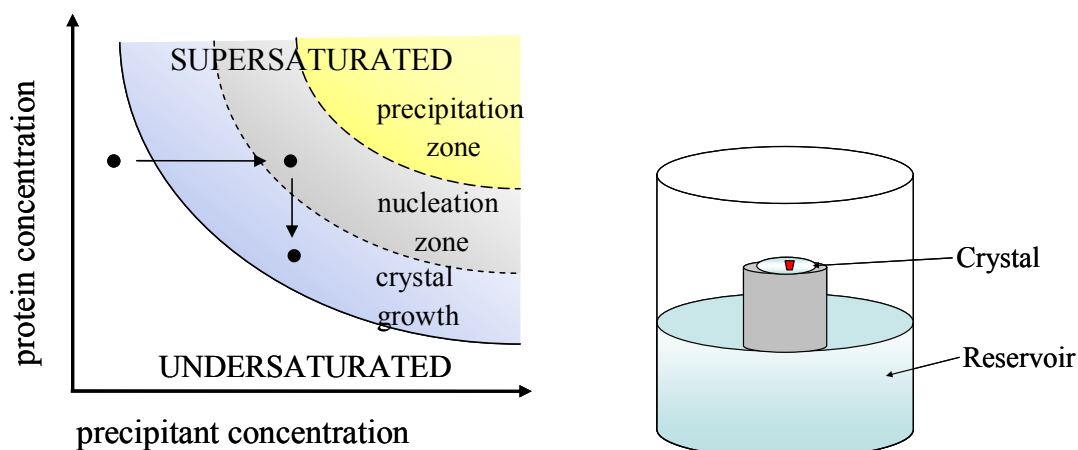


**Figure 17:** left: Phase diagram showing the solubility of a protein in solution in dependence of the precipitant concentration; right: crystallization by the *sitting drop* method

Initially the protein in the drop is in a metastable or undersaturated state concerning crystal nucleation. Drop and reservoir are connected via gas phase and the vapor pressure for the reservoir is lower which results in a net transfer of water from the protein drop to the reservoir. Through this controlled evaporation, equilibrium between reservoir and drop slowly develops. The concentrations of both protein and precipitant

are increased, and the sample increasingly supersaturates resulting in precipitation or ideally crystal nucleation and finally crystal growth.

Footprint Screens (Stura *et al.*, 1994), the Nextal Screens Classics, PACT Suite, the PEGS and MPD Suite (Qiagen, Hilden, Germany), the Hampton Screens 1-2, the Peg/Ion Screen (Hampton Research, USA) and JB Screens 1-10 (Jena Bioscience, Jena, Germany) served as initial screens. 1  $\mu$ l of a 5-7.5 mg/ml protein solution was mixed with 1  $\mu$ l of the reservoir solution for initial screening. These setups were stored at 20°C.

#### 4.2.6.2 Cryo-Cooling

Data collection of crystals at room temperature leads to radiation damage, whereas crystals at 100 K can be exposed much longer to X-rays without loss of diffraction quality.

However, freezing of the crystals facilitates the formation of ice crystals. This should be avoided as the internal order of the crystal is affected and the ice rings disturb the diffraction pattern of the protein. Therefore it is crucial to find a cryoprotectant that prevents this phenomenon and also guarantees optimal data quality. On the other hand, it is important that the protectant does not manipulate or even destroy the crystal to conserve its physical state (Garman and Owen, 2006).

#### 4.2.6.3 Data Collection

First data were collected in-house using a Rigaku copper rotating anode at a wavelength of 1.54 Å. Diffraction images were recorded on a mar345 imageplate detector (Mar Research, Norderstedt, Germany). In order to get higher resolution data, well-diffracting crystals were flash-frozen in liquid nitrogen and further data were collected at EMBL Hamburg, at the synchrotron beamlines BW7B and X13.

#### 4.2.6.4 Structure Determination

The smallest repeating unit within a crystal is called unit cell characterized by the lattice constants  $a$ ,  $b$ ,  $c$  and the three base vectors with angles  $\alpha$ ,  $\beta$ ,  $\gamma$  spanned in between. The repetition of this unit cell by translation forms the regularly ordered, 3-dimensional crystal.

X-ray beams can be described as electromagnetic waves that interact with the electrons in the crystal, producing scattering. In the case of elastic scattering, there is no energy

change with the molecule. Hence, the scattered waves have the same energy and frequency as the incident waves.

In case of destructive interference, the diffracted X-ray beams are not in phase, thus deleting one another. All diffracted waves are in phase when the diffracted X-ray beams fulfill Bragg's law and constructive interference occurs:

$$2d_{hkl}\sin\theta = n\lambda \quad (\text{Eq. 4.2.6.4a}).$$

In this process, the set of parallel lattice planes with index  $hkl$  and distance  $d_{hkl}$  produces a diffracted beam when the X-ray beams of the wavelength  $\lambda$  hit a plane in an angle of  $\theta$  and are reflected at the same angle.

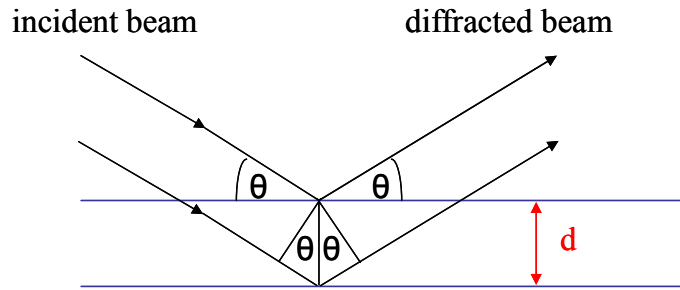
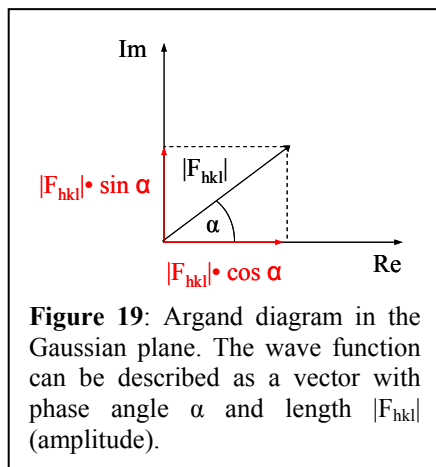


**Figure 18:** Two beams reflected by two parallel lattice planes; the difference in path length is  $2d\sin\theta$  whereas constructive interference occurs if  $2d\sin\theta$  is equal a multiple interger of the wavelength  $\lambda \rightarrow 2d_{hkl}\sin\theta = n\lambda$  (Bragg's law).

Diffracted X-rays can be characterized by the structure factors  $F_{hkl}$ :

$$F_{hkl} = \sum_j f_j e^{2\pi i(hx + ky + lz)} \quad (\text{Eq. 4.2.6.4b}).$$

The summation considers all scattering factors  $f_j$  within the cell and therefore  $F_{hkl}$  is a



function of all atom positions in the unit cell.

As  $F_{hkl}$  is a vector with an orientation given by the phase angle  $\alpha_{hkl}$  and a length given by the amplitude  $|F_{hkl}|$ , the structure factor can be represented as product (see figure 19):

$$F_{hkl} = |F_{hkl}| e^{i\alpha_{hkl}} \quad (\text{Eq. 4.2.6.4c}).$$

The structure factor describes a diffracted beam producing a diffraction spot on the detector. As the phenomenon of X-ray diffraction occurs at the

electron shell, the atomic scattering factor depends on the electron density distribution and the structure factor can be presented in the following way:

$$F_{hkl} = \int_V \rho(x, y, z) e^{2\pi i(hx + ky + lz)} dV \quad (\text{Eq. 4.2.6.4d})$$

where  $V$  is the volume of the unit cell.

By means of an X-ray diffraction experiment, the 3-dimensional electron density function  $\rho(x, y, z)$  of the crystal ought to be determined. However, only the intensities of the spots proportional to the square of the amplitudes of the structure factors can be measured:

$$I_{hkl} \sim |F_{hkl}|^2 \quad (\text{Eq. 4.2.6.4e}).$$

The phase information is lost during the diffraction experiment and can only be determined indirectly. This dilemma is referred to as the “phase problem” in crystallography, as the electron density can only be calculated by fourier transform with informations about both amplitude and phase:

$$\rho(x, y, z) = \frac{1}{V} \sum_{hkl} F_{hkl} e^{-2\pi i(hx + ky + lz)} \quad (\text{Eq. 4.2.6.4f}).$$

#### 4.2.6.5 Phase Determination

For macromolecules, phase information can be obtained by following methods:

- Molecular replacement (MR)
- Isomorphous replacement (MIR/SIR)
- Anomalous dispersion (MAD: multiple wavelength anomalous dispersion /SAD)
- Combination of isomorphous replacement and anomalous dispersion (MIRAS: multiple isomorphous replacement /SIRAS)

##### 4.2.6.5.1 Molecular Replacement

The method of molecular replacement is one of the principal techniques to determine the structure of macromolecules (Rossmann and Blow, 1962). A homologous model structure is used to obtain an atomic model from which estimates of the phases can be computed. Those serve as initial phases for the unknown structure.

The method is based on the fact that proteins sharing homologies in their sequence have a similar structure. Consequently, the level of sequence identity between phasing model and target structure and also the completeness of the model play an important role for the success of this method. As a rule of thumb, the amino acid sequences should be at least by 40% identical.

Several programs for molecular replacement exist, including *MOLREP* (Vagin and Teplyakov, 1997), *PHASER* (Storni *et al.*, 2004), *CNS* (Brünger *et al.*, 1998), *AMoRe* (Navaza, 1994) and *EPMR* (Kissinger *et al.*, 1999).



Usually, the process of locating the phasing model in the unit cell is divided into two independent steps. First, the right orientation of the model is determined by a rotation search using a rotation function. Afterwards, the right position of the model is found by a translational search using a translation function. Within the molecular replacement six variables need to be determined, three parameters to specify orientation and three parameters to specify position. The resulting structure factors of the positioned phasing model are then used as an initial estimate of the searched phases.

The rotation function determines the best orientation of the search model. This exploits the fact that intramolecular vectors (Patterson vectors) depend only on the orientation of the molecule and not on the position in the unit cell. If the search model and the target protein are oriented in the same way within the unit cell, Patterson-maps should look similar. This concurrence of Patterson peaks is examined by the determination of the rotation function maxima calculated by the computer programs.

Subsequently, comparisons of the structure factors are employed to locate the best position of the model protein via translational search. For each trial position the observed structure factor amplitudes  $|F_{obs}|$  of the native data set are calculated and compared to the structure factor amplitudes  $|F_{calc}|$ . The R-factor compares both sets of structure factor amplitudes for every reflection:

$$R = \frac{\sum ||F_{obs}| - |F_{calc}||}{\sum |F_{obs}|} \quad (\text{Eq. 4.2.6.5.1}).$$

In the case of consistent structure factor amplitudes a small difference and thus a low R-factor are expected.

#### 4.2.6.5.2 MAD

Absorption edges for heavy atoms are in the range of X-ray wavelengths used in an X-ray diffraction experiment. If the wavelength of the incident photons is in the range of the specific absorption edge and hence the photons have high enough energy, X-ray photons are absorbed by the heavy atoms and re-emitted with an altered phase producing anomalous scattering (Hendrickson *et al.*, 1988).

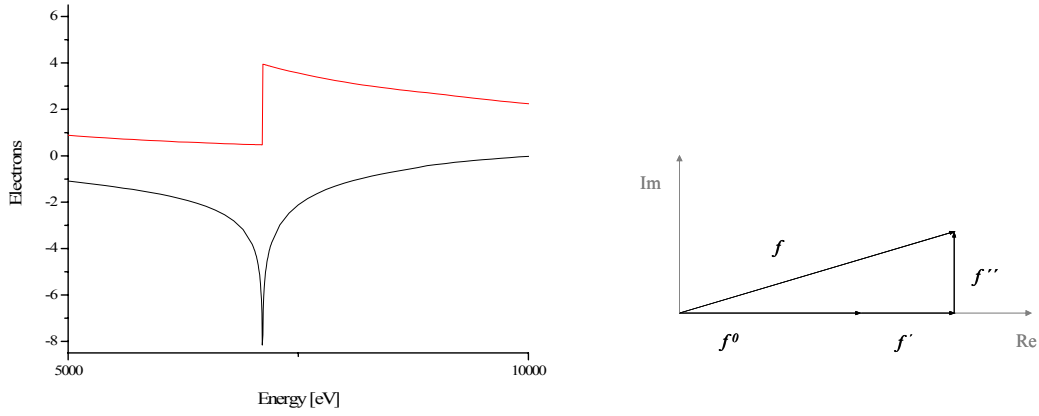


**Figure 20:** left: Theoretical absorption edge of iron (7112 eV) and values for  $f'$  (black line) and  $f''$  (red line) (<http://www.bmsc.washington.edu/scatterer>). Right: The anomalous contribution to the atomic scattering factor consists of the real part  $f'$  and the imaginary part  $f''$ .

The scattering of an atom for which anomalous scattering occurs is wavelength-dependent and can be written as

$$f(\lambda) = f^0 + f'(\lambda) + i f''(\lambda) \quad (\text{Eq. 4.2.6.5.2a}).$$

In this case,  $f^0$  is the normal scattering contribution,  $f'$  is the real scattering component and  $f''$  is the anomalous signal.  $f''$  can be obtained from a fluorescence scan, while  $f'$  can be calculated from  $f''$  as the scattering components  $f'$  and  $f''$  are related via the Kramers-Kronig relationship:

$$f'(\omega) = \frac{2}{\pi} \int_0^{\infty} \frac{\omega' f''(\omega') \partial \omega'}{\omega^2 - \omega'^2} \quad (\text{Eq. 4.2.6.5.2b}).$$

Friedel's law states that the reflection ( $hkl$ ) and the - by inversion through the origin - related reflection ( $-\bar{h}, -\bar{k}, -\bar{l}$ ) have equal amplitude and opposite phase. Whenever there is anomalous dispersion, Friedel's law is broken

$$(|F_{hkl}| \neq |F_{\bar{h}\bar{k}\bar{l}}|) \quad (\text{Eq. 4.2.6.5.2c}).$$

From this discrepancy, phase information can be obtained. By Patterson methods, the location of heavy atoms can be determined at first.

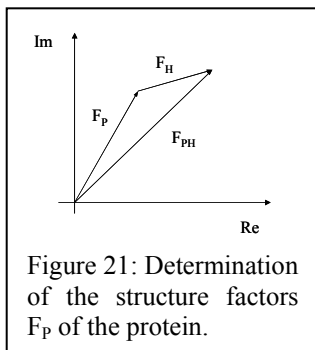
The Patterson function in its general form is a variation of the Fourier sum for which only the amplitude is required:

$$P(u, v, w) = \frac{1}{V} \sum_{hkl} |F(hkl)|^2 \cos[2\pi(hu + kv + lw)] \quad (\text{Eq. 4.2.6.5.2d}).$$

The difference Patterson map is calculated with coefficients  $(\Delta F)^2 = (|F_P| - |F_{PH}|)^2$  showing interatomic vectors with amplitudes contributed by the heavy atoms solely.

$$\Delta P(u, v, w) = \frac{1}{V} \sum_{hkl} |\Delta F(hkl)|^2 \cos[2\pi(hu + kv + lw)] \quad (\text{Eq. 2.2.6.5.2e}).$$

A MAD experiment comprises several datasets around the absorption edge of the heavy atom. In case of metalloproteins, datasets are recorded at the edge of the incorporated metal. A peak dataset at the maximum of  $f''(\lambda)$  is collected as well as the inflection dataset (minimum of  $f''(\lambda)$ ) and the high remote dataset (medium values for  $f''(\lambda)$  and  $f'(\lambda)$ ).



Once the positions of the heavy atoms are found, structure factors of the protein can be determined. For this, the structure factor can be written as  $F_P = F_{PH} - F_H$  where  $F_P$  is the structure factor of the remote dataset,  $F_{PH}$  is the structure factor of the peak dataset and  $F_H$  is the structure factor of the heavy atom.

#### 4.2.6.5.3 Isomorphous Replacement

Isomorphous replacement is a method for the determination of initial phases for a new structure (Green *et al.*, 1954). Phases are derived from several data sets collected from native crystals and isomorphous crystals into which heavy atoms have been soaked that must not disturb crystal packing or the conformation of the protein. These heavy atoms cause perturbations in the diffraction pattern resulting in differences between native and derivative structure factors.

#### 4.2.6.6 Graphical Representation

Molecular graphics were made with *PyMOL* (DeLano Scientific LLC, San Francisco, USA) (DeLano, 2002). The final model was validated with the program *PROCHECK* (Laskowski *et al.*, 1993). Surface was calculated with the program *AREAIMOL* (Lee and Richards, 1971) included in the CCP4 suite. Electrostatic surface potentials were calculated with *DELPHI* (Honig and Nicholls, 1995) based on the numerical solution of the Poisson-Boltzmann equation, assuming standard charges for amino acids.

## 5 Results

### 5.1 Purification of the Recombinant Peroxidases from *G. sulfurreducens*

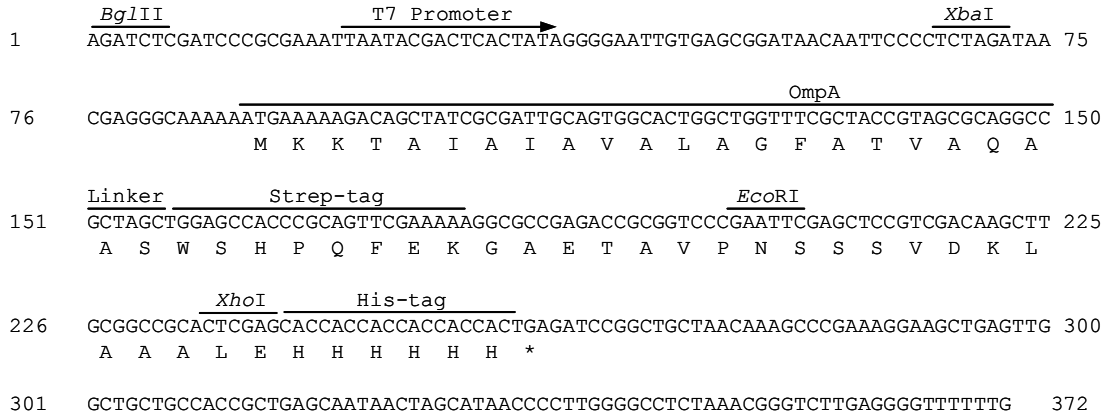


**Figure 22:** Organization of the pETSN-22 expression vector insert region. The OmpA signal sequence is cleaved off after secretion of the apoprotein into the periplasm.

The *Geobacter sulfurreducens* cytochrome *c* peroxidases MacA and CcpA were overproduced in *E. coli* strain BL21(DE3) by coexpressing the pEC86 plasmid encoding the *c*-type cytochrome maturation genes *ccmABCDEFGH* (see figure 14) (Thöny-Meyer, 1997). The expression vector pETSN-22 was created for this purpose and provides an N-terminal signal sequence for the secretion of the protein into the periplasm, an N-terminal *Strep*-tagII and a C-terminal His-tag. The *macA* gene (978 bp) and the *ccpA* gene (975 bp) were cloned via the *EcoRI* and *XhoI* restriction sites into pETSN-22. In order to obtain a construct without His-tag, the stop codon of the genes was retained.

Protein expression could be optimized by reducing the expression rate of the apoprotein. The leakiness of the promoter was exploited, thus without addition of IPTG the basal transcription level was sufficient for the production of holoprotein.

The original expression vector pASK-IBA44 with its *tet* promoter was unsuitable because this construct just produced apoprotein. This might be due to the fact that a relatively high rate of protein expression can be harmful for correct posttranslational processing (Londer *et al.*, 2005).

### 5.1.1 Purification of CcpA

The cells were cultivated and broken as described previously (see 4.2.1.1 and 4.2.3.1). After centrifugation, the soluble fraction was loaded onto a *Strep*-tactin column (4.2.3.2). The fractions containing CcpA were pooled and concentrated by ultrafiltration (30,000 Da molecular weight cut-off; Vivaspin) (Sartorius, Göttingen, Germany). Furthermore, the protein was purified and rebuffered by size exclusion chromatography (Superdex 200) (GE Healthcare, München, Germany). Protein of the right size could be separated from misfolded protein which elutes in the exclusion volume making the size exclusion chromatography an essential step in spite of the observed electrophoretic homogeneity after the affinity step.

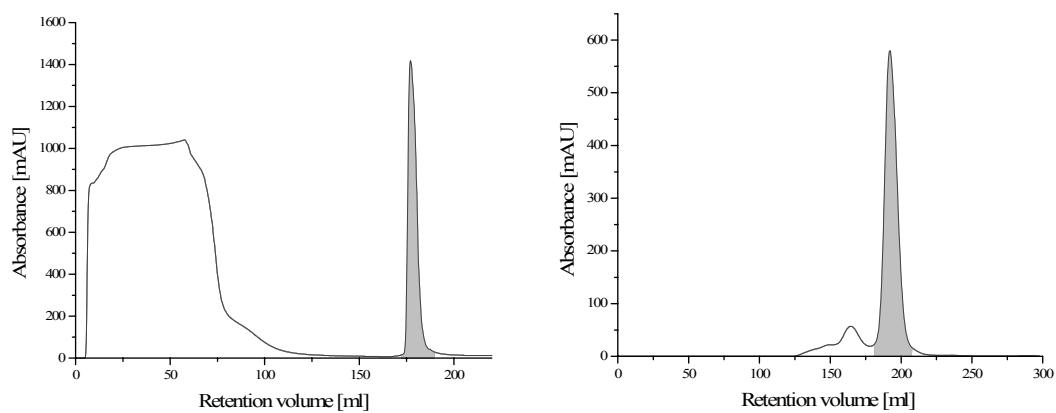


**Figure 23:** left: Chromatogram of the *Strep*-tactin column; right: Chromatogram of the S200 gel filtration column; the pooled fractions are indicated in grey.

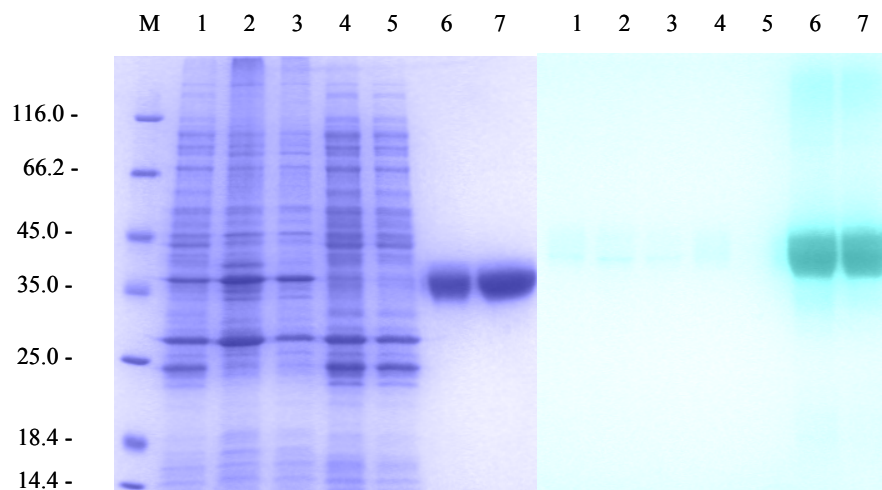


**Figure 24:** left: Coomassie-stained gel, right: Heme-stained gel; M: marker with corresponding molecular weight in kDa, 1: cell extract, 2: 20,000 x g pellet, 3: 100,000 x g pellet, 4: 100,000 x g supernatant, 5: flowthrough *Strep*-tactin column, 6: pool after *Strep*-tactin column, 7: pool after gel filtration; 15  $\mu$ g protein per lane were applied.

Molecular weight prediction with the ExPaSy webservice (<http://www.expasy.org>) (Bjellqvist *et al.*, 1993) results in 36.78 kDa per monomer if linker and *Strep*-tag are

taken into account. The addition of 616 Da per heme group leads to a calculated molecular weight of 38.02 kDa and subsequently of 76.04 kDa per dimer. CcpA elutes at 191.97 ml from the S200 column which corresponds to a molecular weight of 73.94 kDa according to the calibration curve  $y = -0.0155x + 7.8445$ . Furthermore, a pI of 8.7 was calculated by *Compute pI* from the ExPaSy webservice.

### 5.1.2 Purification of MacA

The purification of MacA was performed in analogy to the procedure for CcpA.

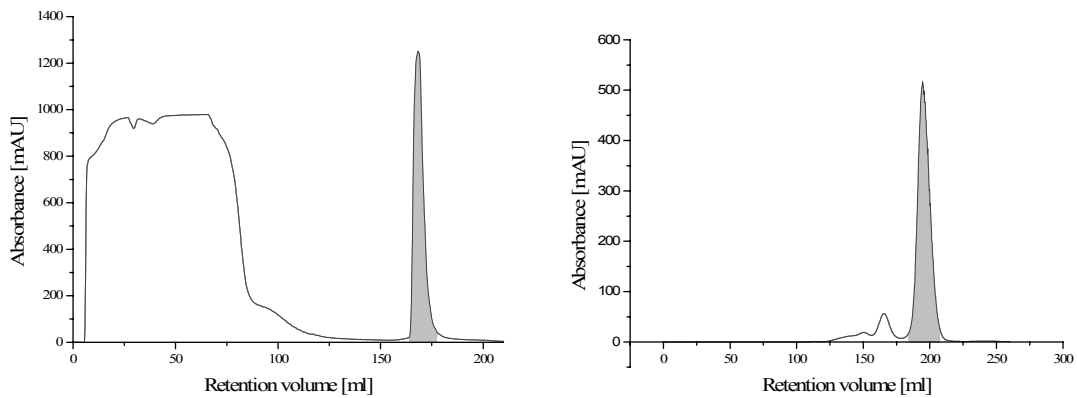


**Figure 25:** left: Chromatogram of the *Strep*-tactin column; right: Chromatogram of the gel filtration column S200; the pooled fractions are indicated in grey.

According to the ExPaSy-webservice, MacA has a molecular weight of 37.06 kDa and of 38.29 kDa including the two heme groups. Thus, the theoretical molecular weight of the dimer is 76.58 kDa while MacA elutes at 194.55 ml corresponding to a molecular weight of 67.45 kDa. A theoretical pI of 8.9 was calculated.

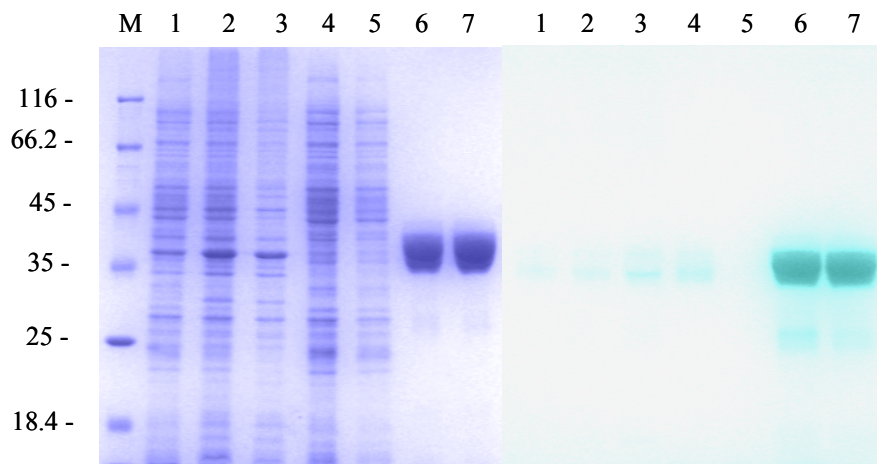


**Figure 26:** left: Coomassie-stained gel, right: Heme-stained gel; M: marker with corresponding molecular weight in kDa, 1: cell extract, 2: 20,000 x g pellet, 3: 100,000 x g pellet, 4: 100,000 x g supernatant, 5: flowthrough *Strep*-tactin column, 6: pool after *Strep*-tactin column, 7: pool after gel filtration; 12  $\mu$ g protein per lane were applied.

### 5.1.3 Representative Purification of CcpA and MacA

MacA and CcpA were purified from 5 l expression cultures that had been harvested at OD<sub>600</sub> of 5-6.

Purification step	MacA			CcpA		
	Protein [mg]	A <sub>405</sub> /A <sub>280</sub>	specific activity [ $\mu\text{mol min}^{-1} \text{mg}^{-1}$ ]	Protein [mg]	A <sub>405</sub> /A <sub>280</sub>	specific activity [ $\mu\text{mol min}^{-1} \text{mg}^{-1}$ ]
Soluble fraction	1008	0.05	0.027	935	0.06	0.013
<i>Strep</i> -tactin	30	4.10	0.954	48	2.16	0.836
Superdex 200	17.5	4.21	2.066	26.6	3.86	2.005

CcpA was purified from 20 g cells yielding 1.33 mg g<sup>-1</sup> cells. The yield of MacA was lower with 0.92 mg g<sup>-1</sup> cells.

## 5.2 Electron Excitation Spectra

The oxidized form of CcpA shows a typical *c*-type cytochrome spectrum with absorption maxima at 406.5 nm and at 530 nm. The extinction coefficient at 406.5 nm was determined to  $\epsilon_{406.5 \text{ nm}} = 231,000 \text{ M}^{-1} \text{ cm}^{-1}$ . Upon reduction with 1 mM ascorbate, one heme is reduced and the Soret band shifts to 411 nm while  $\alpha$ - and  $\beta$ -bands become apparent. Additional incubation with CaCl<sub>2</sub> shifts the  $\gamma$ -band to 417 nm, a shoulder at lower wavelength remains corresponding to the second non-reduced heme group. An additional band at 630 nm is slightly more pronounced upon addition of calcium and indicates a Fe(III) high spin signal.

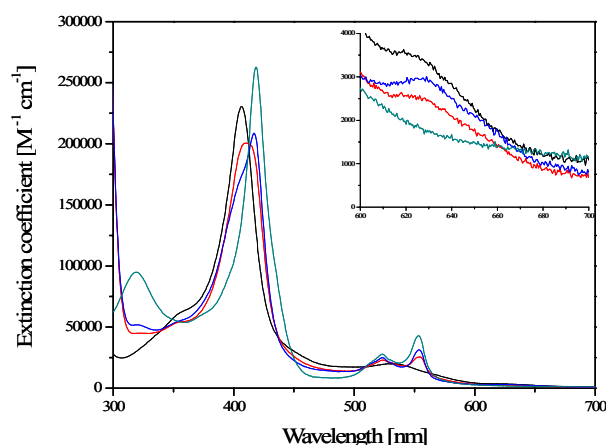


**Figure 27:** Electron excitation spectra of CcpA in 20 mM Tris pH 8, 150 mM NaCl buffer; native enzyme (oxidized, black line), ascorbate-reduced enzyme (1 mM ascorbate, pH 7.2; 15 minutes incubation, red line), addition of 1 mM CaCl<sub>2</sub> to the ascorbate-reduced enzyme (blue line), dithionite-reduced enzyme (green line).

In the dithionite-reduced form of CcpA, the Soret band has its absorption maximum at 418.5 nm; the  $\beta$ -band is visible at 523 nm and the  $\alpha$ -band at 553.5 nm.

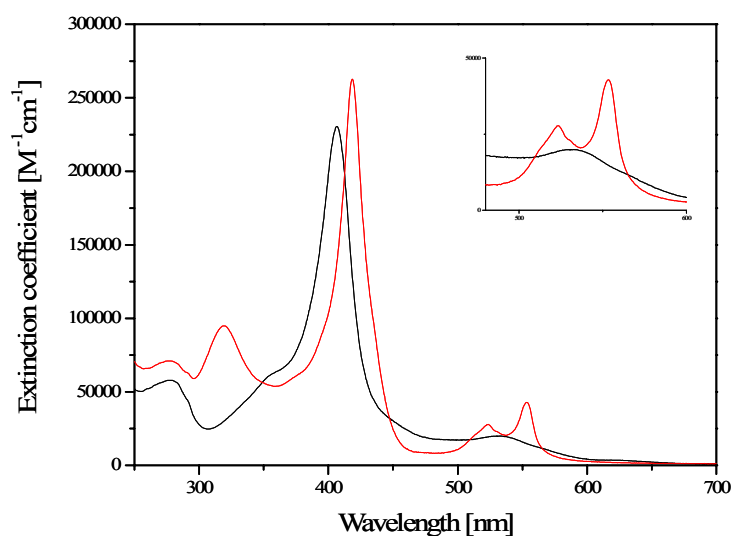


**Figure 28:** Electron excitation spectra showing the oxidized (black) and reduced (red) form of CcpA in 20 mM Tris pH 8, 150 mM NaCl buffer.

The oxidized form of MacA also reveals a typical spectrum of a *c*-type cytochrome with absorption maxima at 406.5 nm and at 525 nm.

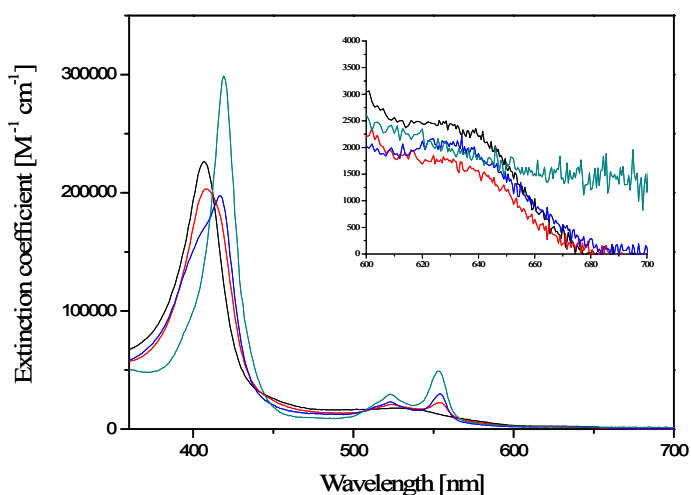


**Figure 29:** Electron excitation spectra of MacA in 20 mM Tris pH 8, 150 mM NaCl buffer; native enzyme (oxidized, black line), ascorbate-reduced enzyme (1 mM ascorbate, pH 7.2; 15 minutes incubation, red line), addition of 1 mM  $\text{CaCl}_2$  to the ascorbate-reduced enzyme (blue line) and dithionite-reduced enzyme (green line).

The extinction coefficient at 406.5 nm was determined to  $226,000 \text{ M}^{-1} \text{ cm}^{-1}$ . Upon reduction with ascorbate and additional incubation with  $\text{CaCl}_2$  spectroscopic features



are generated resembling those of CcpA. The fully-reduced spectrum of MacA exhibits absorption maxima at 419 nm, 523 nm and 553 nm.

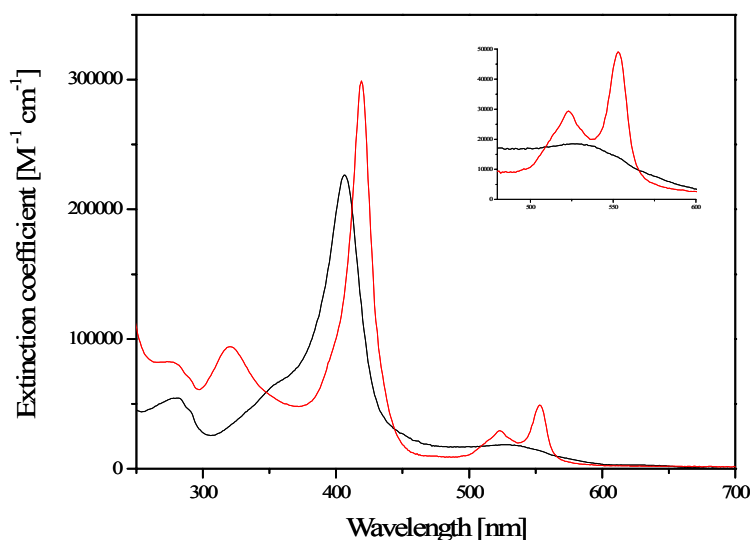


**Figure 30:** Electron excitation spectra of MacA in 20 mM Tris pH 8, 150 mM NaCl buffer; oxidized (black) and reduced (red) form.

### 5.3 Peroxidase Activity Assay

Both diheme *c*-type cytochromes from *Geobacter sulfurreducens* revealed peroxidase activity as determined by the ABTS method (see 4.2.5.2). Usually, the physiological electron donor of cytochrome *c* peroxidases, ferrocycytochrome  $c_{550}$ , serves as electron donor in the activity assay (Gilmour *et al.*, 1994). Initially, an analogous assay containing bovine heart cytochrome *c* as electron donor was performed as *Geobacter sulfurreducens* lacks any homologs of cytochrome *c* (Butler *et al.*, 2004). Just like the cytochrome *c* peroxidase of *Pseudomonas nautica* (Alves *et al.*, 1999), MacA did not show any significant activity using bovine heart ferrocycytochrome *c* as electron donor. Hence, ABTS was used to detect peroxidase activity.

Oxidized MacA revealed a specific activity of  $0.064 \mu\text{mol min}^{-1} \mu\text{g}^{-1}$  at a concentration of  $18 \mu\text{M H}_2\text{O}_2$ . As cytochrome *c* peroxidases are active in the mixed valence state, the enzyme was incubated with ascorbate, ascorbate and calcium or dithionite prior to the assay (see 5.2 and 4.2.5.2). Only the reduction of the enzyme with dithionite had an effect on the activity so that following activities were determined for the reduced enzyme.

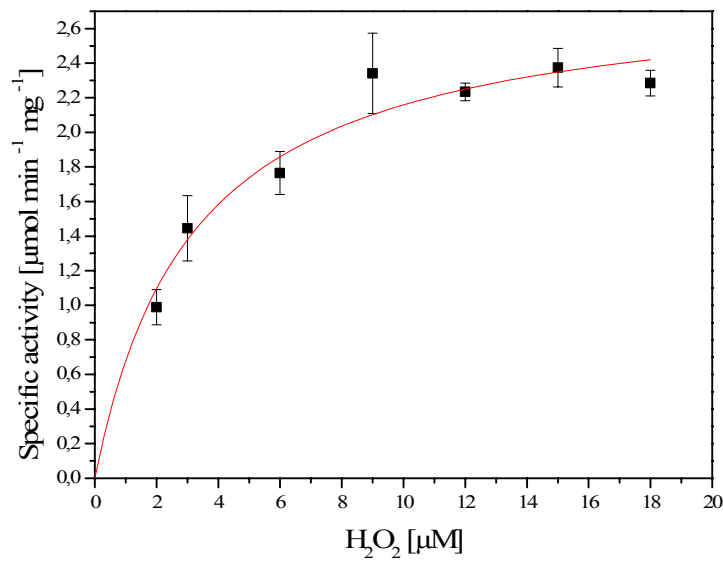


**Figure 31:** Effect of the hydrogen peroxide concentration on the specific activity of MacA. The reaction was started upon addition of MacA ( $c = 391$  nM). Each value represents an average of three measurements. The curve was fitted by the Hill-function  $y = \frac{v_{\max} \cdot x^n}{k^n + x^n}$  with  $n = 1$ .

The curve obtained for the specific activity in dependence on H<sub>2</sub>O<sub>2</sub> obeys Michaelis-Menten kinetics. Based on the fitting by the Hill-function and Hill coefficient  $n = 1$ ,  $v_{\max} = 2.85 \pm 0.18 \mu\text{mol min}^{-1} \text{mg}^{-1}$  and  $K_M = 3.20 \pm 0.70 \mu\text{M H}_2\text{O}_2$  were obtained for MacA.

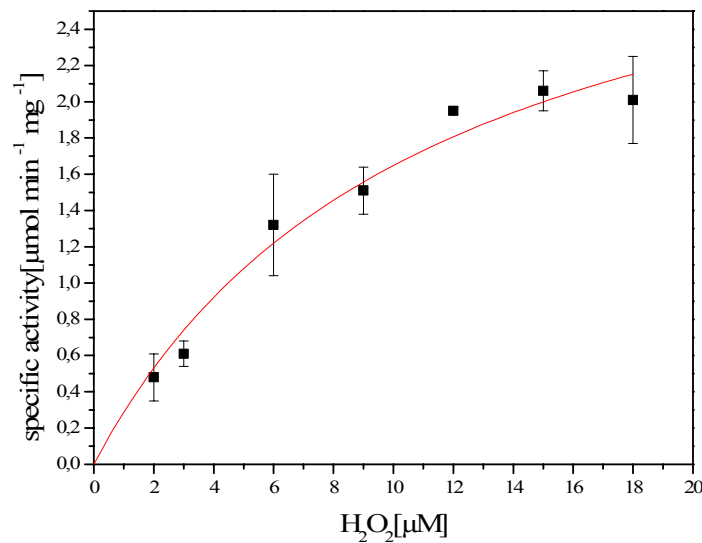


**Figure 32:** Effect of the hydrogen peroxide concentration on the specific activity of CcpA. The reaction was started upon addition of H<sub>2</sub>O<sub>2</sub> ( $c = 900$  nM). Each value represents an average of three measurements. The curve was fitted by the Hill-function.

The peroxidase activity of CcpA is in a similar range as the activity of MacA. The values for  $v_{\max} = 3.48 \pm 0.47 \mu\text{mol min}^{-1} \text{mg}^{-1}$  and  $K_M = 11.14 \pm 3.06 \mu\text{M H}_2\text{O}_2$  are obtained from the fitted curve. In the range of low  $\text{H}_2\text{O}_2$  concentration, the activity is lower than the activity of MacA resulting in  $v_{\max}$  and  $K_M$  values that were presumably overestimated. Especially, the  $K_M$  value is expected to be much lower. Therefore, these values have to be regarded as approximate because hydrogen peroxide concentrations above  $18 \mu\text{M}$  do not increase the specific activity.

## 5.4 Sequence Analysis

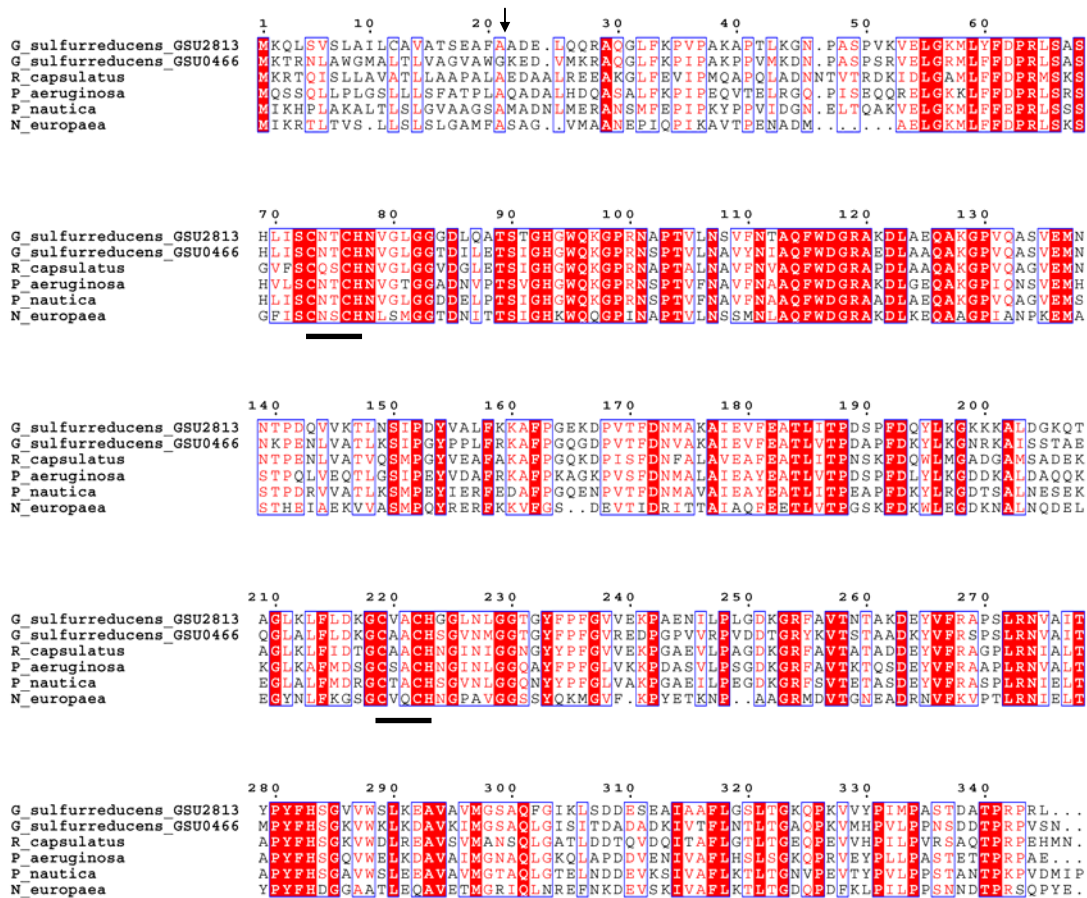


**Figure 33:** Multiple sequence alignment of CcpA (GSU2813), MacA (GSU0466) and related cytochrome *c* peroxidases from *Rhodobacter capsulatus*, *Pseudomonas aeruginosa*, *Pseudomonas nautica* and *Nitrosomonas europaea*. Identical sequences are colored in red and areas of homology are indicated by red letters. The predicted signal sequence cleavage sites of CcpA and MacA were obtained from the SignalP server and are indicated with an arrow. Heme-binding motifs are highlighted with bars. The sequence alignment was generated by ClustalW (Thompson *et al.*, 1994).

BLAST searches (BLASTP 2.2.15) (Altschul *et al.*, 1997) were performed in order to identify other bacterial diheme cytochrome *c* peroxidases in sequence databases. Both *Geobacter sulfurreducens* enzymes are 68% identical with respect to the mature protein. The sequence identity between the peroxidase from *P. aeruginosa* and CcpA and MacA

are 66% and 58%, respectively. Apart from the homologs listed below, cytochrome *c* peroxidases from many other organisms were found in the BLAST (e.g. from *Geobacter metallireducens*, *Geobacter uraniumreducens* and *Rhodospirillum rubrum*).

## 5.5 Crystallization and Structure Determination

### 5.5.1 Crystallization of CcpA and Data Collection

In many PEG (polyethylene glycol) containing conditions, crystals were visible already after one day. But in most of these conditions extremely thin needles grew from one single center of nucleation (figure 34A).

Only in some conditions 2- or even 3-dimensional crystals appeared. In the condition containing 15% PEG 3350, 0.1 M sodium citrate pH 5.4 and 20% 2-propanol, the third dimension was developed better compared to all the other crystallization conditions. However, a diffraction test showed that crystals were disordered in one direction and therefore were not suitable for diffraction data collection.

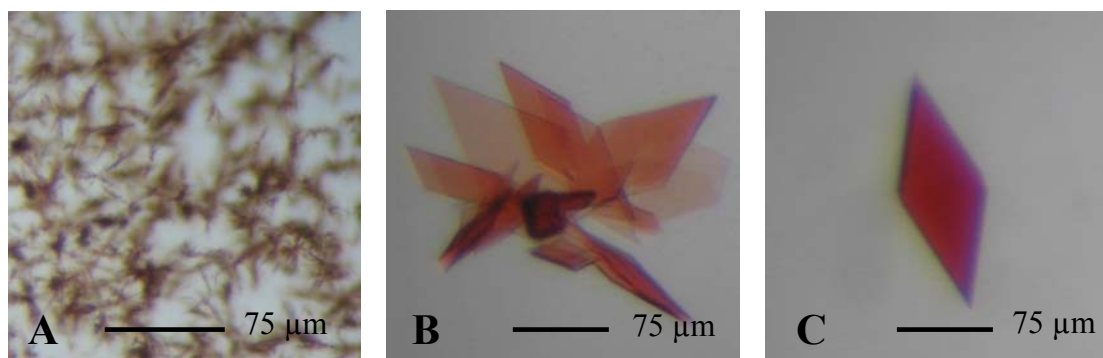


**Figure 34:** (A) Needle clusters of CcpA appearing in many different PEG containing conditions. (B + C) CcpA crystals obtained from the condition containing 15% PEG 3350, 0.1 M sodium citrate pH 5.4 and 20% 2-propanol.

Starting from the condition 41 of the Nextal Screen *The PEGS* (0.1 M HEPES pH 7.5 and 20 % PEG 10,000), crystals were reproduced and improved.

Several techniques were employed to reduce the number of nucleation centers, the speed of crystal growth and to improve the thin 3<sup>rd</sup> dimension of the crystals. The application of the Additive Screen (Hampton Research, USA) as well as the reduction of the temperature to 4°C and seeding techniques were involved herein. But for all conditions the huge number of nucleation centers is common even if the sample was filtered directly before pipetting into crystallization plates.

Variation of PEGs, pH and buffer finally lead to the crystallization condition 16% PEG 10,000 and 0.1 M HEPES pH 7.4. Crystals were thin plates that were grown together and tended to break easily.

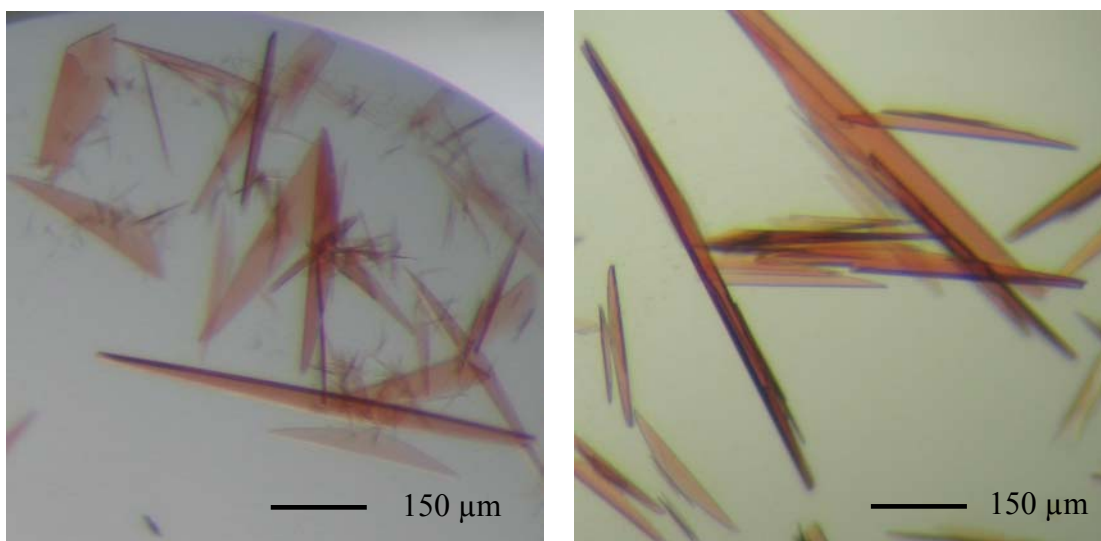


**Figure 35:** Final crystals used for structure determination of CcpA.

The crystals were soaked in a protective cryo solution containing 10% 2R,3R-butanediol in the reservoir solution, mounted in nylon loops and flash-frozen in liquid nitrogen.

At the in-house X-ray source, the crystals diffracted to 2.6 Å. In order to reach higher resolution, 300 diffraction images were collected at the EMBL beamline BW7B (DESY, Hamburg) where the crystals diffracted to 1.89 Å.

Data were indexed and integrated with the program *DENZO* (Otwinowski and Minor, 1997), scaling was performed with the program *SCALEPACK*.

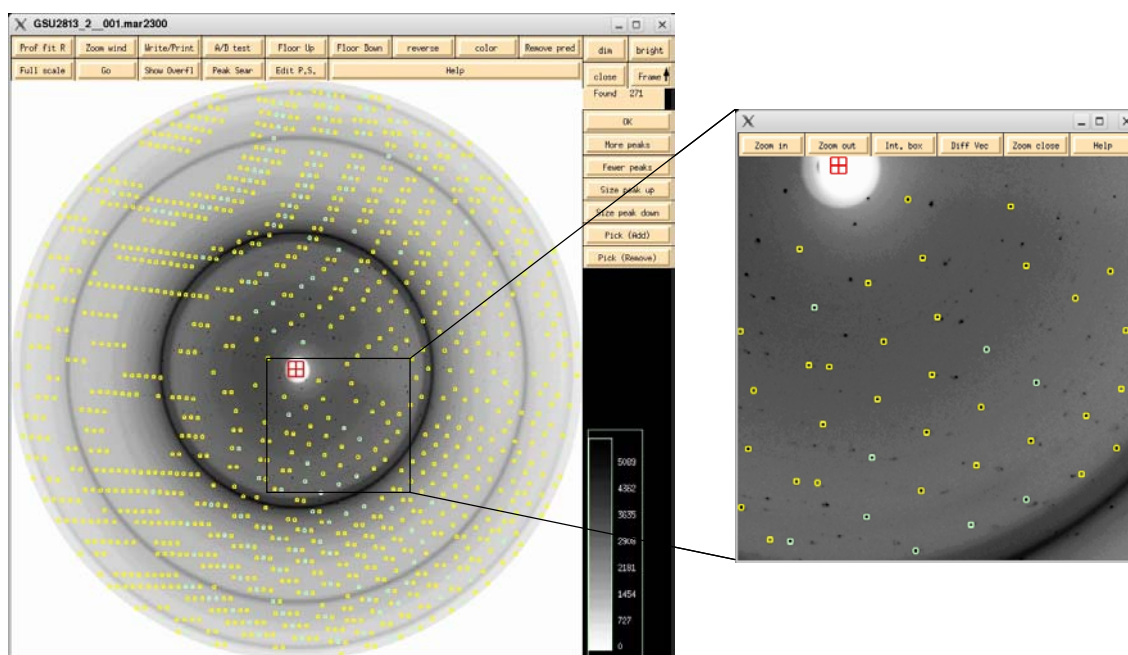


**Figure 36:** Diffraction image used for indexing. The image was recorded at the EMBL beamline BW7B while the crystal was rotated 1° per image during exposure. Data were collected at a wavelength of 0.8423 Å.

The crystals of CcpA belonged to the triclinic space group P1 with unit cell parameters  $a = 54.2 \text{ \AA}$ ,  $b = 55.8 \text{ \AA}$ ,  $c = 78.6 \text{ \AA}$ ,  $\alpha = 68.7^\circ$ ,  $\beta = 71.8^\circ$ ,  $\gamma = 57.8^\circ$  and an estimated mosaicity of 0.6. As crystals were grown together in most cases, it was always a problem of indexing the datasets properly. Several lattices were present (see figure 36) and visible on the diffraction image so that in many cases indexing failed. Even although there were icerings, this dataset was most suitable for structure determination of CcpA as the dataset could be indexed.

Resolution ( $\text{\AA}$ )	50.00 - 2.00 (2.03 – 2.00)
Redundancy	3.0 (2.9)
Number of observations	361320
Number of unique reflections	48703
Completeness (%)	95.2 (97.1)
I/ sigma	9.6 (2.2)
$R_{\text{sym}}$	0.099 (0.421)

**Table 1:** Data collection statistics for CcpA. Numbers in parentheses refer to the values within the highest resolution shell.  $R_{\text{sym}} = (\sum |I - \langle I \rangle| / \sum I)$

There are two monomers in the asymmetric unit and the solvent content of the crystal is 48.70% with a Matthews coefficient (Matthews, 1968) of  $V_M = 2.42 \text{ \AA}^3 / \text{Da}$ . Due to deteriorating data quality, only data up to a resolution of  $2 \text{ \AA}$  were used for refinement.

### 5.5.2 Structure Determination of CcpA and Refinement

The structure was solved by molecular replacement using the program *MOLREP* (Vagin and Teplyakov, 1997) from the CCP4 suite (Collaborative Computational Project Number 4, 1994) with data to a resolution of  $3.5 \text{ \AA}$ . Cytochrome *c* peroxidase of *Pseudomonas aeruginosa* (pdb accession code 1EB7) (Fülöp *et al.*, 1995) sharing 66% sequence identity with CcpA served as search model. A preliminary model was obtained with data collected in-house. Different residues were mutated using the mutation function in *COOT* (Emsley and Cowtan, 2004). This model was subsequently used as search model for molecular replacement using synchrotron data.

Resolution (Å)	72.357-2.0
r.m.s.d. in bond length (Å)	1.690
r.m.s.d. in bond angles (°)	0.014
R <sub>work</sub> (%) / R <sub>free</sub> (%)	21.4 / 27.0
Figure of merit	0.718
Average B-factor for the protein (Å <sup>2</sup> )	chain A: 24.45, chain B: 21.99
Average B-factor for waters (Å <sup>2</sup> )	25.13

**Table 2:** Data statistics from the refinement using the synchrotron data set.  $R_{\text{work}} = \sum ||F_{\text{obs}}| - |F_{\text{calc}}|| / \sum |F_{\text{obs}}|$ , where  $|F_{\text{obs}}|$  and  $|F_{\text{calc}}|$  are structure factor amplitudes from the data and the model, respectively. In order to monitor  $R_{\text{free}}$  (Brünger, 1992), 5.1% of the reflections were excluded from the refinement. The figure of merit for a reflection (hkl) is  $m = |F(\text{hkl})_{\text{best}}| / |F(\text{hkl})|$  where  $F(\text{hkl})_{\text{best}} = \sum P(\alpha) F_{\text{hkl}}(\alpha) / \sum P(\alpha)$ .

Further model building was performed with the graphics program *COOT*. In order to get a consistent model of the protein structure, the model was refined against experimental amplitudes and phases after every round of model rebuilding. After rebuilding and 10 refinement cycles in Refmac5 (Murshudov *et al.*, 1997) water molecules were added automatically by *COOT* and subsequently manually by checking the electron density peaks and taking the possibility of hydrogen bond formation into account.

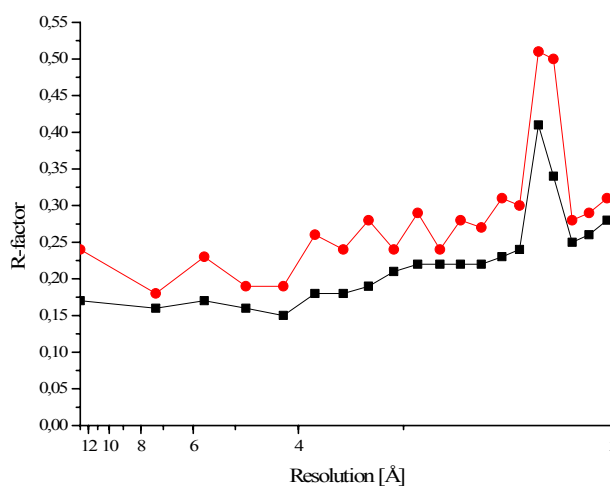


**Figure 37:** R-factor versus resolution. The ice ring around 2.24 Å influences R<sub>work</sub> (black) and R<sub>free</sub> (red).

Despite the ice ring and the resulting bad statistics in the resolution shell between 2.25-2.31 Å, data could be used to 2 Å. The final model of CcpA after the last refinement with Refmac5 had R-factors of R<sub>work</sub> = 21.4% and R<sub>free</sub> = 27.0%, containing

637 residues and 4 heme groups in two monomers, as well as 481 waters. At the amino-terminal end, an alanine belonging to the linker between protein and *Strep*-tag was defined in the electron density. In molecule A, all residues were modeled, but in molecule B residues 220-230 are missing. This flexible loop is absent in most of the cytochrome *c* peroxidase structures determined up to now (Fülöp *et al.*, 1995; Dias *et al.*, 2004; De Smet *et al.*, 2006).

### 5.5.3 Structure Analysis of CcpA

The Ramachandran plot (Ramachandran *et al.*, 1963) was calculated with *PROCHECK* (Laskowski *et al.*, 1993) in order to analyze the model quality. 85.9% of the residues are located in the most favorite regions, 13% in the allowed regions, 0.8% in generously allowed regions and 0.4% in the disallowed region.

Of these, the side chains of residues A144, A241 and A279 are not well defined in the electron density, with B values of 31.0 Å<sup>2</sup>, 38.5 Å<sup>2</sup> and 35.2 Å<sup>2</sup>, respectively. Rebuilding of these residues in allowed conformations and subsequent refinement resulted again in disallowed conformations.

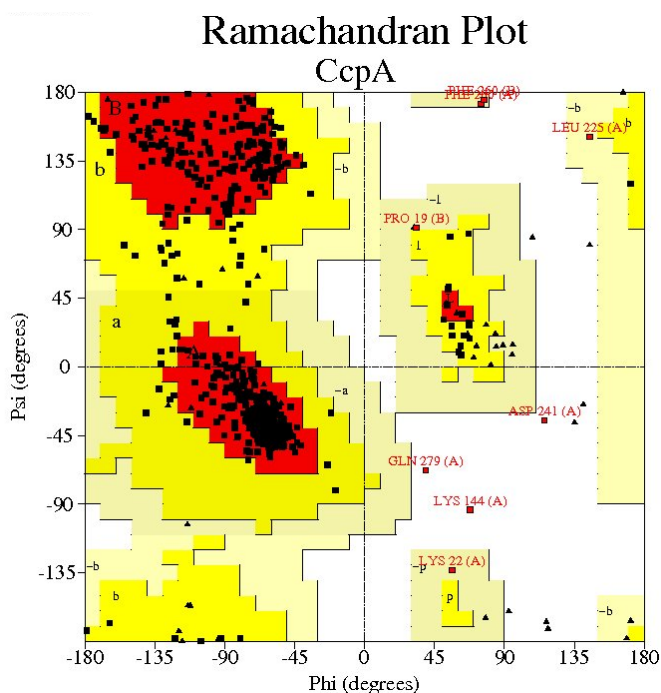


**Figure 38:** Ramachandran plot. The red area displays the most favourable region, the yellow area is the additional allowed region and the beige area is the generously allowed region. Glycines are presented as triangles.

### 5.5.4 Crystallization and Data Collection of MacA

Crystals used for the structure determination were obtained from the condition 1 A of the home-made Footprint Screen 2 (Stura *et al.*, 1994). Initially, many little crystals appeared within one drop. Variation of the protein to reservoir ratio improved the



crystal size and finally, by using 2  $\mu\text{l}$  protein and 1  $\mu\text{l}$  reservoir, fewer but bigger crystals grew in the conditions around the initial Footprint Screen 2 condition.

Several hexagonal crystal forms appeared, but only the trapezoid prism shaped crystals were tested as the others macroscopically seemed to be accreted to each other. MacA crystals for structure determination were finally taken from the condition 0.1 M ammonium acetate pH 5.5, 1.3 M sodium/ potassium phosphate and 6% ethanol.

Lithium sulfate served as cryoprotectant. The cryoprotectant solution was mixed freshly out of 40  $\mu\text{l}$  of 0.1 M ammonium acetate pH 5.5, 1.3 M sodium/ potassium phosphate and 210  $\mu\text{l}$  of 3 M lithium sulfate to avoid precipitation of cryosolution ingredients.

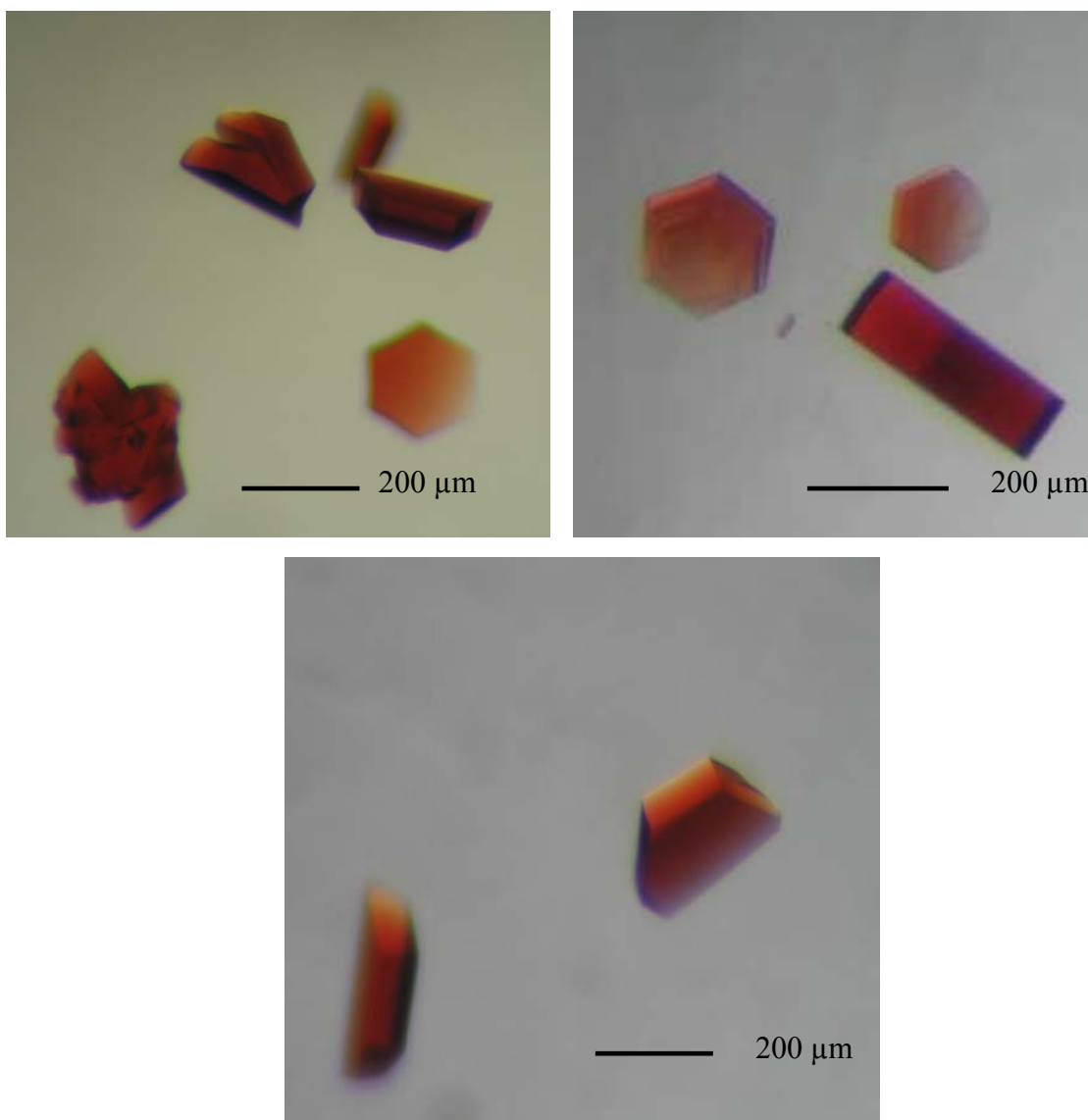


**Figure 39:** MacA crystals. Crystals grew overnight at 20°C in 0.1 M ammonium acetate pH 5.5, 1.3 M sodium, potassium phosphate and 6% ethanol.

At the X-ray home-source, MacA crystals diffracted to 2.05 Å. Higher resolution data were collected at the EMBL beam line X13 (DESY, Hamburg) at an X-ray wavelength of 0.801 Å. Diffraction images were recorded with a CCD-detector while rotating the

crystal around  $0.5^\circ$  per image during exposure. The crystal measured at the synchrotron diffracted to  $1.84 \text{ \AA}$  and belonged to the spacegroup  $P6_522$  with unit cell parameters  $a = b = 118.0 \text{ \AA}$ ,  $c = 242.0 \text{ \AA}$ ,  $\alpha = \beta = 90^\circ$ ,  $\gamma = 120^\circ$  and an estimated mosaicity of 0.4.

The data were indexed and integrated with the program *DENZO* (Otwinowski and Minor, 1997). Scaling was performed with the Bruker program *SADABS* and statistics were gained from the Bruker program *XPREP*.

A Matthews coefficient of  $2.99 \text{ \AA}^3/\text{Da}$  was calculated, corresponding to a solvent content of 58.5%.

Resolution ( $\text{\AA}$ )	50.01 – 1.95 (2.05-1.95)
Redundancy	13.49 (8.35)
Number of observations	988380
Number of unique reflections	73166
Completeness (%)	99.9 (99.5)
I/sigma	16.10 (2.84)
$R_{\text{pim}}$	0.0246 (0.1836)

**Table 3:** Data collection statistics for MacA. Numbers in parentheses refer to the values within the highest resolution shell. The R-factor  $R_{\text{pim}}$  represents the precision indicating merging R-factor (Weiss

and Hilgenfeld, 1997):  $R_{\text{pim}} = \sum_{hkl} \sqrt{\frac{1}{N-1} \sum_i |I_i(hkl) - \overline{I(hkl)}|^2} / \sum_{hkl} \sum_i I_i(hkl)$ .

### 5.5.5 Structure Determination of MacA and Refinement

The structure of MacA was determined by molecular replacement using the known structure model for the cytochrome *c* peroxidase of *P. aeruginosa* (pdb accession code 1EB7) (Fülöp *et al.*, 1995) as search model. Both proteins share a sequence identity of 58%. For molecular replacement, the program *MOLREP* was used with experimental data to  $3.5 \text{ \AA}$ . Two molecules per asymmetric unit were found.

The initial model was acquired with in-house data. First model building implicated the mutation of residues different from the model with the mutation function of the program *COOT*. Subsequently, synchrotron data were used to refine to a resolution of  $1.95 \text{ \AA}$ .

Resolution (Å)	102.06-1.95
r.m.s.d. in bond length (Å)	1.570
r.m.s.d. in bond angles (°)	0.014
R <sub>work</sub> (%) / R <sub>free</sub> (%)	20.6 / 25.6
Figure of merit	0.803
Average B value for the protein (Å <sup>2</sup> )	Chain A: 32.02, Chain B: 32.92
Average B value for waters (Å <sup>2</sup> )	39.94

**Table 4:** Data statistics from the refinement of the synchrotron data.  $R_{\text{work}} = \sum ||F_{\text{obs}}| - |F_{\text{calc}}|| / \sum |F_{\text{obs}}|$ , where  $|F_{\text{obs}}|$  and  $|F_{\text{calc}}|$  are structure factor amplitudes from the data and the model, respectively. In order to monitor  $R_{\text{free}}$  (Brünger, 1992), 5.1% of the reflections were excluded from the refinement.

After the last refinement with Refmac5, the final model of MacA had R-factors of  $R_{\text{work}} = 20.6\%$  and  $R_{\text{free}} = 25.6\%$  and contains two monomers, 608 water molecules, one ethanol molecule, six acetate molecules and 23 phosphate molecules. The modeled protein chain begins with Glu1 and ends with Asn324 while residues A223-225 and B222-226 are missing in the model. This flexible loop is also absent in molecule B of the *Geobacter sulfurreducens* peroxidase CcpA as in most of the bacterial cytochrome *c* peroxidase structures.

### 5.5.6 Structure Analysis of MacA

The stereochemistry of the two MacA molecules in the asymmetric unit is evaluated by the Ramachandran plot that has been generated with *PROCHECK* (Laskowski *et al.*, 1993). According to this, 89.1% of the residues are located in the most favorite regions, 10.3% within the allowed regions, 0.2% in the generously allowed regions and 0.4% in the disallowed region.

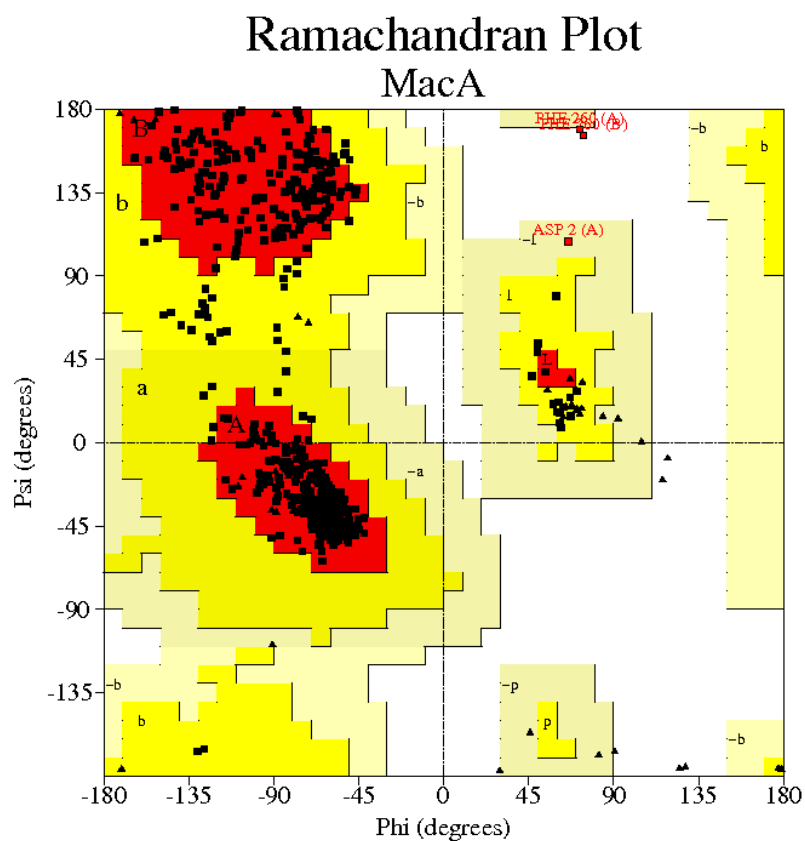


**Figure 40:** Ramachandran plot. The red area displays the most favourable region, the yellow area is the additional allowed region and the beige area is the generously allowed region. Glycines are presented as triangles.

Strikingly, the two residues found in the disallowed region (Phe260) are also located in the disallowed region of the CcpA model (see 5.5.3).

## 5.6 Overall Structures: CcpA and MacA

### 5.6.1 CcpA



**Figure 41:** Overall structure of CcpA from *Geobacter sulfurreducens*.  $\alpha$ -helices are indicated in red and  $\beta$ -strands are indicated in blue. The calcium ion and the heme groups are colored in grey.

The structure of CcpA reveals the typical topology of cytochrome *c* peroxidases (Fülöp *et al.*, 1995; Shimizu *et al.*, 2001; Dias *et al.*, 2004; De Smet *et al.*, 2006) with  $\alpha$ -helices and  $\beta$ -strands as secondary structural motives. Each of the two domains reveals a typical *c*-type cytochrome fold (Moore and Pettigrew, 1990). As in the other determined structures, the two domains are connected by three stretches with the calcium binding site located in the domain interface.

#### 5.6.1.1 Heme Groups

Both domains accommodate one heme group. In the following, distances are referred to molecule A unless stated otherwise. The N-terminal domain is built by residues 17-164 and 303-324 with the heme group attached to the polypeptide chain by the cysteines Cys51 and Cys54. The heme iron is bis-histidinyly coordinated and the dihedral angle between the imidazole planes is  $54.15^\circ$ .

The nitrogen  $N^\delta$  of one axial histidine (His55) interacts with the carbonyl group of proline 81 ( $3.07 \text{ \AA}$ ), as well as the nitrogen  $N^\delta$  of the second axial ligand (His71), is oriented by the interaction with the C=O group of proline 108 ( $2.82 \text{ \AA}$ ).

The position of the heme group is further stabilized by interactions of the propionates with the water molecules 153 and 154 and the main chain nitrogen atom of Trp94. The other propionate interacts with Asn89 and the water molecules 137 and 138.

The C-terminal domain comprises residues 1-16 and 165-302. The second heme group is located within this domain and is attached to the polypeptide chain via the cysteines of the Cys197-X-Y-Cys200-His201-...-Met275 motif while the iron is histidine-methionine coordinated. The imidazole ring of histidine 201 is oriented by the carbonyl group of proline 248 (3.12 Å).

The heme group imposes stereogeometrical restraints on the protein fold by the interaction of the propionate with the main chain nitrogen and the side chain nitrogen N<sup>δ</sup> of histidine 261 as well as with the main chain nitrogen of valine 216. The other propionate interacts with the main chain nitrogen of phenylalanine 260 and the water molecules 128, 400 and 402.

The two heme groups are arranged roughly perpendicular to each other with an iron-iron distance of 21.05 Å. The shortest distance between the heme groups is via the propionates (9.99 Å) that point inside the protein.

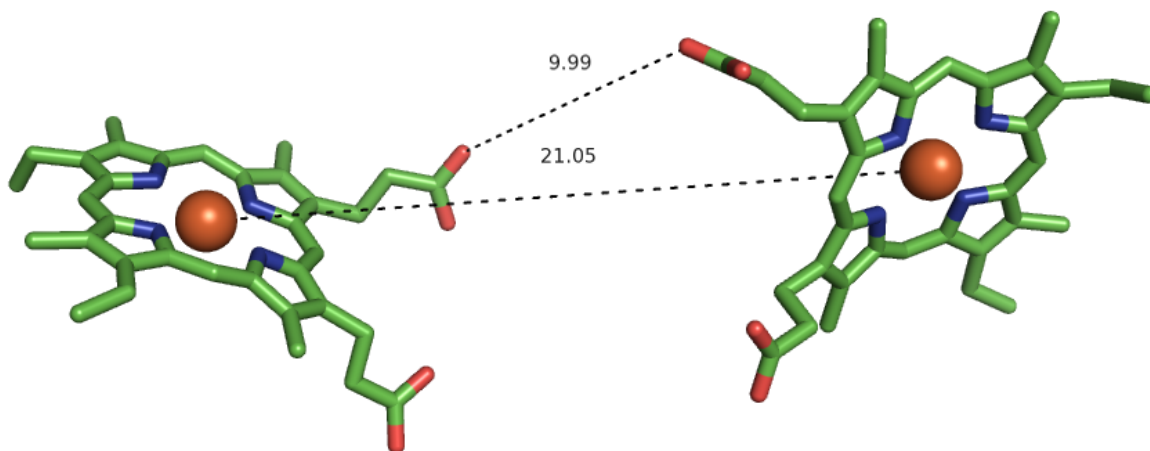


**Figure 42:** Heme group arrangement in CcpA.

### 5.6.2 MacA

The structure of MacA shows the overall scaffold seen in the other bacterial cytochrome c peroxidases (see 5.6.1).



**Figure 43:** Stereo view of the MacA monomer.  $\alpha$ -helices are indicated in red and  $\beta$ -strands are indicated in blue. The calcium ion and the heme groups are colored in grey.

#### 5.6.2.1 Heme Groups

The two heme groups are arranged roughly perpendicular to each other with an iron-iron distance of 21.19 Å. The closest distance between the cofactors is 9.59 Å via the propionates.

The N-terminal domain is made up by the residues 15-166 and 302-324 with one heme group attached to the polypeptide chain by cysteines Cys51 and Cys54. As in CcpA, the iron is ligated by the two histidines 55 and 71. Carbonyl groups of other residues form hydrogen bonds with the  $N^\delta$  of the iron coordinating histidines, thus orienting the histidine imidazole ring. Nitrogen  $N^\delta$  of histidine 55 is bonded to the carbonyl group of proline 81 (2.79 Å). In a similar way, histidine 71 is interacting with the carbonyl group of alanine 111 (2.82 Å) while in CcpA the carbonyl group interacting with the  $N^\delta$  of His71 belongs to proline 108. The dihedral angle between the imidazole planes is 45.51°.

The electron transferring heme group is stabilized by asparagine 89, arginine 246 and by the water molecule 188 forming hydrogen bonds to one of the propionates. The other propionate interacts with tryptophan 73 and the water molecules 275 and 416.

Histidine 71 is located in a flexible loop that has to be released from the iron in the active form as hydrogen peroxide has to get access to the active center. In order to determine the structure of the active enzyme, crystals of the *P. pantotrophus* cytochrome *c* peroxidase in its mixed valence state have been produced by Echalier and coworkers (2006).

Photoreduction of MacA crystals and reduction with dithionite or ascorbate were attempted. Subsequently, datasets of those crystals were recorded and evaluated, but no difference electron density around this putatively flexible loop was detected (data not shown). Growth of reduced crystals under anaerobic conditions in order to determine the structure of active MacA did not succeed so far.

The C-terminal domain comprises residues 1-14 and 167-301. The heme group located in this domain is coordinated by the residues Cys197-X-Y-Cys200-His201-...-Met275 and the iron is ligated by a histidine and a methionine. The orientation of the histidine 201 is maintained by interaction with the carbonyl group of proline 248 (2.92 Å).

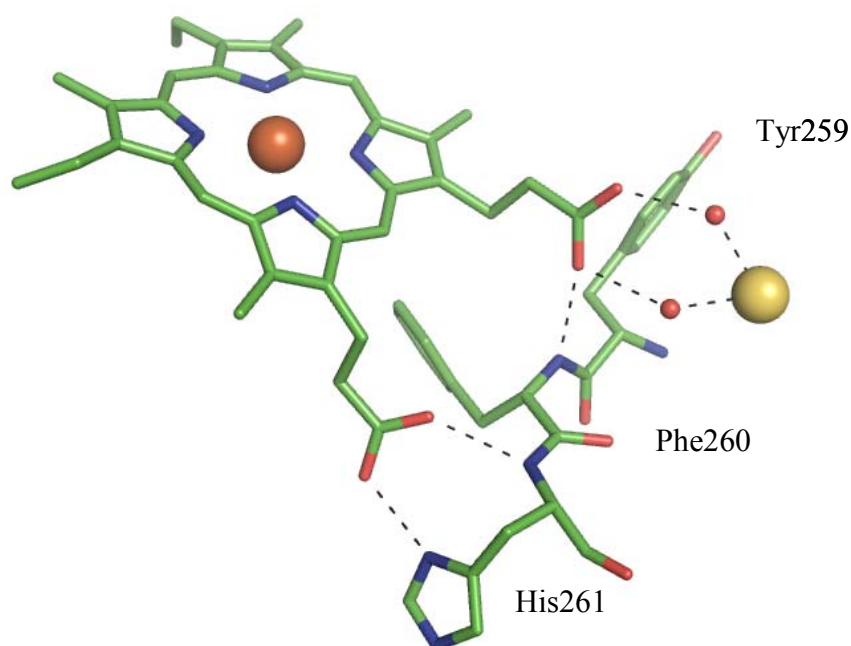


**Figure 44:** Stereochemical restraints imposed by the heme group in MacA. The iron is colored in brown, the water molecules are colored in red and the calcium ion is colored in yellow.

One propionate is stabilized by the main chain nitrogen from His 261 as well as by the nitrogen  $N^{\delta}$  of the imidazole ring and the main chain nitrogen of valine 216. The water molecules 110 and 118 as well as the main chain nitrogen of phenylalanine 260 stabilize the other propionate. These hydrogen bonds formed by the propionates and the main



chain nitrogen atoms of Phe260 and His261 impose stereochemical restraints that are the reason for the disallowed confirmation of Phe260 in both peroxidases from *Geobacter sulfurreducens*. This stereochemical feature has also been reported for the cytochrome *c* peroxidase from *Pseudomonas nautica* (Dias *et al.*, 2004).

### 5.6.3 Comparison of the Overall Structure to Other Peroxidases

On the basis of their pdb (protein data bank) coordinates, families of structurally similar proteins to MacA and CcpA were searched with the DALI server (Holm and Sander, 1993). The cytochrome *c* peroxidase of *P. aeruginosa* already served as search model in molecular replacement for both, CcpA and MacA. Likewise, the peroxidase of *P. aeruginosa* is the first hit upon DALI database search with Z-values of 42.7 in case of MacA and 44.5 in case of CcpA. The similarity to the other database hits only arises due to the classical *c*-type cytochrome fold of the two domains which is reflected by rather low Z-values (maximum 4.4).

MacA and CcpA have 69% identical amino acid residues. Their similarity is maintained on the structural level and is reflected by the root-mean-square deviation (rmsd) of 0.924 Å for 302 aligned residues.

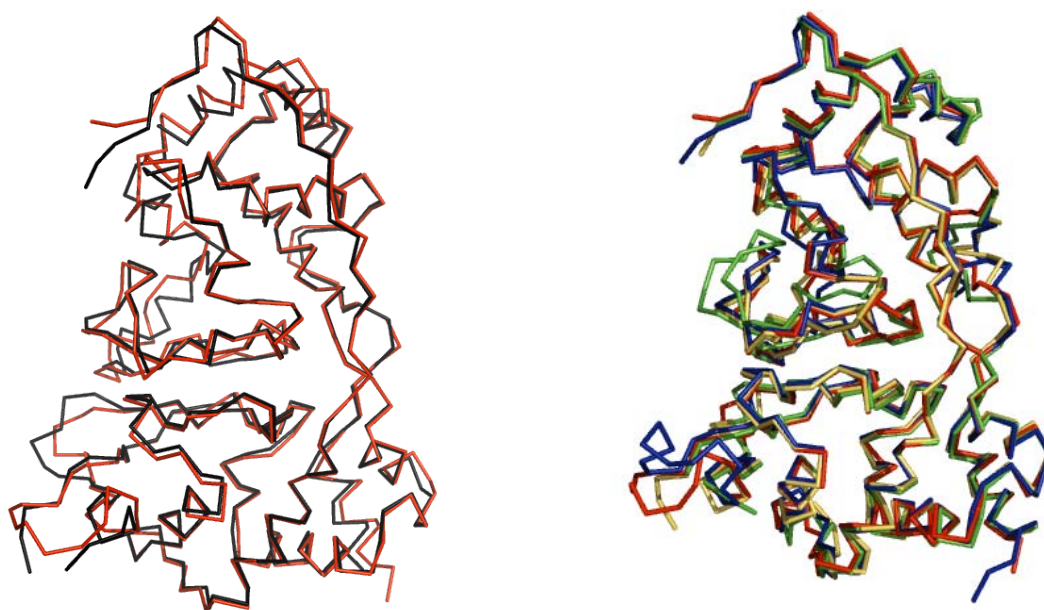


**Figure 45:** left: MacA (black) and CcpA (red) from *Geobacter sulfurreducens*. Right: Comparison of the oxidized form of cytochrome *c* peroxidases from different organisms, CcpA from *G. sulfurreducens* (red), *P. pantotrophus* (blue), *P. aeruginosa* (yellow) and *P. nautica* (green).

As expected from sequence alignment, CcpA, MacA and peroxidases from other organisms are very similar. Especially, the residues coordinating the heme groups and in the domain interface where electron transfer between the heme groups takes place are conserved (see figure 33). The most prominent differences are found in the loop

comprising the axial iron ligand histidine 71 and in the loop formed by the residues 219-232 which is not complete in most Ccp structures. In CcpA this loop is very flexible with B-factors higher than  $50 \text{ \AA}^2$ .

	CcpA-1EB7	CcpA-1RZ6	CcpA-2C1U
Aligned residues	308	301	306
RMSD ( $\text{\AA}$ )	0.973	1.264	1.122

**Table 5:** Pairwise superposition of CcpA from *Geobacter sulfurreducens* with 1RZ6 (*Pseudomonas nautica*), 2C1U (*Paracoccus pantotrophus*) and 1EB7 (*Pseudomonas aeruginosa*). Superposition of the molecules was performed with lsqman (Kleywegt, 1996). The comparison of MacA to the Ccp of *P. aeruginosa* which served as model for the molecular replacement gave a rmsd of  $1.081 \text{ \AA}$  for 300 residues.

#### 5.6.4 Crystal Packing and Accessible Surface

The accessible surface of CcpA has a size of  $15,047 \text{ \AA}^2$  (molecule B:  $14,515 \text{ \AA}^2$ ). As mentioned above, bacterial Ccps are believed to form functional dimers. In the dimer an area of  $26,871 \text{ \AA}^2$  is accessible, therefore the dimer interface has a size of  $2,691 \text{ \AA}^2/2$  reminiscent of the dimer interface of the inactive *P. nautica* IN form ( $2412 \text{ \AA}^2$ ) (Dias *et al.*, 2004).

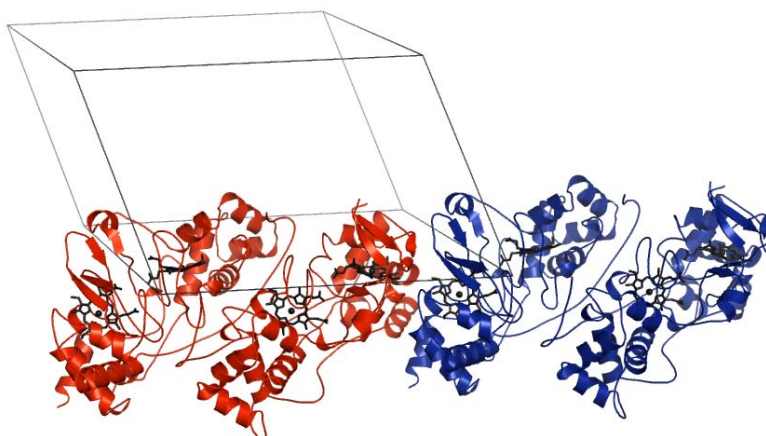


**Figure 46:** The crystal of CcpA is formed by the translation of the dimer in the three directions in space (space group P1).

The monomer of MacA provides a total accessible surface area of  $14,677 \text{ \AA}^2$  (molecule B:  $14,456 \text{ \AA}^2$ ). In the crystal two large interface areas between the monomers are present. The typical dimer formed by the other cytochrome *c* peroxidases has an accessible surface area of  $26,007 \text{ \AA}^2$  and a dimer interface of  $3126 \text{ \AA}^2/2$  resembling the dimer interface of the active *P. nautica* OUT form ( $3031 \text{ \AA}^2$ ) (Dias *et al.*, 2004). On the

other hand, the alternative dimer has an accessible surface of 26,056 Å<sup>2</sup> with a dimer interface of 3,077 Å<sup>2</sup>/2.

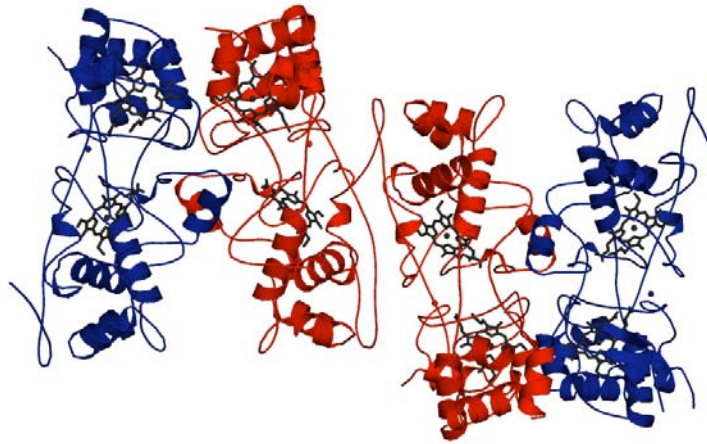


**Figure 47:** The crystal packing of MacA in space group P6<sub>5</sub>22 creates two possible dimer interfaces. According to cytochrome *c* peroxidases from other organisms, the red monomers belong to the functional dimer. For CcpA, this crystal packing is impossible due to side chains constraining each other.

### 5.6.5 Electrostatic Potential

The most apparent difference of MacA and CcpA compared to the other bacterial cytochrome *c* peroxidases resides in their different electrostatic potentials. Much of the divergence is due to the substitution of charged residues located on the surface, with more positively charged residues and the loss of many negatively charged residues. Therefore MacA and CcpA are more basic than e.g. the *P. aeruginosa* cytochrome *c* peroxidase.

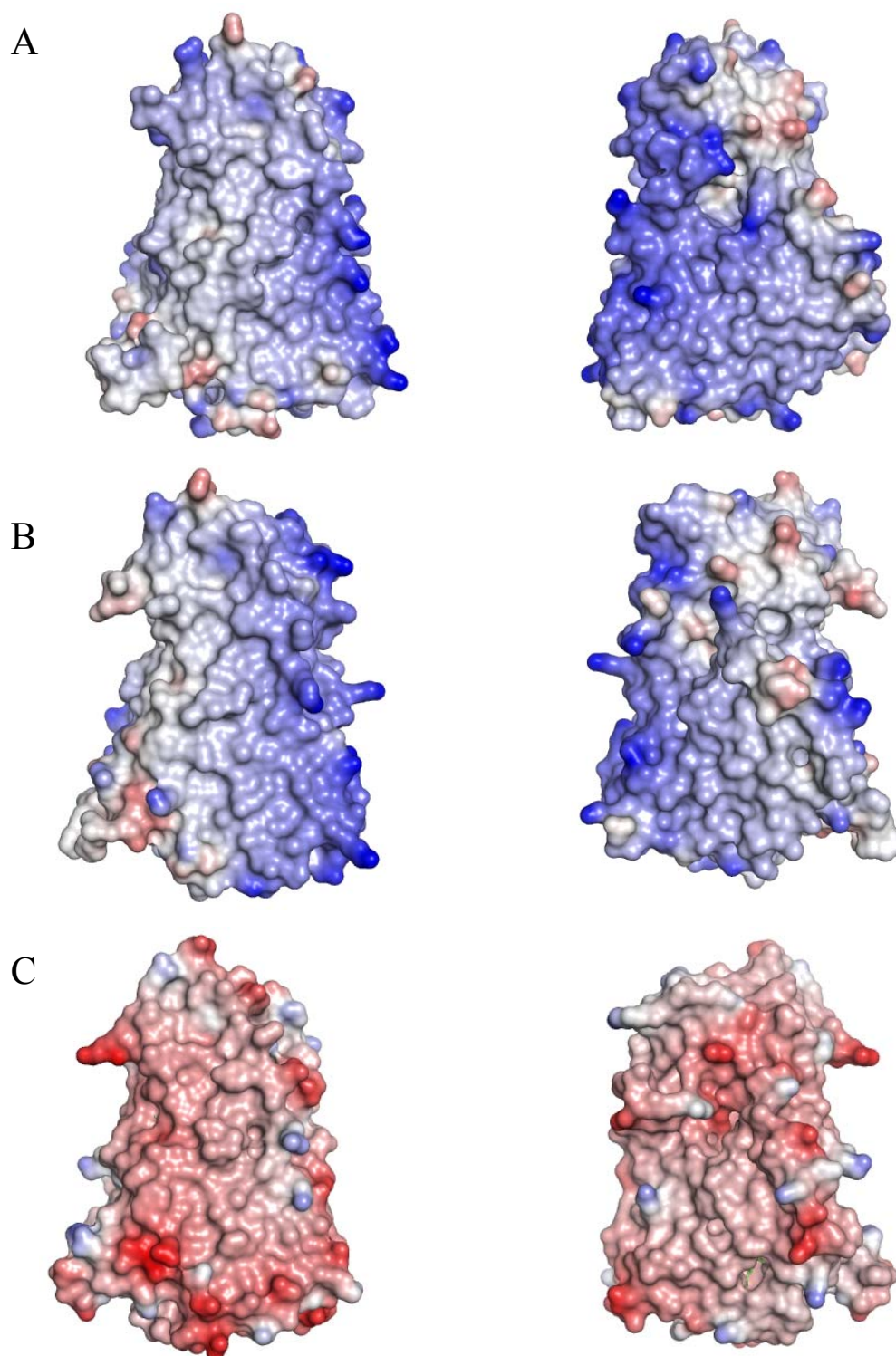


**Figure 48:** Comparison of the electrostatic surface potentials of the (A) CcpA monomer, (B) MacA monomer and (C) the *P. aeruginosa* Ccp monomer (pdb accession code 1EB7). The molecules on the right hand side have been rotated 180° (y-axis). The blue patches represent the basic, positively charged parts on the surface; the red patches represent the acidic, negatively charged parts on the protein surface. The electrostatic surface potentials were calculated with *DELPHI* (Honig and Nicholls, 1995) and presented with *PYMOL* (DeLano, 2002) in a range of -402 to 402 kT.

### 5.6.6 Calcium Binding Site

The calcium binding site is located in the hydrophobic interface between the two domains. In both peroxidases of *Geobacter sulfurreducens*, the ion is equidistant from each iron ( $\sim 12.6$  Å to the His-Met coordinated iron and  $\sim 12.1$  Å to the bis-histidinyll coordinated iron). The B-factors for  $\text{Ca}^{2+}$  in MacA are  $23.66$  Å<sup>2</sup> and  $23.77$  Å<sup>2</sup>, respectively, and in CcpA, they are  $16.70$  Å<sup>2</sup> and  $18.61$  Å<sup>2</sup>, respectively.

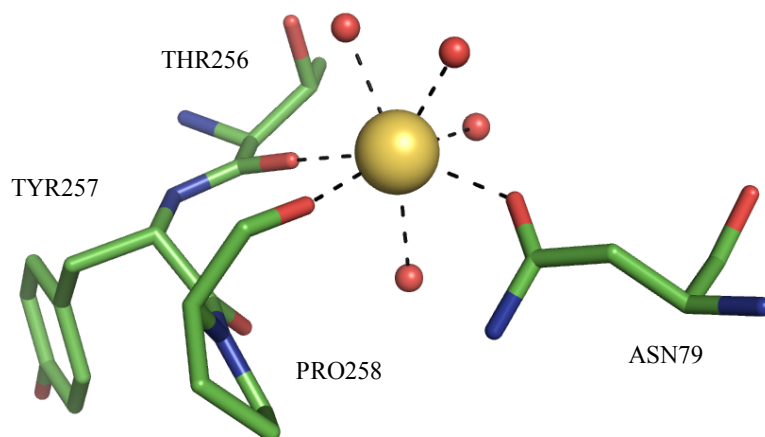


**Figure 49:** Calcium binding site of CcpA. The calcium ion is colored in yellow, the water molecules are colored in red.

In MacA as well as in CcpA, the amino acids complexing the calcium ion are asparagine 79, the carbonyl group of threonine 256 and the carbonyl group of proline 258. The cis conformation of Pro258 and Met257 in MacA and of Pro258 and Tyr257 in CcpA, respectively, might be due to the restraints imposed by the calcium ion coordination geometry. Furthermore, the calcium ion is coordinated by four water molecules so that the seven ligands are bound in distorted pentagonal bipyramidal geometry to the calcium ion.

These protein ligands are located in highly conserved regions within bacterial cytochrome *c* peroxidases. Likewise, one of the propionates is coordinated to two of the coordinating water molecules as found in other peroxidases (see figure 44).

Not only the calcium binding site contributes to the interaction of the two domains, also the residues 244-246 and 94-96 are interacting with each other via the main chain as well as residues 90-91 and 208 do in case of MacA. The side chains of Asn205 and Trp94 also make contact between both domains. In CcpA, the contact is mainly established by the interaction of the two  $\beta$ -strands comprising the residues 95-97 and 243-245.

### 5.6.7 B-Factor Analysis

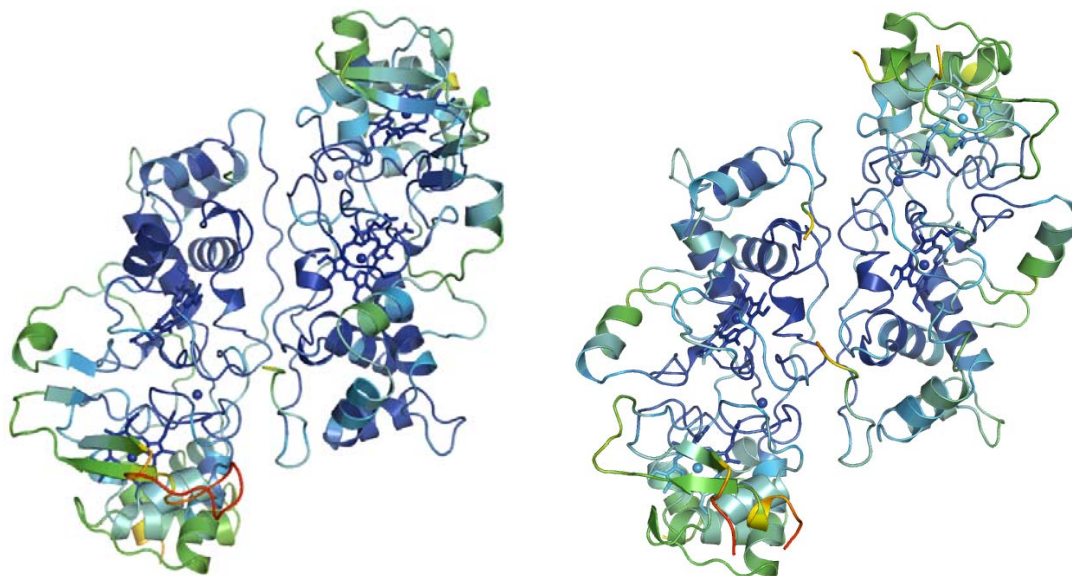


**Figure 50:** Cartoon representation of CcpA (left) and MacA (right). The structures are colored according to the B-factors (Debye-Waller factors) where blue symbolizes low and red symbolizes high B-factors.

In regions around the heme groups of both MacA and CcpA, the B-factors are lower which is reflected by the dark blue color. Residues located in the interface between both monomers as well as residues around the calcium binding site are the most rigid. Flexible loops are found in domain of the electron transferring heme.

## 5.7 Structure Determination of RoxA

### 5.7.1 Crystallization, Data Collection and Structure Determination of RoxA

Due to the similarity of the rubber oxygenase A (RoxA) from *Xanthomonas* sp. strain 35Y to bacterial cytochrome *c* peroxidases (Jendrossek and Reinhardt, 2003), this project was taken over in order to evaluate and compare the structure of RoxA to those of CcpA and MacA. Crystallization, structure determination and initial model building was performed by Prof. Oliver Einsle.

RoxA was crystallized in 8% PEG 8000 and 0.1 M Hepes pH 7.5. 10% (v/v) of 2R,3R-butanediol served as cryoprotectant.

The crystal belonged to the monoclinic space group  $P2_1$  with unit cell parameters of  $a = 72.4 \text{ \AA}$ ,  $b = 97.1 \text{ \AA}$ ,  $c = 101.1 \text{ \AA}$ ,  $\alpha = 90^\circ$ ,  $\beta = 98.39^\circ$  and  $\gamma = 90^\circ$  and diffracted to  $1.68 \text{ \AA}$ . The data were integrated with *DENZO* (Otwinowski and Minor, 1997) and scaled with the Bruker program *SADABS*.

RoxA has a calculated, sequence-derived molecular weight of 74.1 kDa. There are two monomers in the asymmetric unit and the solvent content is 48.14% with a Matthews coefficient of  $V_M = 2.37 \text{ \AA}^3/\text{Da}$  (Matthews, 1968).

Different attempts of phase determination had to be performed as initial trials to solve the structure of RoxA by Fe-SAD failed due to the low phasing power. Two high redundant datasets for Fe-SAD were recorded and the iron sites were immediately found by this method. However, the structure could only be solved by Fe-MAD with data recorded at four different wavelengths. The MAD experiment was performed at the EMBL in Hamburg at the synchrotron beamline X 12.

	High redundancy	Peak	Inflection	High resolution
Wavelength (Å)	1.7316	1.7384	1.7398	0.9184
Resolution (Å)	2.4	2.7	2.7	1.68
Redundancy	56.5	5.7	7.2	4.9
No. of observations	3 159 992	698 564	782 909	764 808
No. of unique reflections	54970	36932	37559	156762
Completeness (%)	98.3 (92.3)	94.9 (80.6)	96.5 (80.6)	96.6 (86.6)
I/ sigma	30.2 (6.5)	16.7 (5.7)	19.9 (6.5)	8.9 (1.5)
R <sub>sym</sub> (%)	0.164 (0.632)	0.091 (0.251)	0.089 (0.251)	0.116 (0.711)

**Table 6:** Data collection statistics for RoxA. Numbers in parentheses refer to the values within the highest resolution shell.  $R_{\text{sym}} = (\sum |I - \langle I \rangle| / \sum I)$

The iron sites were acquired with ShelxD (Schneider and Sheldrick, 2002) and phasing was performed in Sharp (La Fortelle *et al.*, 1997). The density of both monomers was averaged with Ave (Kleywegt and Read, 1997) to improve the quality of the electron density. Initial model building was performed in *COOT*.

### 5.7.2 Structure Determination of RoxA and Refinement

Initial refinement was performed in *CNS* (Brünger *et al.*, 1998) providing higher geometry-restraints. Subsequently, alternating cycles of model building in *COOT* and refinement in Refmac5 were performed. Water molecules were added automatically and later on manually in *COOT*.

After the final refinement in Refmac5, the R-factors reached  $R_{\text{work}} = 17.7\%$  and  $R_{\text{free}} = 22.6\%$ .

Resolution (Å)	100.00 - 1.80
Rms deviation in bond length (Å)	1.612
Rms deviation in bond angles (°)	0.015
$R_{\text{work}}$ (%) / $R_{\text{free}}$ (%)	17.7 / 22.6
Figure of merit	0.829
Average B value for the protein (Å <sup>2</sup> )	Chain A: 20.51, Chain B: 22.59
Average B value for waters (Å <sup>2</sup> )	29.93

**Table 8:** Data statistics from the refinement of the RoxA structure.  $R_{\text{work}} = \sum ||F_{\text{obs}}| - |F_{\text{calc}}|| / \sum |F_{\text{obs}}|$ , where  $|F_{\text{obs}}|$  and  $|F_{\text{calc}}|$  are structure factor amplitudes from the data and the model, respectively. In order to monitor  $R_{\text{free}}$  (Brünger, 1992), 5% of the reflections were excluded from the refinement.

Altogether 647 amino acids and two heme groups per monomer, two Hepes molecules and 1457 water molecules could be modeled. From Ala15 to Leu662, the amino acids could be continuously built into the electron density.

### 5.7.3 Structure Analysis of RoxA

The quality of the final RoxA model was verified with the Ramachandran plot and is fully satisfactory for this resolution. 89.2% of the residues are in the most preferred region, 10.3% are found in the additional allowed regions and 0.1% in the generously



allowed region. Strikingly, as well as in the models of CcpA and MacA, phenylalanines (Phe301 and Phe516) are located within the disallowed region.

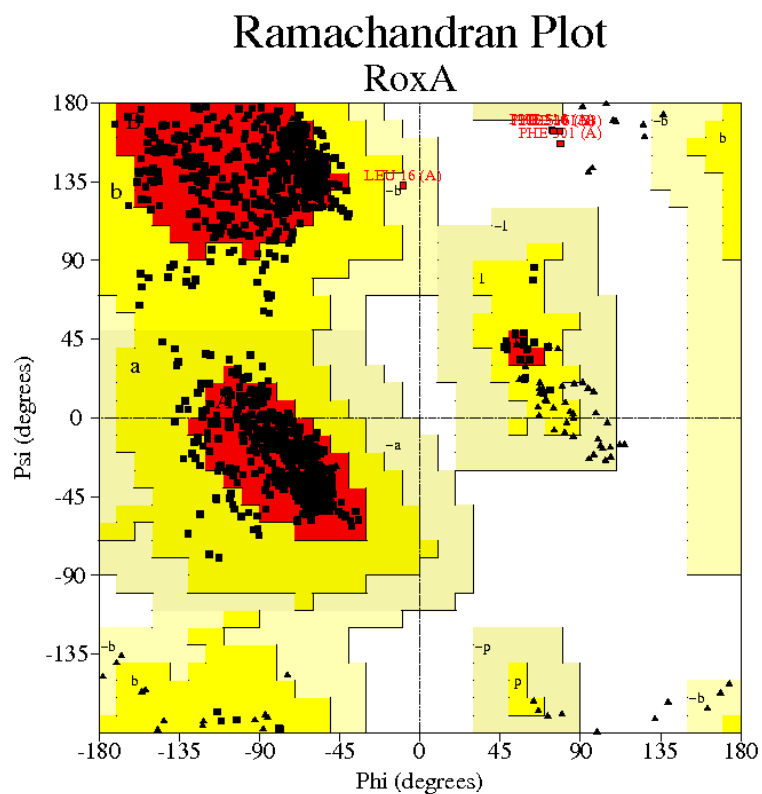


**Figure 51:** Ramachandran plot. The red area displays the most favorable region, the yellow area is the additional allowed region and the beige area is the generously allowed region. Glycines are presented as triangles.

## 5.8 Overall Structure of RoxA

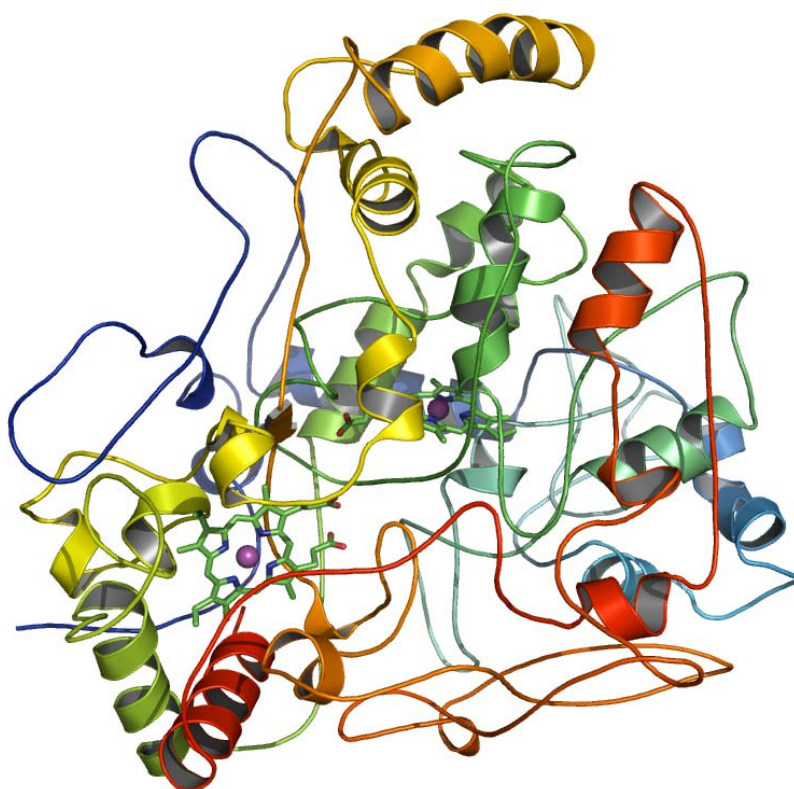


**Figure 52:** Cartoon representation of RoxA. The peptide chain is colored blue from the N-terminal end to red at the C-terminal end. The heme groups are displayed as sticks.

RoxA is a monomeric enzyme that consists of one compact domain of  $\sim 60 \text{ \AA} \times 60 \text{ \AA} \times 65 \text{ \AA}$  with  $\alpha$ -helices representing the main secondary structural motif and an unusually large portion of loops. Two short antiparallel  $\beta$ -strands comprising residues 420-422 and residues 500-502 face each other and shield the bis-histidinyl coordinated heme group from the solvent. The accessible surface of molecule A is  $22,660 \text{ \AA}^2$  (molecule B:  $22,657 \text{ \AA}^2$ ).

Both molecules in the asymmetric unit are very similar, reflected by a root-mean square deviation of  $0.18 \text{ \AA}$ .

### 5.8.1 Heme Groups

Both heme groups are fully buried within the protein. They are oriented approximately perpendicular to each other with an iron-iron distance of  $21.46 \text{ \AA}$ . The shortest distance between the heme groups is via the propionates ( $9.17 \text{ \AA}$ ).

One heme group is attached to the peptide chain by the cysteines Cys390 and Cys393 while the iron is coordinated by two histidines 394 and 641. Nitrogen  $N^\delta$  of His394 interacts with the carbonyl group of proline 504 ( $2.76 \text{ \AA}$ ) while nitrogen  $N^\delta$  of His641

forms a hydrogen bond to its own carbonyl group (2.77 Å), thus orienting the imidazole ring. The dihedral angle between the imidazole planes is 59.74°.

One propionate is stabilized by interactions with the water molecules 87 (2.82 Å), 86 (3.01 Å) and 80 (2.62 Å) as well as with the main chain nitrogen of Phe516 (2.78 Å). The other propionate interacts with the main chain nitrogen of His517 (2.60 Å), the nitrogen N<sup>δ</sup> of His517 (2.51 Å) and with the hydroxyl group of threonine 428 (2.80 Å). As seen above, the coordination of Phe516 and His517 imposes stereogeometrical restraints which explain the localization of Phe516 in the disallowed region of the Ramachandran plot.

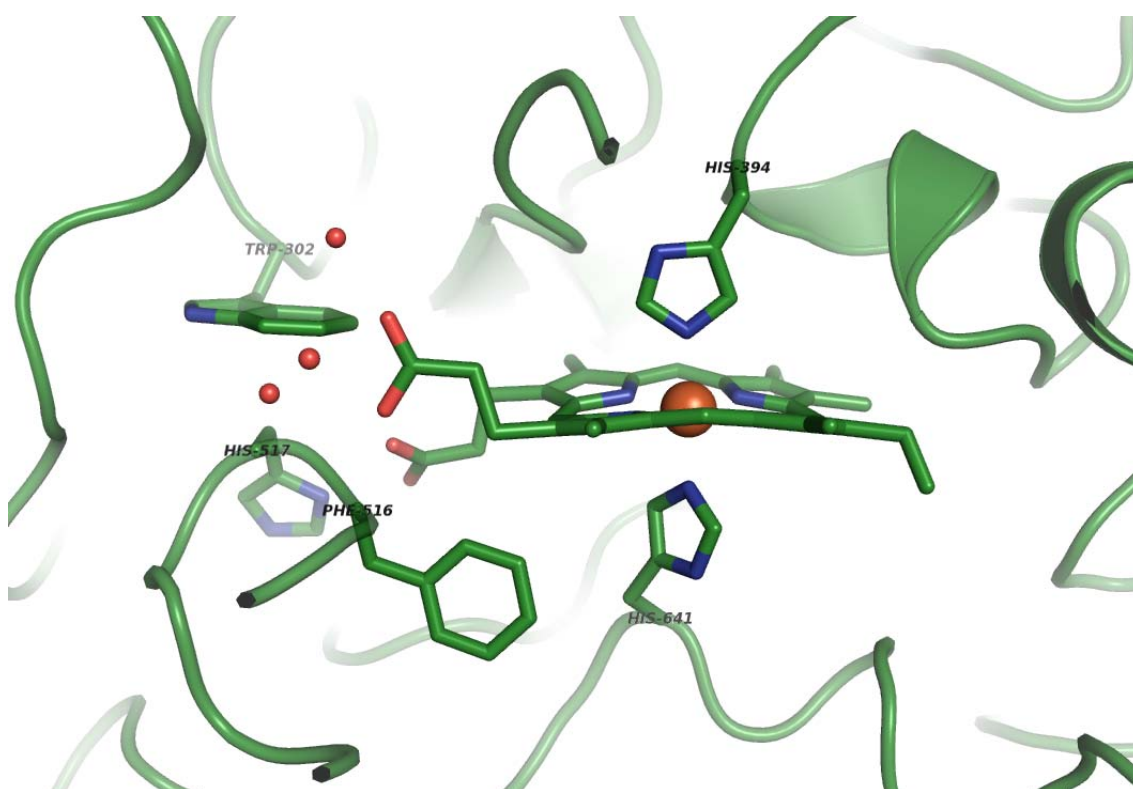


**Figure 53:** Stick representation of the bis-histidinyly coordinated heme group. The water molecules 80, 86 and 87 are included in the picture.

The second heme group is attached to the peptide chain via the cysteines Cys191 and Cys194. In the crystallized form of RoxA, the heme group has only one protein-derived axial ligand, His195. In a distance of 2.10 Å, a water molecule is positioned. The nitrogen atom N<sup>δ</sup> of His195 is not oriented by the peptide chain but forms a hydrogen bond with water molecule 1272 (2.93 Å).

One propionate is oriented through interactions with the hydroxyl group of threonine 286 (2.68 Å), the nitrogen N<sup>e</sup> of arginine 432 (2.68 Å), the main chain nitrogen of tryptophan 302 (2.86 Å) and the nitrogen N<sup>n</sup> of arginine 432 (2.93 Å). The other propionate interacts with the main chain nitrogen of Phe301 (2.73 Å) which explains the restrained stereogeometry of Phe301 located in the disallowed region of the

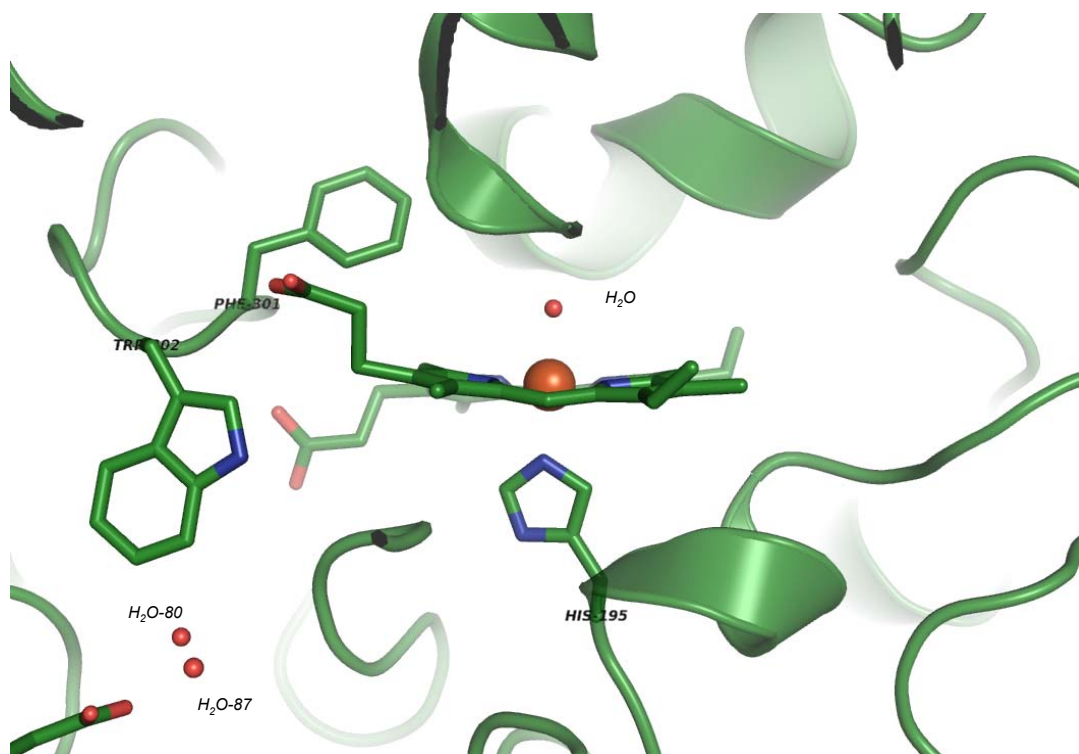


**Figure 54:** Stick representation of the histidine coordinated heme group.

Ramachandran plot. The water molecules 89 (2.59 Å) and 1273 (2.68 Å) as well as the nitrogen N<sup>1</sup> of arginine 294 represent further ligands of this propionate.

### 5.8.2 Disulfide Bridges

There are two disulfide bridges in the structure of RoxA, Cys574-Cys586 and Cys32-Cys88. They are located at the surface of the protein, distant from the heme groups, and are presumed to stabilize the protein.

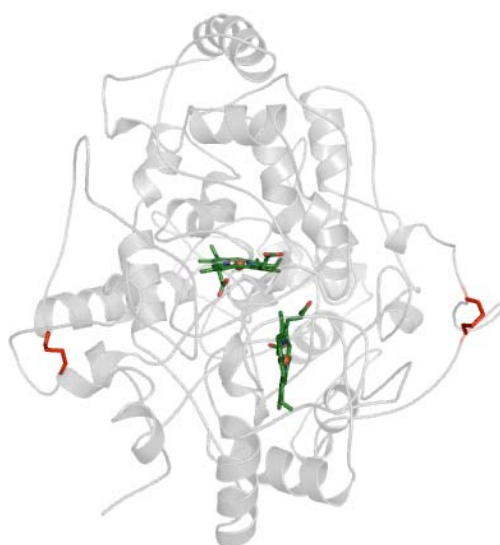


**Figure 55:** Cartoon representation of RoxA. The two heme groups are colored in green, the disulfide bridges are colored in red. The molecule is rotated around 90° (y-axis) in comparison to figure 52.

### 5.8.3 Surface Properties

RoxA exhibits a differential distribution of negatively and positively charged residues on the surface. The lower part is quite basic compared to other proteins. As depicted in figure 56, both heme groups are accommodated in this lower part of the enzyme.

The heme group in the center of RoxA representing the active site has only one axial ligand (His195). The substrate probably gains access to the reaction center from the upper, more hydrophobic part of the enzyme.

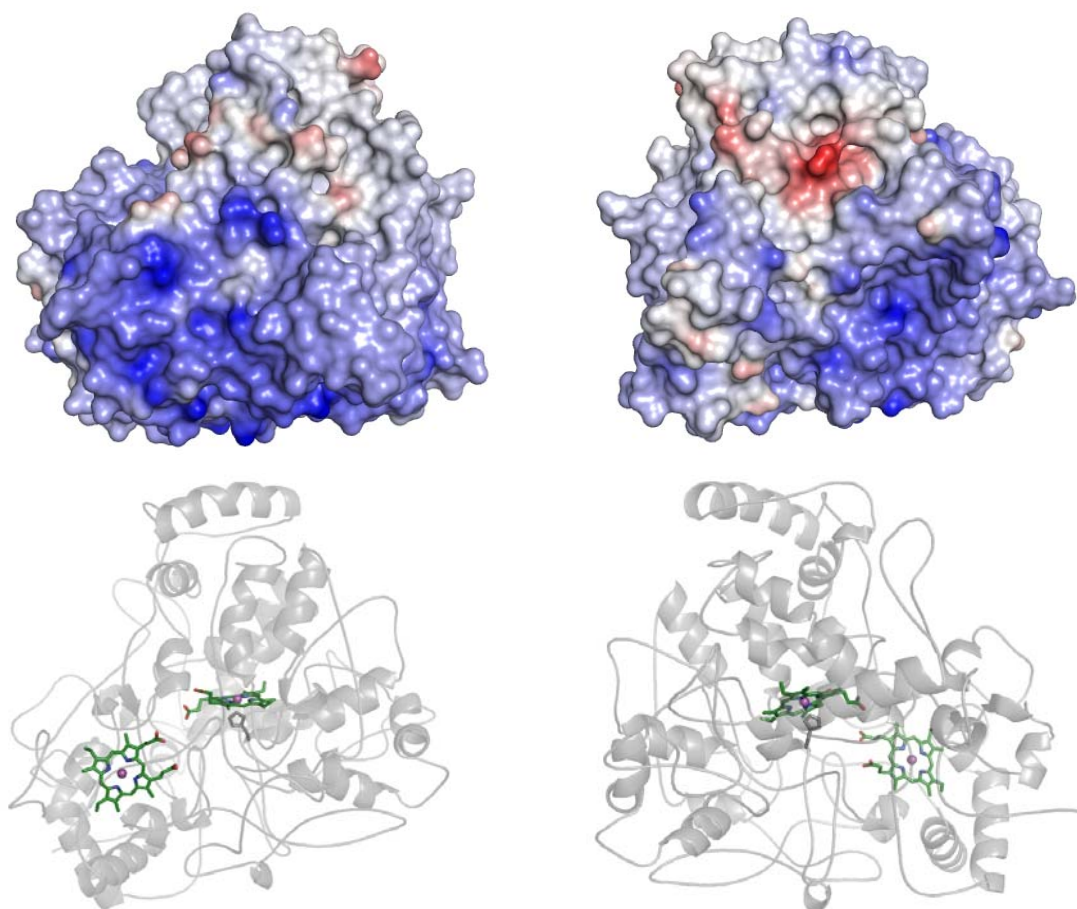


**Figure 56:** Surface representation of RoxA colored according to the electrostatic surface potential. On the left hand side, the molecule is oriented comparable to figure 3.8 and on the right hand side, it is rotated around  $180^\circ$  (y-axis). Blue patches indicate basic residues while red patches indicate acidic residues. The electrostatic surface potential is calculated with *DELPHI* (Honig and Nicholls, 1995) and presented with *PYMOL* (DeLano, 2002) in the range of -403 to 403 kT. The heme group orientation is indicated below.

## 6 Discussion

### 6.1 The Physiological Role of CcpA and MacA in *Geobacter sulfurreducens*

In contrast to the reduction of soluble electron acceptors that can diffuse into bacterial cells, the reduction of insoluble iron oxides by *Geobacter* species requires electron transfer from the cytoplasm to the outside of the outer membrane where the reduction of insoluble ferric iron occurs (see figure 3). The genus *Geobacter sulfurreducens* has adapted to these demands by the large number of *c*-type cytochromes (Méthé *et al.*, 2003). Some of these *c*-type cytochromes have been shown to be required for optimal electron transfer to iron (Leang *et al.*, 2003; Lloyd *et al.*, 2003; Butler *et al.*, 2004; Mehta *et al.*, 2005). The identification of key players involved in the electron transport to and finally the reduction of insoluble iron is based on genetic studies and growth experiments with knock-out mutants of *Geobacter sulfurreducens* performed by Lovley and coworkers.

First indications that MacA and CcpA could be involved in electron transport to iron were found by the comparison of *G. sulfurreducens* cells grown on Fe(III) citrate and fumarate (Butler *et al.*, 2004). Both proteins were detected in the membrane fraction and could be extracted from it by treatment with low salt (150 mM NaCl). MacA as well as CcpA can be heterologously expressed in *E. coli* and subsequently purified as soluble proteins in a buffer containing at least 150 mM NaCl (see results 5.1). The positively charged surface (see figure 48) is consistent with the idea that both proteins are peripherally associated to the membrane. Depending on pH and ionic strength, any positively charged protein can make contact to the negatively charged membrane by non-specific electrostatic interactions.

The suggestion that MacA and probably also CcpA might be central intermediates in the reduction of Fe(III) in *Geobacter sulfurreducens* arose from the finding that cells grown on Fe(III) citrate revealed higher levels of *macA* mRNA and that the *macA* deletion mutant showed a decreased ability to reduce Fe(III) citrate compared to the wild type (Butler *et al.*, 2004). The *Geobacter sulfurreducens* knock-out mutant of OmcB, a proposed key player in the dissimilatory iron reduction pathway (see figure 3) (Leang *et al.*, 2003), revealed a significant up-regulation of the *ccpA* expression level compared to the wild type grown in acetate-limiting Fe(III) citrate continuous culture (Leang *et al.*,

2005). This indicates that CcpA may play a role in an alternative electron transport chain to the terminal ferric iron reductase under these conditions.

Otherwise, CcpA and MacA reveal typical spectroscopic features (see results 5.2) and a typical threedimensional structure (see results 5.6) of bacterial diheme cytochrome *c* peroxidases as well as peroxidases activity *in vitro* (see results 5.3).

### 6.1.1 Gene Expression of *ccpA* and *macA* in the *rel<sub>Gsu</sub>* Mutant

Evidence that CcpA and MacA are not necessarily involved in Fe(III) reduction but rather in stress response was provided by the analysis of the *rel<sub>Gsu</sub>* mutant of *Geobacter sulfurreducens* (DiDonato *et al.*, 2006). The gene *rel<sub>Gsu</sub>* encodes a RelA/ SpoT homolog predicted to be involved in stress response. In bacteria and plants, the stringent response occurs in reaction to limiting growth conditions with the signal molecule guanosine 3',5'-bispyrophosphate (ppGpp) acting as a broad regulator during the adaptation of the organism to a variety of environmental conditions (Chatterji and Ojha, 2001; Braeken *et al.*, 2006). In *E. coli*, two paralogous enzymes, RelA and SpoT, were detected that catalyze the synthesis and degradation of ppGpp (Magnusson *et al.*, 2005). However, in *G. sulfurreducens* (DiDonato *et al.*, 2006), as in several other organisms (Wendrich and Marahiel, 1997; Wendrich *et al.*, 2000), one homolog of RelA/ SpoT is assumed to be responsible for both, synthesis and degradation of ppGpp. For *G. sulfurreducens*, it was shown that genes involved in protein synthesis are up-regulated and genes involved in stress responses and electron transport are down-regulated in the *rel<sub>Gsu</sub>* mutant (DiDonato *et al.*, 2006). Genes that are down-regulated include *pilA*, *omcS*, *omcB*, *macA*, *ccpA*, desulfoferrodoxin and the rubrerythrin encoding gene GSU2814. In addition to the finding that the oxidative stress response was impaired in the *rel<sub>Gsu</sub>* mutant, the capacity of Fe(III) reduction was also lower compared to the wild type. Thus, the study illustrates the complexity of the regulation of both, the stringent response and the Fe(III) reduction in *G. sulfurreducens*. But probably, the stringent response plays an important role in adjusting growth in a substrate-limiting environment and hence, the decreased ability of the *rel<sub>Gsu</sub>* mutant to reduce Fe(III) is only a consequence of the oxidative stress.

### 6.1.2 Gene Expression of *ccpA* and *macA* in the *rpoS* Deletion Mutant

On the transcriptional level, sigma factors represent further prokaryotic regulators of the stress response. It is well known that they confer specific binding of the RNA polymerase to promoter sites, thus initiating transcription (Wosten, 1998).

*G. sulfurreducens* has at least six genes encoding homologs of sigma factors (Nunez *et al.*, 2004).

Expression analysis showed that the sigma factor  $\sigma^S$  (RpoS) of *G. sulfurreducens* activates genes involved in oxidative stress resistance and adaptation to nutrient limitation. Activation of these genes by RpoS corresponds to a decreased gene expression in the *rpoS* mutant.

The *macA* gene is RpoS dependent (Nunez *et al.*, 2006) and is significantly down-regulated in the *rpoS* mutant during growth on fumarate, as well as the genes encoding CcpA and the proteins ferredoxin (GSU3187), rubredoxin (GSU3188) and desulfoferredoxin (GSU0720) which are implicated in the oxidative stress response. The transcriptional regulation of these genes is consistent with the role of RpoS in oxidative stress response which is additionally confirmed by the decreased tolerance of oxygen during growth of the *rpoS* mutant. (Nunez *et al.*, 2004)

During growth on Fe(III) citrate a similar change in gene expression is observed in case of *macA* suggesting that the expression is not regulated by the electron acceptor. Likewise, the expression of *ccpA* is positively regulated by RpoS in the presence of Fe(III) (Nunez *et al.*, 2006).

As the expression levels of *ccpA* and *macA* are diminished in the *rpoS* mutant (Nunez *et al.*, 2006), a decrease in the reduction of Fe(III) citrate is expected for the *rpoS* mutant if CcpA or MacA were directly involved in electron transfer to Fe(III). But the mutation in the *rpoS* gene only effected the reduction of insoluble Fe(III) and not the reduction of fumarate or soluble iron in form of Fe(III) citrate (Nunez *et al.*, 2004).

### 6.1.3 Genome Regions of *ccpA* and *macA*

The genetic arrangement of the *ccpA* region differs from that of *macA*. The region around the *ccpA* gene contains a rubrerythrin-encoding gene (GSU2814) which has been implicated in oxidative stress response in anaerobic microorganisms (Fournier *et al.*, 2003) and a glutaredoxin gene (GSU2812).



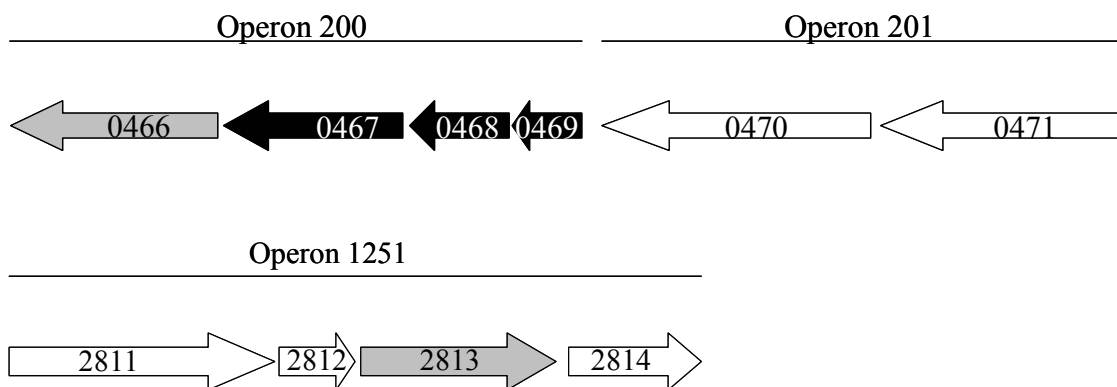


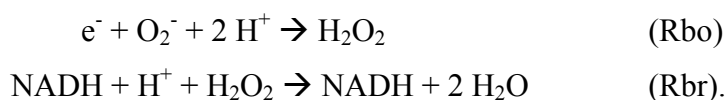
**Figure 57:** Genome region of *MacA* (GSU0466) and *CcpA* (GSU2813). GSU0467 and GSU0468 are hypothetical proteins with most similar proteins found in *G. uraniumreducens* Rf4 and *G. lovleyi* SZ (BLASTP). According to *The Institute of Genomic Research* (TIGR) GSU0469 is annotated as a hypothetical protein, GSU0470 as sigma-54 dependent response regulator and GSU0471 as sensor histidine kinase. GSU2811 is annotated as cytochrome *c* Hsc, GSU2812 as glutaredoxin family protein and GSU2814 as rubrerythrin. The operons are designated according to [www.geobacter.org/research/genomescan/Gsul\\_annotation.txt](http://www.geobacter.org/research/genomescan/Gsul_annotation.txt).

Upstream of the *macA* gene, a sigma-54 dependent response regulator and a sensor histidine kinase are located. The presence of genes encoding proteins involved in the oxidative stress response in the immediate surrounding of the *ccpA* and *macA* genes strongly indicates that both proteins are involved in stress regulation.

#### 6.1.4 Description of the *macA* Deletion Mutant

Growth experiments with the *macA* deletion mutant lead to the conclusion that *MacA* is not required for the toleration of oxidative stress (Butler *et al.*, 2004). However, *Geobacter sulfurreducens* tolerates O<sub>2</sub> (Lin *et al.*, 2004) and possesses several enzymes that putatively participate in the elimination of reactive oxygen species (Méthé *et al.*, 2003).

The superoxide dismutase (SOD) catalase oxidative stress defense system generates oxygen and hydrogen peroxide from superoxide (SOD) and subsequently catalyzes the conversion from hydrogen peroxide to oxygen and water (catalase). An alternative system consists of rubrerythrin (Rbr) and rubredoxin oxidoreductase (Rbo, also called desulfoferrodoxin) and is suggested to play a role in cytoplasmic oxidative stress response in anaerobic microorganisms (Lumppio *et al.*, 2001):



By this system, superoxide and hydrogen peroxide are reduced to water without the generation of oxygen which is especially important for the detoxification of reactive oxygen species in anaerobes. In addition to the possible presence of proteins involved in oxidative stress response, CcpA was detected in the same membrane fraction of *Geobacter sulfurreducens* as MacA (Butler *et al.*, 2004). Expression of CcpA is still possible in the *macA* mutant so that CcpA could have taken over the function of MacA. *Geobacter sulfurreducens* cells grown on ferric citrate instead of fumarate revealed a higher expression of Rbo and lower expression of SOD (Khare *et al.*, 2006). In addition, a cytosolic protein was identified as a catalase/ peroxidase in ferric iron grown but not in fumarate grown cultures, thus illustrating that the mechanism of protection against oxidative stress is differentially regulated under various growth conditions. The presence of several proteins involved in the “decomposition” of hydrogen peroxide explains that wild type cells as well as *macA* deficient mutant cells exposed to low concentrations of hydrogen peroxide survive.

The fact that growth of the *macA* mutant was significantly inhibited during growth on iron (Butler *et al.*, 2004) does not necessarily lead to the conclusion that MacA is an intermediate in the electron transfer chain to iron. On one hand, the experiments with the *macA* deletion mutant were performed with the soluble iron source Fe(III) citrate which may result in unexpected and unrecognized consequences. Furthermore, MacA might influence the expression levels of proteins directly involved in electron transfer (Kim *et al.*, 2005) leading to the observed, inhibited Fe(III) reduction in the *macA* deletion mutant.

MacA was more highly expressed during growth on Fe(III) than on fumarate (Butler *et al.*, 2004), but in another study no correlation between the expression pattern of MacA and iron (III) reduction was exhibited (Ding *et al.*, 2006). Instead, new *c*-type cytochrome candidates (GSU0105, GSU0701, GSU2515) have been discovered, that might also be involved in the electron transfer pathway to Fe(III) (Ding *et al.*, 2006).

### 6.1.5 Inspection of the *omcB* Deletion Mutant

The *omcB* deletion mutant can adapt to growth on soluble Fe(III) but not on insoluble Fe(III), pointing out that there are differences in electron transfer to soluble Fe(III) citrate and to the environmentally relevant iron oxides (Leang *et al.*, 2005). Furthermore, this study demonstrates that there are different mechanisms of electron transport to Fe(III) citrate as OmcB is not required for the growth on soluble Fe(III). The adaption of the *omcB* deletion mutant to growth on Fe(III) citrate was accompanied

by increased transcription levels of electron transfer protein encoding genes GSU0594, GSU2494, GSU2495, GSU2503 (OmcT), GSU2504, GSU2811 and GSU2813 (CcpA). Up-regulation of the *relA* homolog as well as other stress response protein encoding genes indicates that the *omcB* deletion mutant is exposed to oxidative stress, thus explaining the increased transcription levels of CcpA.

### 6.1.6 Implications for the Function of CcpA and MacA

The identification of many proteins that are putatively involved in Fe(III) reduction indicates a network of *c*-type cytochromes acting in electron transfer to insoluble iron. The finding that the disruption of one single gene impairs the Fe(III) reduction can have many reasons and does not necessarily prove the identification of an intermediate in the Fe(III) reduction pathway. The high number of *c*-type cytochromes in the genome of *Geobacter sulfurreducens* provides the possibility of several alternative electron transfer chains, depending on the physiological and metabolic state of the cells. This hypothesis is supported by the study of Ding and coworkers (2006) that illustrates the difference in expression pattern depending on the metabolic state (differences in late-log and mid-log phase cultures). Furthermore, solid iron oxides represent the most abundant electron acceptors in subsurface environments, but in most laboratory experiments soluble iron citrate is used for comparative analysis of the physiological or metabolic adaptation to the presence or absence of metals. This means that many of the observed effects may not be connected to the dissimilatory metal reduction.

It was proposed above that *Geobacter sulfurreducens* can employ different mechanisms in the reduction of Fe(III) that may involve any electron transferring protein including CcpA and MacA. But CcpA and MacA reveal *in vitro* peroxidase activity, and in addition, the transcription and expression patterns of CcpA and MacA discussed precedingly suggest that both enzymes are involved in stress response rather than in electron transfer to insoluble Fe(III) oxides.

## 6.2 Bacterial Cytochrome *c* Peroxidases

### 6.2.1 Dimer Formation

The heterologous expression of CcpA and MacA (see results 5.1) allowed an easier handling of the cells and the purification by affinity chromatography facilitated the specific purification. Size exclusion chromatography of both enzymes revealed a molecular weight of 73.94 kDa for CcpA and of 67.45 kDa for MacA resulting from

dimer formation as observed in other bacterial cytochrome *c* peroxidases (Arciero and Hooper, 1994; Gilmour *et al.*, 1994; Alves *et al.*, 1999; De Smet *et al.*, 2001). The lower value of 67.45 kDa provided by size exclusion chromatography in comparison to the calculated molecular weight of 76.58 kDa for the MacA dimer might be explained by a monomer-dimer equilibrium (Alves *et al.*, 1999) rather than by proteolysis (see results 5.5.5).

The dimeric appearance of CcpA and MacA becomes visible in the crystal packing (see figures 46 and 47). However, MacA exhibits a further, large interface in the crystal packing that has nearly the same area as the expected dimer interface. The mutation of one residue in both possible dimer interfaces did not have any effect on the retention time in size exclusion chromatography (data not shown), such that the formation of an alternative dimer cannot be excluded at this point.

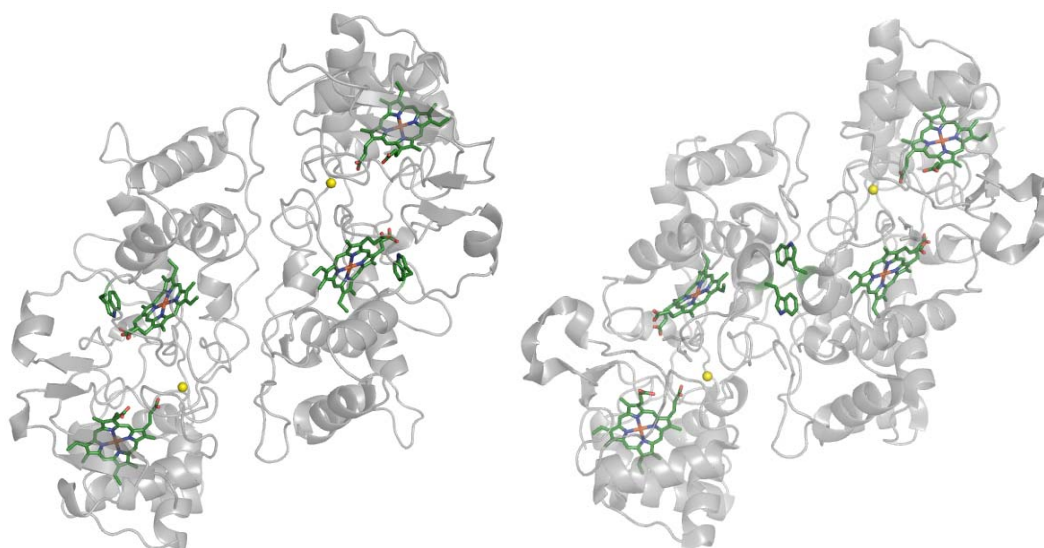


**Figure 58:** Dimer of CcpA from *Geobacter sulfurreducens* (left) and of the *Nitrosomonas europaea* (*Nie*) cytochrome *c* peroxidase. The calcium ion is colored in yellow and the heme groups are colored in green. Tryptophan 73 from CcpA and the homologous tryptophan 61 of the *Nie* cytochrome *c* peroxidase are depicted in stick mode.

Like the dimer interface in other cytochrome *c* peroxidases (Fülöp *et al.*, 1995), the dimer interface in the CcpA as well as in the MacA dimer is hydrophobic by nature. In the active form of the enzyme, the contact between the two monomers is additionally stabilized by a  $\pi$ -stacking interaction. The flexible loop of the *Nitrosomonas europaea* peroxidase carrying His59 (Shimizu *et al.*, 2001) as well as the flexible loop of the *Paracoccus pantotrophus* enzyme containing His85 (Echalier *et al.*, 2006) are oriented towards the dimer interface where the side chain of two related tryptophan residues form contact. In the structures of the oxidized forms of CcpA and MacA, the conformation of the corresponding loop places Trp73 close to the heme group.

### 6.2.2 Electron Excitation Spectra

The electron excitation spectra of MacA and CcpA show a weak absorption maximum at 640 nm in the oxidized as well as in the ascorbate-reduced and calcium-treated protein (see 5.2). This signal suggests a high spin/ low spin equilibrium of one heme group. Cytochrome *c* peroxidases of *Paracoccus denitrificans* (Gilmour *et al.*, 1993) and *Pseudomonas stutzeri* (Timoteo *et al.*, 2003) also show a weak absorption band at 630 nm that has been shown to be due to high spin/ low spin equilibrium in the high potential heme. However, the formation of the high spin state at the low potential heme is correlated to the enzyme activation in *Paracoccus denitrificans* (Gilmour *et al.*, 1994).

The cytochrome *c* peroxidase of *Pseudomonas stutzeri* exhibits no difference between the spectrum of the ascorbate-reduced and the ascorbate-reduced and calcium-treated enzyme (Timoteo *et al.*, 2003), in accordance with the calcium-independent activity of the enzyme. Obviously, the cytochrome *c* peroxidase of *Pseudomonas stutzeri* does not need additional calcium for high spin formation when the enzyme is reduced with ascorbate only. The spectra of CcpA and MacA suggest that there is a difference in the activity of untreated and calcium-treated enzyme. However, no calcium-dependent increase could be detected for the cytochrome *c* peroxidases of *Geobacter sulfurreducens* so far (see results 5.3).

### 6.2.3 The Calcium Binding Site

The calcium binding site localized in the domain interface is occupied in most of the cytochrome *c* peroxidase structures (Fülöp *et al.*, 1995; Shimizu *et al.*, 2001; Echalié *et al.*, 2006) including the CcpA and MacA structures (see results 5.6.6), but is missing in the low pH structure of the *Pseudomonas nautica* IN-form (Dias *et al.*, 2004). The protein of *Pseudomonas nautica* was crystallized at a pH value of 4 which might have caused non-physiological conformations. Hence, the oxidized and mixed valence structures of *Paracoccus pantotrophus* cytochrome *c* peroxidase (Echalié *et al.*, 2006) are consulted in the following to compare the inactive and active state of the enzyme.

The cytochrome *c* peroxidase from *Paracoccus denitrificans* was proposed to have two different calcium binding sites (Gilmour *et al.*, 1995). One is usually occupied (site I), corresponding to the calcium binding site identified in most of the structures of cytochrome *c* peroxidases, and the other is empty or only partially occupied in the oxidized enzyme (site II). Binding of Ca<sup>2+</sup> to site II of the *Paracoccus denitrificans*

enzyme corresponds to the dimerization state and is essential for the formation of the high spin state at the low potential heme (Gilmour *et al.*, 1995).

Members of the bacterial diheme cytochrome *c* peroxidases vary in the affinity of site II for  $\text{Ca}^{2+}$ . The enzymes of *Pseudomonas nautica* and *Paracoccus denitrificans* behave similarly (Alves *et al.*, 1999), but the enzymes of *Rhodobacter capsulatus* and *Pseudomonas stutzeri* do not require added  $\text{Ca}^{2+}$  for activation (De Smet *et al.*, 2001; Timoteo *et al.*, 2003).

Both enzymes from *Geobacter sulfurreducens*, MacA and CcpA, show high affinity for calcium at site I as the  $\text{Ca}^{2+}$  ion was found in the structures even without addition of calcium throughout the whole purification procedure (see 4.2.3.2, 4.2.3.3 and 5.1). The second calcium binding site proposed to be involved in dimerization (Gilmour *et al.*, 1995; Atack and Kelly, 2007) has neither been found in the structures of CcpA and MacA nor in any cytochrome *c* peroxidases structure, although CcpA and MacA form dimers (see 5.1.1 and 5.1.2).

Until now, the exact role of the second calcium binding site remains unclear because it could not be identified so far and is inconsistent through the cytochrome *c* peroxidases of different species. Furthermore, physiological concentrations of free  $\text{Ca}^{2+}$  are between 100 to 300 nM (Dominguez, 2004) and thus are much lower than the calcium concentration of 1 mM employed in the calcium treatment of the enzymes.

#### 6.2.4 Enzyme Activity

Bacterial cytochrome *c* peroxidases are located in the periplasm where their likely function is the protection of the cell against reactive oxygen species. The enzyme catalyzes the conversion of hydrogen peroxide to water by transferring electrons from electron donors such as cytochrome *c* and pseudoazurin to  $\text{H}_2\text{O}_2$  (Timoteo *et al.*, 2003; Pauleta *et al.*, 2004a; Pauleta *et al.*, 2004b). However, in *Geobacter sulfurreducens*, no homologs of putative electron donors could be identified (Butler *et al.*, 2004).

As are CcpA and MacA, the cytochrome *c* peroxidase from *Neisseria gonorrhoeae* is associated with the membrane (Turner *et al.*, 2003; Butler *et al.*, 2004), but in contrast to the *Geobacter sulfurreducens* enzymes, the *Neisseria gonorrhoeae* protein was also found membrane-associated when it was expressed heterologously in *E. coli*. It is unclear why the protein is membrane-associated (Atack and Kelly, 2007), but one possibility is that the cell keeps the enzyme in closer proximity to its electron donor in the membrane.

Due to the positively charged surface of CcpA and MacA, a peripheral association of the proteins to the membrane is possible so that electrons might be received directly from electron transport proteins located in the inner membrane, such as the cytochrome  $bc_1$  complex. A BLAST search pointed out that *Geobacter sulfurreducens* has neither a homolog of cytochrome  $c_1$  nor of cytochrome  $f$ . Instead, *Geobacter sulfurreducens* possesses unusual  $bc_1$ -complexes consisting of typical cytochrome  $b$  and iron-sulfur protein subunits, but having replaced the cytochrome  $c_1$  and cytochrome  $f$ , respectively, by a different  $c$ -type cytochrome (Yanyushin *et al.*, 2005).

Cytochrome  $c$  and the cytochrome  $c$  peroxidase are thought to interact electrostatically in *Paracoccus denitrificans*, *Pseudomonas aeruginosa* and in *Pseudomonas nautica* (Atack and Kelly, 2007). *In vitro*, horse heart cytochrome  $c$  can also act as electron donor, thus replacing the physiological electron donor in the assay (De Smet *et al.*, 2001). However, docking simulations revealed that the physiological electron donor cytochrome  $c_{550}$  of *Paracoccus denitrificans* and horse heart cytochrome  $c$  bind at different positions of the cytochrome  $c$  peroxidase, with horse heart cytochrome  $c$  between the two heme groups (Pettigrew *et al.*, 1999).

The fact that enzyme activity of CcpA and MacA could not be detected with bovine heart cytochrome  $c$  might be due to the significantly different surface potential of the two enzymes compared to other cytochrome  $c$  peroxidases (see 5.3 and 5.6.5).

The low activity of oxidized MacA (see 5.3) can be explained by the fact that the oxidized enzyme can neither provide enough reducing equivalents, nor an accessible active site. The enzyme of *Paracoccus denitrificans* is most active when the high potential heme is reduced and the low potential heme is oxidized in high spin state (Gilmour *et al.*, 1994). Reduction of the enzyme with ascorbate or diaminodurol enhances the activity 15-fold compared to the oxidized enzyme. Additional incubation with  $Ca^{2+}$  doubles the activity in *Paracoccus denitrificans* supporting the hypothesis that the mixed valence high spin form of the enzyme is the active form and  $Ca^{2+}$  promotes this state. The calcium effect can be replaced by  $Mg^{2+}$  (Gilmour *et al.*, 1994).

The specific activity of reduced CcpA and MacA is within the range of  $2 \mu\text{mol min}^{-1} \text{mg}^{-1}$  (see results 5.3) while the cytochrome  $c$  peroxidase of e.g. *Pseudomonas nautica* reveals a specific activity of  $\sim 100 \mu\text{mol min}^{-1} \text{mg}^{-1}$  (Alves *et al.*, 1999), approximately 50-fold higher. However, comparison of enzyme activities of the cytochrome  $c$  peroxidase of *Pseudomonas aeruginosa* and *Rhodobacter capsulatus* revealed a large difference as well, with a turnover number of  $90 \text{ s}^{-1}$  and  $1060 \text{ s}^{-1}$ , respectively (De Smet *et al.*, 2006). Furthermore, different enzyme activities were determined with different

electron donors (Timoteo *et al.*, 2003). The physiological electron donor of the cytochrome *c* peroxidase of *Nitrosomonas europaea* is not identified yet (Arciero and Hooper, 1994) so that the activity was determined with horse heart cytochrome *c* as electron donor. The turnover number of  $3 \text{ s}^{-1}$  shows clearly that the absolute value of the activity depends on the method. In comparison, MacA has a turnover number of  $35 \text{ s}^{-1}$ . In case of *Paracoccus denitrificans*, calcium activation was required in order to obtain optimal enzyme activity (Gilmour *et al.*, 1994). Pre-incubation had no effect on the activity of the *Pseudomonas stutzeri* enzyme with cytochrome *c*<sub>551</sub> as electron donor. The presence of calcium even inhibited the oxidation of horse heart cytochrome *c* (Timoteo *et al.*, 2003).

All these results indicate that absolute values for the enzyme activity strongly depend on the electron donor as well as on the treatment of the enzyme.

### 6.2.5 Catalytic Reaction Mechanism of Cytochrome *c* Peroxidases

The mechanism of hydrogen peroxide reduction differs within eukaryotic monoheme cytochrome *c* peroxidases and diheme bacterial cytochrome *c* peroxidases how they store oxidizing equivalents and the type of heme they use. In contrast to the eukaryotic cytochrome *c* peroxidases, the bacterial enzymes do not generate a free radical intermediate.

Several studies indicate that upon reduction of the C-terminal, high potential heme and in the presence of calcium, the active site gets accessible to the substrate (De Smet *et al.*, 2006), thus representing the active state of the enzyme. Two models of the activation mechanism have been proposed (Prazeres *et al.*, 1995; De Smet *et al.*, 2006). In the first model, the N-terminal heme represents the peroxidatic center and would switch from low spin to high spin state while the active site is accessible from the solvent upon release of the sixth heme ligand. In the second model, in addition to a spin change a ligand switch is proposed. In the low potential heme, the distal histidine would be replaced by a methionine packing in the mixed valence form of *Paracoccus pantotrophus* against one edge of the distal surface of the active site heme group (De Smet *et al.*, 2006), while the high potential heme would lose the distal methionine. In contrast to the prevailing opinion, this activation mechanism would place the active site at the high potential heme.

Structural data of the *Nitrosomonas europaea* and *Paracoccus pantotrophus* peroxidases showing that the N-terminal heme group is penta-coordinated and that the distal histidine is released in the active form of the enzyme favor the first model. In



addition, mutagenesis of the proposed switch ligand methionine to leucine in the *Rhodobacter capsulatus* enzyme results in an enzyme that is less active than the wild type. But the fact that the leucine mutant is still active supports the first model more than the second one (De Smet *et al.*, 2006).

Independent of the difference in the reaction mechanism between the *Nitrosomonas europaea* enzyme type and the other peroxidases, there is still a difference in the regulation of the accessibility for the hydrogen peroxide to the active site. The enzyme of *Nitrosomonas europaea* is unable to protect the active site in reaction to a decrease of electron supply (Pettigrew *et al.*, 2006), in contrast to the other peroxidases that can regulate the resting and the mixed valence state so that the binding of hydrogen peroxide can be avoided under conditions of insufficient electron availability.

In the structure of the active *Nitrosomonas europaea* enzyme as well as in the structure of the active *Paracoccus pantotrophus* cytochrome *c* peroxidase (Shimizu *et al.*, 2001; Echalié *et al.*, 2006), a glutamic acid is in close proximity to the active site and is proposed to act as the initial proton acceptor from hydrogen peroxide in a way similar to chloroperoxidase (Sundaramoorthy *et al.*, 1995; Sundaramoorthy *et al.*, 1998). In chloroperoxidase, the catalytic base essential to promote the cleavage of the O – O bond and thus to form compound I is glutamic acid rather than histidine as in other peroxidases (Poulos and Kraut, 1980).

This glutamic acid residue is conserved among the bacterial cytochrome *c* peroxidases. Probably due to the flexibility of the loop, the residue is missing in the oxidized structure of the *Paracoccus pantotrophus* enzyme. In the oxidized structures of MacA and CcpA, the glutamic acid is distant to the active site and need to be rearranged if the residue is considered as heterolytic catalyst. But even if the residue is missing in the oxidized *Paracoccus pantotrophus* structure, it is expected to be located in a similar way. Upon enzyme activation, the loop is rearranged and brings the glutamic acid residue in close proximity to the active center (figure 59).

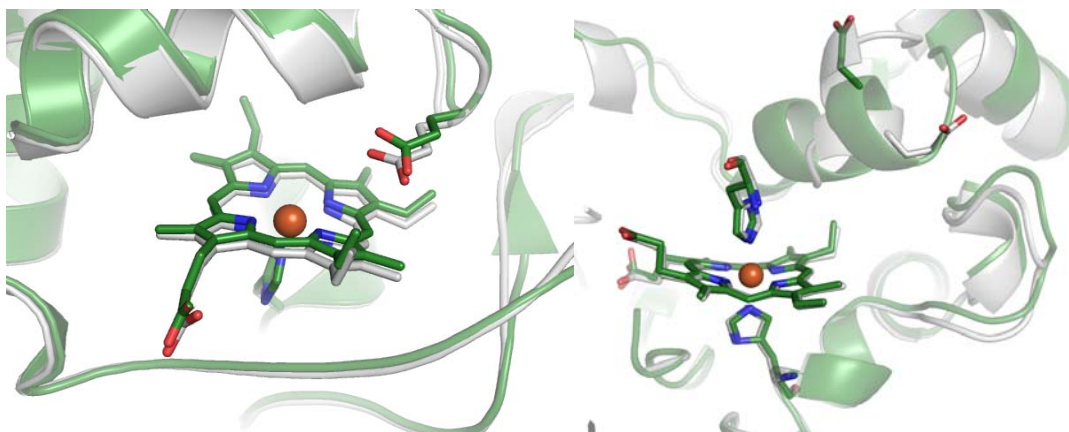


**Figure 59:** left: Glutamic acid as putative catalytic base. The heme groups, the proximal histidine and the glutamic acid are shown in stick mode. The distal histidine in the oxidized form of the cytochrome *c* peroxidase of *Nitrosomonas europaea* (green, pdb accession code 1IQC) and in the mixed valence form of the cytochrome *c* peroxidase of *Paracoccus paracoccus* (grey, pdb accession code 2C1V) is released from the heme. Right: The glutamic acid in the oxidized, inactive form of MacA (grey) and CcpA (green) points away from the active center.

Site-directed mutagenesis of the glutamic acid residue to a leucine leads to the loss of activity in *Rhodobacter capsulatus* indicating that glutamic acid is essential for the activity (De Smet *et al.*, 2006). However, the expected pH-dependent change in activity upon mutation of Glu117 to a histidine or a lysine was not observed as all the three glutamic acid mutants of *Rhodobacter capsulatus* were inactive.

Upon reduction of hydrogen peroxide, one electron is drawn from the reduced high potential heme getting re-oxidized. The second electron is extracted from the low potential heme forming an oxo-ferryl center (Ellfolk *et al.*, 1983). While one of the two substrate oxygens leaves as water, the other is bound to the iron forming the  $\text{Fe}^{\text{IV}} = \text{O}$  species of compound I. Subsequently, compound I is reduced yielding compound II. According to DeSmet *et al.* (2006), the low potential heme group then is penta-coordinated and a water molecule is released. Atack and Kelly (2007) however suggest a  $\text{Fe}^{3+} - \text{OH}$  group at the low potential heme and the release of a water molecule in a subsequent step. The final reduction of the high potential heme closes the reaction cycle.

The cytochrome *c* peroxidase of *Nitrosomonas europaea* represents the only exception known so far. In comparison to other bacterial cytochrome *c* peroxidases, the active site of the *Nitrosomonas europaea* enzyme is able to bind substrate in the oxidized state (Shimizu *et al.*, 2001; Bradley *et al.*, 2004). The suggested mechanism is more similar to that of eukaryotic cytochrome *c* peroxidases (see figure 8), as the formation of a stable radical  $\text{Fe}^{\text{IV}} = \text{O} \text{R}^{\bullet}$  is involved in the generation of compound I while the nature

of the residue R is not clear so far. However, the possibility that the  $\text{Fe}^{\text{IV}} = \text{O} \text{R}^+$  state is an intermediate as well in the other cytochrome *c* peroxidases cannot be excluded, because the reduction by an electron from the electron-transferring heme is very rapid (Pettigrew *et al.*, 2006).

### 6.2.6 Electron Transfer in Cytochrome *c* Peroxidases

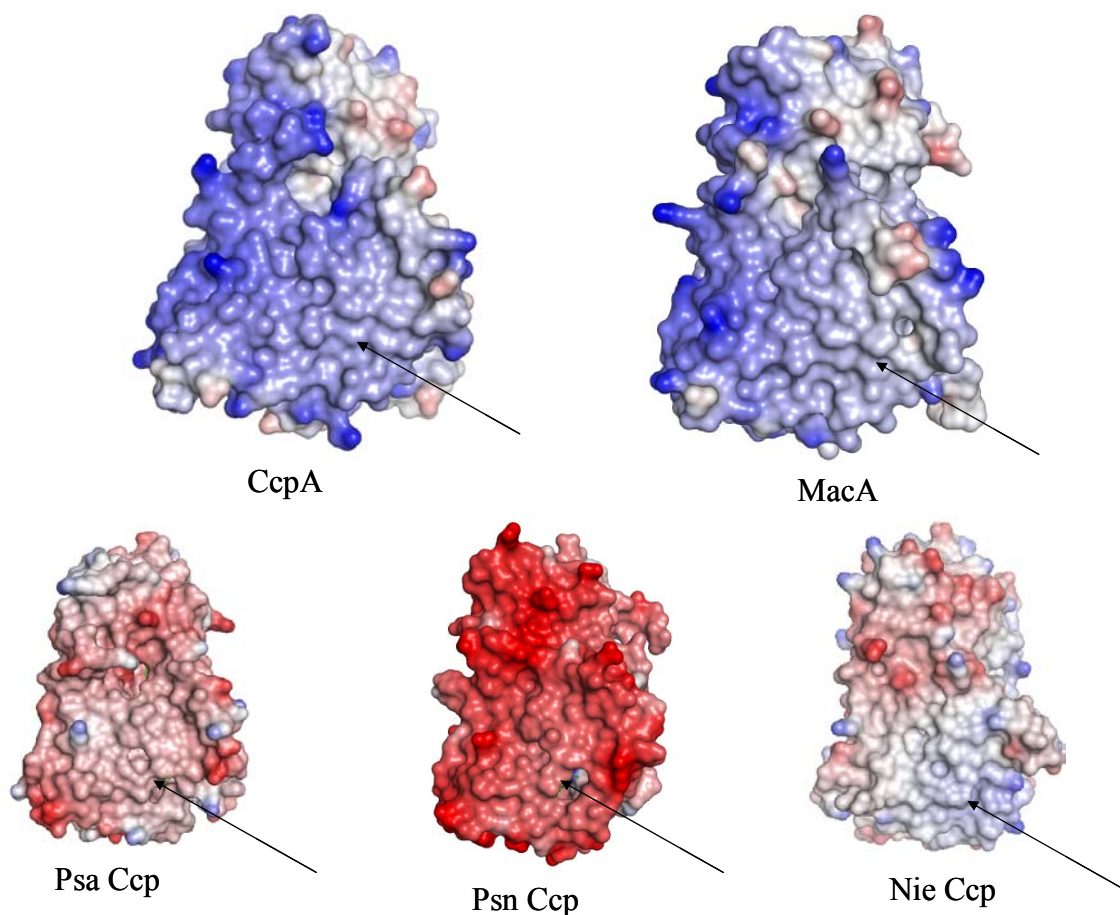


**Figure 60:** Electrostatic surface potential of several cytochrome *c* peroxidases. The cytochrome *c* peroxidases of *Geobacter sulfurreducens* are compared to the enzymes of *Pseudomonas aeruginosa* (Psa), *Pseudomonas nautica* (Psn) and *Nitrosomonas europaea* (Nie). The site of the electron transferring heme is indicated with arrows.

The high potential heme is directly accessible from the surface. The proposed interaction surfaces for the small redox proteins surround the exposed edge of the electron transferring heme. It was shown for *Paracoccus pantotrophus* that cytochrome *c* and pseudoazurin bind competitively at the same site close to the electron-transferring heme and the pair of electrons is delivered one at a time to the electron-transferring heme (Pauleta *et al.*, 2004a).

Besides the activation of the enzyme and the reaction cycle, the cytochrome *c* peroxidase enzymatic reaction involves also electron transfer between the two heme groups. Neither the heme distance nor the orientation of the cofactors is altered in the different redox states (Echalier *et al.*, 2006), so that the electrons have to overcome a distance of at least 10 Å from one propionate to the other.

Electron transfer between redox centers often occurs over distances of 10-20 Å through the mechanism of electron-tunneling (Canters, 1992; Page *et al.*, 2003). Several routes for electron transfer from the high potential heme to the low potential heme have been proposed (Fülöp *et al.*, 1995). One pathway includes the proximal histidine of the high potential heme, the protein backbone and the propionate of the low potential heme. Alternatively, the electrons could leave the heme via the propionates and reach the proximal histidine of the low potential heme via the calcium and the protein backbone. However, the most likely pathway exhibits the shortest distance and the most direct way for electron transfer via the propionates and involves the conserved tryptophan lying in the same plane as the high potential heme, perpendicular to the low potential heme. This region in between the two heme groups is conserved within the cytochrome *c* peroxidases (see figure 12 and 33) and probably reflects the precisely and optimally evolved electron-conducting pathway between the two hemes.

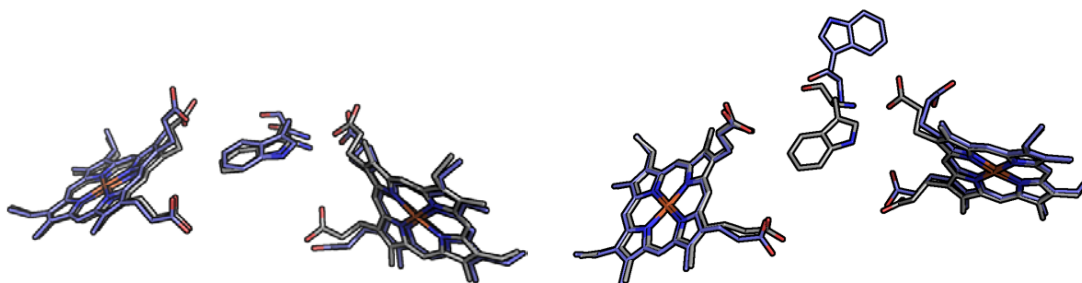


**Figure 61:** Arrangement of the heme groups and the tryptophan. Left: Oxidized (blue) and mixed valence state (grey) form of *Paracoccus pantotrophus* cytochrome *c* peroxidases. Right: IN (blue) and OUT (grey) form of *Pseudomonas nautica* cytochrome *c* peroxidases.

Comparing both crystal forms, the IN and the OUT form of *Pseudomonas nautica*, a rearrangement in the tryptophan residue thought to be involved in electron transfer occurs (Dias *et al.*, 2004). Phe93 is moving out of the pathway in the OUT form allowing Trp94 to occupy the position between both propionates. However, this conformation of Trp94 in the IN form is so far only observed in the *Pseudomonas nautica* structure and might be due to the crystallization conditions (see 6.2.3). The disruption of the calcium binding site probably causes this conformational change of the tryptophan, thus the localization of the tryptophan in between the heme groups as

observed in the structures of CcpA and MacA represents the physiological conformation.

### 6.3 RoxA

In many cases, comparing 3D structures may reveal biologically interesting similarities that are not detected by sequence comparison alone. The sequences of RoxA (74.1 kDa) and MacA (38.3 kDa) are not very similar concerning the whole amino acid sequence. However, several sequence regions are conserved.

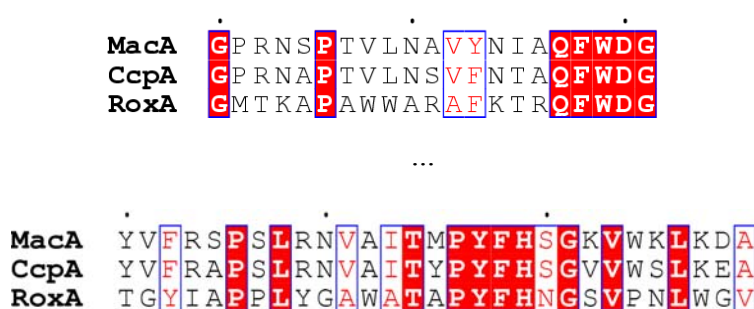


**Figure 62:** Alignment of the RoxA sequence to the sequences of the *G. sulfurreducens* peroxidases CcpA and MacA. In the upper part, the sequences of MacA and CcpA comprise residues 76-96, and the sequence of RoxA comprises residues 284-304. In the lower part, the sequences of MacA and CcpA comprise residues 243-271, and the sequence of RoxA comprises residues 499-527.

Structurally similar proteins should be detected with DALI by a multiple alignment of structural neighbours. The database search resulted in the identification of three *c*-type cytochromes with maximal Z-value of 4.7 indicating that the similarity is not very high. The sequence of RoxA has no significant similarity to any protein in the data base except for short sequence parts comprising amino acids that are located in between the two heme groups in bacterial diheme cytochrome *c* peroxidases (see figure 62) (Jendrossek and Reinhardt, 2003). However, a DALI search did not uncover structural similarities among RoxA and the cytochrome *c* peroxidases.

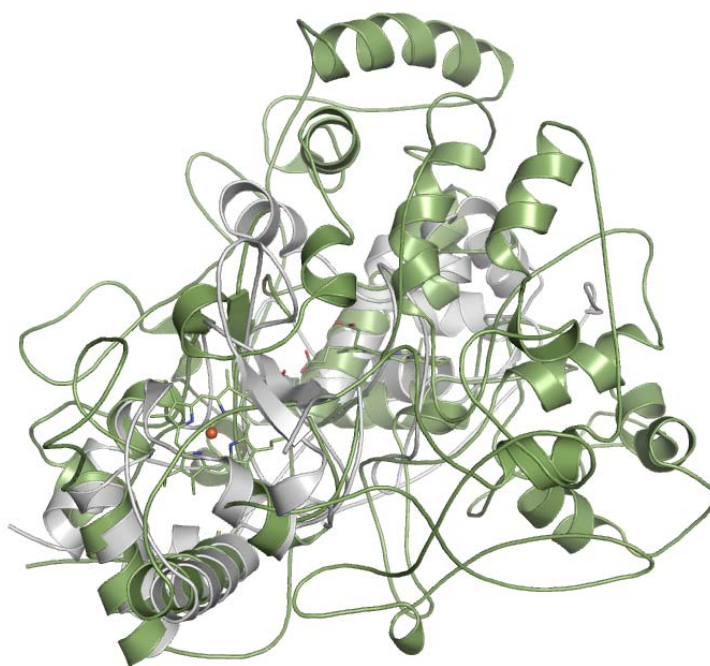


**Figure 63:** Superposition of RoxA and the cytochrome *c* peroxidase MacA from *Geobacter sulfurreducens* by fitting of the heme groups in *PYMOL*. RoxA is colored in green and the MacA monomer is colored in grey.

RoxA is monomeric and the two domain structure of MacA can be placed inside the structure of RoxA by superimposing both heme groups (see figure 63). Concerning the overall structure of RoxA and the monomer of MacA, a representative of cytochrome *c* peroxidases, the two structures are quite different. By closer examination of the amino acids around the heme groups, however, similarities among the two enzymes become apparent.

The calcium binding site is localized in the interface between the two peroxidase domains, thus serving the stability of the enzyme. In the structure of RoxA, two facing loops are arranged in a similar way, but instead of a calcium ion, a lysine interacts with the carbonyl groups of Thr512 and Pro514. The fact that this stabilization is important and promotes the right positioning of important residues in electron transfer between the hemes is shown by the IN-form of the *Pseudomonas nautica* cytochrome *c* peroxidase which lacks the calcium ion due to non-physiological crystallization conditions (see figure 61).

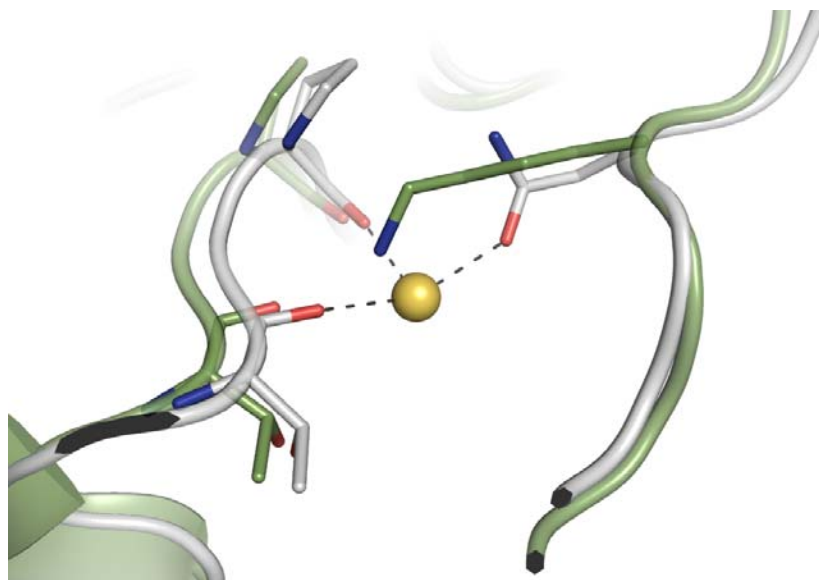


**Figure 64:** Superposition of RoxA and MacA by fitting the heme groups. MacA (grey) involves a calcium binding site in stabilizing the loops. The contact between the two loops in RoxA (green) is maintained by the interaction of lysine with two carbonyl groups (2.72 Å and 2.85 Å distances). This calcium ion is absent in the RoxA structure.

The electron-transferring heme in cytochrome *c* peroxidase is histidine-methionine coordinated and is directly accessible from the surface. In the structure of RoxA, the corresponding bis-histidinyll coordinated heme group is near the surface but is shielded from the solvent by amino acids. The second heme group is proposed to be the active site and is penta-coordinated in the crystallized form of RoxA with a histidine as proximal iron ligand.

Electron transfer between both heme groups seems to be very similar to that in bacterial cytochrome *c* peroxidases (see 6.2.6). Not only the distances between the heme groups and the orientation towards each other is homologous, but also important residues proposed to mediate electron transfer are present in the RoxA structure. Trp302 is situated between the propionates and is considered to be essential for the electron transport that runs from the bis-histidinyll coordinated heme group via the propionates and the tryptophan to the active center heme group.

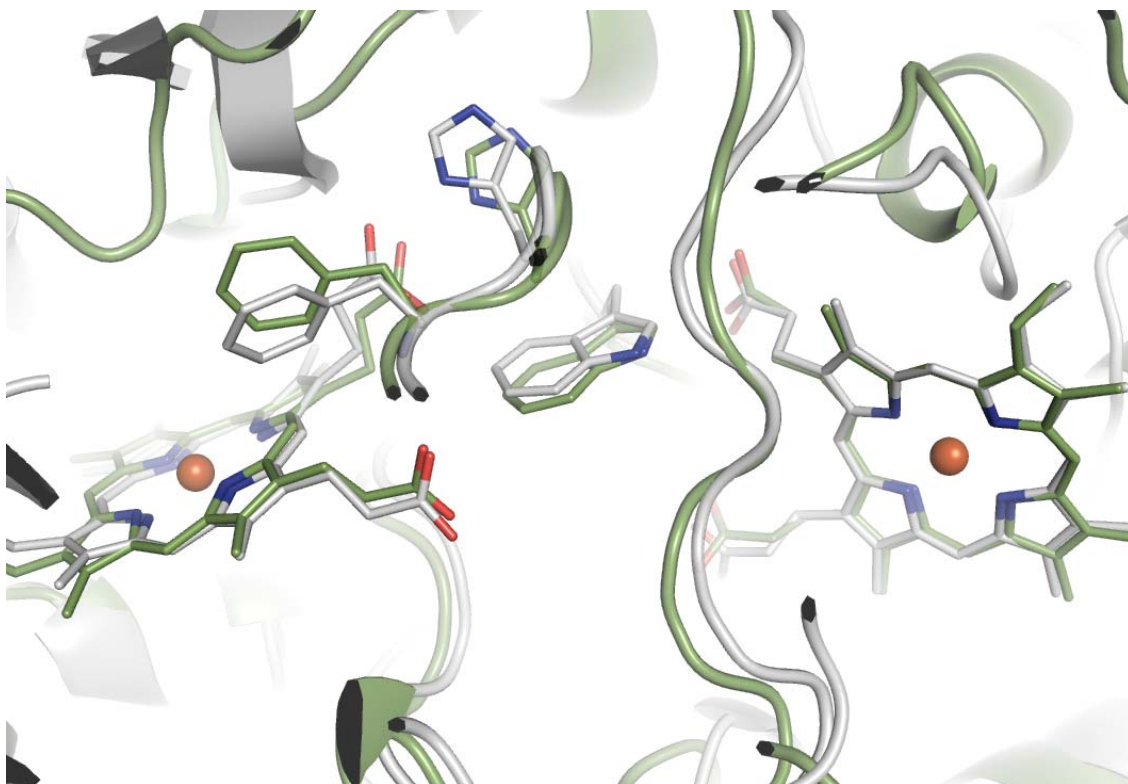


**Figure 65:** Superposition of RoxA and MacA by fitting the heme groups in *PYMOL*. View of the arrangement of the heme groups in MacA (grey) and RoxA (green). Residues with similar conformation include Trp302 (corresponding to Trp94 in MacA), His517 (corresponding to His261 in MacA) and the outlier in the Ramachandran plot Phe516 (corresponding to Phe260 in MacA, see 5.5.6).

The similarity of this region probably corresponds to a similar mode of electron transfer between the two heme groups. However, the mechanism of the reaction itself seems to be different. RoxA is suggested to catalyze a dioxygenase-mediated cleavage of natural rubber (Braaz *et al.*, 2005). The distal heme binding pocket compared to the active form of the *Paracoccus pantotrophus* cytochrome *c* peroxidase exhibits quite different residues and does not seem to be conserved.

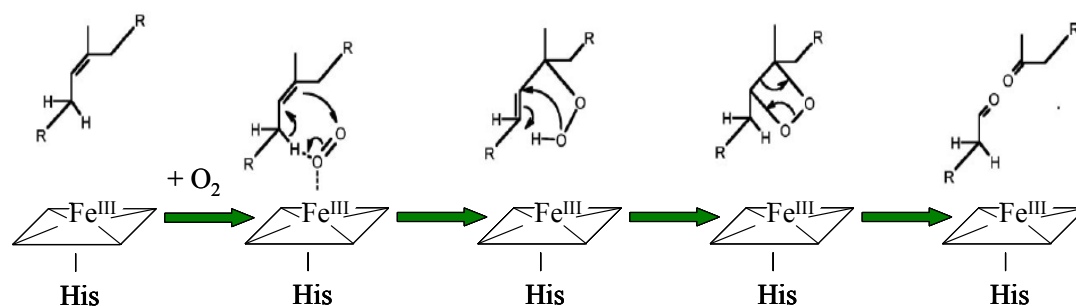


**Figure 66:** Proposed dioxygenase reaction mechanism for the cleavage of natural rubber by RoxA according to Braaz *et al.* (2005).

The access of the substrate to the active site is subject to speculations as the crystallized form of RoxA does not provide access to the active site. In order to create an accessible



reaction center, rearrangements of the protein above the free coordination site of the heme group are necessary. The access of hydrogen peroxide to the active site of the cytochrome *c* peroxidase is achieved by the movement of the loop containing the sixth heme ligand out of the protein. This enzyme activation cannot be transferred to RoxA as the structure above the heme group is totally different with compact  $\alpha$ -helices instead of a flexible loop. However, the  $\alpha$ -helices pointing up can be part of the substrate channel as many hydrophobic residues are located there. Probably, these large required rearrangements cause the low activity of 300 mU/ mg (Braaz *et al.*, 2005).

The assumption that electron transfer between the two heme groups occurs and is necessary for the reaction disagrees with the proposed dioxygenase reaction mechanism suggesting the transfer of the oxygen molecule to the substrate without electron transfer. Several possibilities explaining electron transfer during the enzymatic reaction are taken into account. The alternative that RoxA rather functions as a monooxygenase than as a dioxygenase is consistent with experimental data that do not exclude a monooxygenase mechanism (Braaz *et al.*, 2005). Alternatively, RoxA might catalyze further reactions which require electron transport. This shows that the model (see figure 66) of the dioxygenase mechanism is subject to speculations and needs to be confirmed or adapted.

Due to a similar core of the MauG protein to peroxidases, Pettigrew and coworkers (2006) suggest a different reaction mechanism as proposed by Wang *et al.* (2003) for the MauG protein. According to this, MauG binds methylamine dehydrogenase (MADH) and a reactive species generated by MauG diffuses into the interior of MADH to react with the tryptophan. However, a peroxidase reaction mechanism cannot be considered for RoxA as the protein does not exhibit peroxidase activity (Braaz *et al.*, 2005) but a similar scenario might be possible.

## 7 Danksagung

Die vorliegende Arbeit wurde in der Zeit vom Oktober 2003 bis zum März 2007 in der Abteilung für Molekulare Strukturbiologie an der Georg-August-Universität Göttingen angefertigt.

Dass die Arbeit so zustande gekommen ist, verdanke ich einer Reihe von Menschen, deren Nennung an dieser Stelle meinen Dank ausdrücken soll.

Meinem Doktorvater Prof. Dr. Oliver Einsle danke ich für die interessante Aufgabenstellung, die stetige Unterstützung während dieser Zeit, seinen hilfreichen Anregungen und nicht zuletzt gilt mein besonderer Dank seinem Vertrauen in das Projekt und mich als seine erste Doktorandin.

Herrn Prof. Dr. Ralf Ficner danke ich für die Übernahme des Korreferats.

Herrn Prof. Dr. Jendrossek und seiner Gruppe danke ich für die Kooperation bei dem RoxA-Projekt.

Antje Dickmanns danke ich für die Einarbeitung und die Hilfestellungen zu Beginn meiner Promotionszeit.

Ich danke meinen Laborkollegen Anja, Peer und Haitham für die stets angenehme und lustige Arbeitsatmosphäre im Labor und Daniel speziell für die Hilfe mit Pymol.

Bedanken möchte ich mich weiterhin bei allen Kolleginnen und Kollegen der Abteilung Molekulare Strukturbiologie, die mir hilfreich zur Seite gestanden haben, bei Susana, Wei, Sarah, Andreas und insbesondere bei Julia, die immer auch spannende außeruniversitäre Unternehmungen organisiert und nicht nur mir damit die Promotionszeit äußerst angenehm und abwechslungsreich gestaltet hat.

Meinen anderen bereits promovierten ehemaligen Mitstreitern Jóhanna, Tine und José, die nun in alle Lande verstreut sind, danke ich für unvergessliche DoKo-Abende.

And last but not least danke ich meinen Freunden und meiner Familie für Anregungen und den stetigen Zuspruch, der zum Gelingen dieser Arbeit beigetragen hat. Insbesondere gilt Malte der Dank, der mich in jeder Phase der Doktorarbeit unterstützt und insbesondere die letzten Wochen mit stoischer Ruhe ertragen hat. Vielen Dank!

## 8 Abbreviations

Å	Ångström
ABTS	2,2'-azino-bis(3-ethylbenzthiazoline-6-sulfonic acid)
APS	ammonium persulfate
BCA	bicinchoninic acid
bp	base pairs
ccm	cytochrome <i>c</i> maturation
Ccp	cytochrome <i>c</i> peroxidase
Da	Dalton
DESY	Deutsches Elektronen-Synchrotron
DMRB	dissimilatory metal-reducing bacteria
DMSO	dimethyl sulfoxide
DNA	deoxyribonucleic acid
dNTP	deoxy-nucleoside-triphosphate
EDTA	(Ethylenedinitrilo)tetraacetic acid
EMBL	European Molecular Biology Laboratory
Fe	iron
HEPES	4-(2-Hydroxyethyl)piperazine-1-ethanesulfonic acid
HP	high potential
IPTG	Isopropyl $\beta$ -D-thiogalactoside
$K_M$	Michaelis constant
LB	Luria Bertani medium
LP	low potential
MAD	multiwavelength anomalous dispersion
Mn	manganese
MOPS	3-(N-Morpholino)propanesulfonic acid
mRNA	messenger RNA
NADH	nicotinamide adenine dinucleotide, reduced form
OD <sub>600</sub>	optical density at 600 nm
PAGE	polyacrylamide gel electrophoresis
PCR	polymerase chain reaction
pdb	The RCSB Protein Data Bank
PEG	polyethylene glycol

RNA	ribonucleic acid
r.m.s.d.	root-mean-square deviation
SDS	sodium dodecyl sulfate
TAE	Tris-acetate-EDTA
Tc	Technetium
TE	Tris-EDTA
TEMED	1,2-Bis(dimethylamino)ethane
TMAO	trimethylamine N-oxide
TMBZ	3,3',5,5'-tetramethylbenzidine
Tris	Tris(hydroxymethyl)aminomethane
U	uranium
v/v	volume per volume
w/v	weight per volume
x g	times gravity

### Amino acids

A	Ala	alanine	M	Met	methionine
C	Cys	cysteine	N	Asn	asparagine
D	Asp	aspartate	P	Pro	proline
E	Glu	glutamate	Q	Gln	glutamine
F	Phe	phenylalanine	R	Arg	arginine
G	Gly	glycine	S	Ser	serine
H	His	histidine	T	Thr	threonine
I	Ile	isoleucine	V	Val	valine
K	Lys	lysine	W	Trp	tryptophan
L	Leu	leucine	Y	Tyr	tyrosine

## 9 References

- Ahuja, U. and Thöny-Meyer, L.** (2005). CcmD is involved in complex formation between CcmC and the heme chaperone CcmE during cytochrome c maturation. *J Biol Chem.* **280.** 236-43.
- Altschul, S. F., Madden, T. L., Schaffer, A. A., Zhang, J., Zhang, Z., Miller, W. and Lipman, D. J.** (1997). Gapped BLAST and PSI-BLAST: a new generation of protein database search programs. *Nucleic Acids Res.* **25.** 3389-402.
- Alves, T., Besson, S., Duarte, L. C., Pettigrew, G. W., Girio, F. M., Devreese, B., Vandenberghe, I., Van Beeumen, J., Fauque, G. and Moura, I.** (1999). A cytochrome c peroxidase from *Pseudomonas nautica* 617 active at high ionic strength: expression, purification and characterization. *Biochim Biophys Acta.* **1434.** 248-59.
- Arciero, D. M. and Hooper, A. B.** (1994). A di-heme cytochrome c peroxidase from *Nitrosomonas europaea* catalytically active in both the oxidized and half-reduced states. *J Biol Chem.* **269.** 11878-86.
- Arslan, E., Schulz, H., Zufferey, R., Kunzler, P. and Thony-Meyer, L.** (1998). Overproduction of the *Bradyrhizobium japonicum* c-type cytochrome subunits of the cbb3 oxidase in *Escherichia coli*. *Biochem Biophys Res Commun.* **251.** 744-7.
- Atack, J. M. and Kelly, D. J.** (2007). Structure, mechanism and physiological roles of bacterial cytochrome c peroxidases. *Adv Microb Physiol.* **52.** 73-106.
- Barker, P. D. and Ferguson, S. J.** (1999). Still a puzzle: why is haem covalently attached in c-type cytochromes? *Structure.* **7.** R281-90.
- Bendtsen, J. D., Nielsen, H., von Heijne, G. and Brunak, S.** (2004). Improved prediction of signal peptides: SignalP 3.0. *J Mol Biol.* **340.** 783-95.
- Bjellqvist, B., Hughes, G. J., Pasquali, C., Paquet, N., Ravier, F., Sanchez, J. C., Frutiger, S. and Hochstrasser, D.** (1993). The focusing positions of polypeptides in immobilized pH gradients can be predicted from their amino acid sequences. *Electrophoresis.* **14.** 1023-31.
- Bond, D. R. and Lovley, D. R.** (2003). Electricity production by *Geobacter sulfurreducens* attached to electrodes. *Appl Environ Microbiol.* **69.** 1548-55.
- Braaz, R., Armbruster, W. and Jendrossek, D.** (2005). Heme-dependent rubber oxygenase RoxA of *Xanthomonas* sp. cleaves the carbon backbone of poly(cis-1,4-Isoprene) by a dioxygenase mechanism. *Appl Environ Microbiol.* **71.** 2473-8.

**Braaz, R., Fischer, P. and Jendrossek, D.** (2004). Novel type of heme-dependent oxygenase catalyzes oxidative cleavage of rubber (poly-cis-1,4-isoprene). *Appl Environ Microbiol.* **70.** 7388-95.

**Bradley, A. L., Chobot, S. E., Arciero, D. M., Hooper, A. B. and Elliott, S. J.** (2004). A distinctive electrocatalytic response from the cytochrome c peroxidase of *Nitrosomonas europaea*. *J Biol Chem.* **279.** 13297-300.

**Braeken, K., Moris, M., Daniels, R., Vanderleyden, J. and Michiels, J.** (2006). New horizons for (p)ppGpp in bacterial and plant physiology. *Trends Microbiol.* **14.** 45-54.

**Brünger, A. T.** (1992). Free R value: a novel statistical quantity for assessing the accuracy of crystal structures. *Nature.* **355.** 472-475.

**Brünger, A. T., Adams, P. D., Clore, G. M., DeLano, W. L., Gros, P., Grosse-Kunstleve, R. W., Jiang, J. S., Kuszewski, J., Nilges, M., Pannu, N. S., Read, R. J., Rice, L. M., Simonson, T. and Warren, G. L.** (1998). Crystallography & NMR system: A new software suite for macromolecular structure determination. *Acta Crystallogr D Biol Crystallogr.* **54.** 905-21.

**Bushnell, G. W., Louie, G. V. and Brayer, G. D.** (1990). High-resolution three-dimensional structure of horse heart cytochrome c. *J Mol Biol.* **214.** 585-95.

**Butler, A.** (1998). Acquisition and utilization of transition metal ions by marine organisms. *Science.* **281.** 207-10.

**Butler, J. E., Kaufmann, F., Coppi, M. V., Nunez, C. and Lovley, D. R.** (2004). MacA, a diheme c-type cytochrome involved in Fe(III) reduction by *Geobacter sulfurreducens*. *J Bacteriol.* **186.** 4042-5.

**Caccavo, F., Jr., Lonergan, D. J., Lovley, D. R., Davis, M., Stolz, J. F. and McInerney, M. J.** (1994). *Geobacter sulfurreducens* sp. nov., a hydrogen- and acetate-oxidizing dissimilatory metal-reducing microorganism. *Appl Environ Microbiol.* **60.** 3752-9.

**Chatterji, D. and Ojha, A. K.** (2001). Revisiting the stringent response, ppGpp and starvation signaling. *Curr Opin Microbiol.* **4.** 160-5.

**Chen, Y.-R., Deterding, L. J., Sturgeon, B. E., Tomer, K. B. and Mason, R. P.** (2002). Protein oxidation of cytochrome c by reactive halogen species enhances its peroxidase activity. *JBC.* **277.**

**Childers, S. E., Ciuffo, S. and Lovley, D. R.** (2002). *Geobacter metallireducens* accesses insoluble Fe(III) oxide by chemotaxis. *Nature.* **416.** 767-9.

**Childs, R. E. and Bardsley, W. G.** (1975). The steady-state kinetics of peroxidase with 2,2'-azino-di-(3-ethyl-benzthiazoline-6-sulphonic acid) as chromogen. *Biochem. J.* **145**. 93-103.

**Coates, J. D., Phillips, E. J., Lonergan, D. J., Jenter, H. and Lovley, D. R.** (1996). Isolation of *Geobacter* species from diverse sedimentary environments. *Appl Environ Microbiol.* **62**. 1531-6.

**Collaborative Computational Project, Number 4** (1994). The CCP4 suite: programs for protein crystallography. *Acta Crystallogr D Biol Crystallogr.* **50**. 760-3.

**Coppi, M. V., Leang, C., Sandler, S. J. and Lovley, D. R.** (2001). Development of a genetic system for *Geobacter sulfurreducens*. *Appl Environ Microbiol.* **67**. 3180-7.

**Coppi, M. V., O'Neil, R. A. and Lovley, D. R.** (2004). Identification of an uptake hydrogenase required for hydrogen-dependent reduction of Fe(III) and other electron acceptors by *Geobacter sulfurreducens*. *J Bacteriol.* **186**. 3022-8.

**Daily, H. A.** (1997). Enzymes of heme biosynthesis. *JBIC.* **2**. 411-417.

**De Smet, L., Pettigrew, G. W. and Van Beeumen, J. J.** (2001). Cloning, overproduction and characterization of cytochrome c peroxidase from the purple phototrophic bacterium *Rhodobacter capsulatus*. *Eur J Biochem.* **268**. 6559-68.

**De Smet, L., Savvides, S. N., Van Horen, E., Pettigrew, G. and Van Beeumen, J. J.** (2006). Structural and mutagenesis studies on the cytochrome c peroxidase from *Rhodobacter capsulatus* provide new insights into structure-function relationships of bacterial di-heme peroxidases. *J Biol Chem.* **281**. 4371-9.

**DeLano, W. L.** (2002). The PyMOL Molecular Graphics System.  
<http://www.pymol.org>.

**Dias, J. M., Alves, T., Bonifacio, C., Pereira, A. S., Trincao, J., Bourgeois, D., Moura, I. and Romao, M. J.** (2004). Structural basis for the mechanism of Ca(2+) activation of the di-heme cytochrome c peroxidase from *Pseudomonas nautica* 617. *Structure.* **12**. 961-73.

**DiChristina, T. J.** (2005). Enzymology of electron transport: energy generation with geochemical consequences. *Reviews in Mineralogy and Geochemistry.* **59**. 27-52.

**DiChristina, T. J., Arnold, R. G., Lidstrom, M. E. and Hoffmann, M. R.** (1988). Dissimilative iron reduction by the marine eubacterium *Alteromonas putrefaciens* strain 200. *Water science and technology.* **20**. 69-79.

**DiDonato, L. N., Sullivan, S. A., Methe, B. A., Nevin, K. P., England, R. and Lovley, D. R.** (2006). Role of RelGsu in stress response and Fe(III) reduction in *Geobacter sulfurreducens*. *J Bacteriol.* **188**. 8469-78.

**Ding, Y. H., Hixson, K. K., Giometti, C. S., Stanley, A., Esteve-Nunez, A., Khare, T., Tollaksen, S. L., Zhu, W., Adkins, J. N., Lipton, M. S., Smith, R. D., Mester, T. and Lovley, D. R.** (2006). The proteome of dissimilatory metal-reducing microorganism *Geobacter sulfurreducens* under various growth conditions. *Biochim Biophys Acta*. **1764**. 1198-206.

**Dominguez, D. C.** (2004). Calcium signalling in bacteria. *Molecular Microbiology*. **54**. 291-297.

**Echalier, A., Goodhew, C. F., Pettigrew, G. W. and Fulop, V.** (2004). Crystallization and preliminary X-ray diffraction analysis of a dihaem cytochrome c peroxidase from *Paracoccus denitrificans*. *Acta Crystallogr D Biol Crystallogr*. **60**. 331-3.

**Echalier, A., Goodhew, C. F., Pettigrew, G. W. and Fülöp, V.** (2006). Activation and catalysis of the di-heme cytochrome c peroxidase from *Paracoccus pantotrophus*. *Structure*. **14**. 107-17.

**Einsle, O., Stach, P., Messerschmidt, A., Simon, J., Kroger, A., Huber, R. and Kroneck, P. M.** (2000). Cytochrome c nitrite reductase from *Wolinella succinogenes*. Structure at 1.6 Å resolution, inhibitor binding, and heme-packing motifs. *J Biol Chem*. **275**. 39608-16.

**Ellfolk, N., Ronnberg, M., Aasa, R., Andreasson, L. E. and Vanngard, T.** (1983). Properties and function of the two hemes in *Pseudomonas* cytochrome c peroxidase. *Biochim Biophys Acta*. **743**. 23-30.

**Ellfolk, N. and Soininen, R.** (1970). *Pseudomonas* cytochrome c peroxidase. I. Purification procedure. *Acta Chem Scand*. **24**. 2126-36.

**Emsley, P. and Cowtan, K.** (2004). Coot: model-building tool for molecular graphics. *Acta Cryst*. **D60**. 2126-2132.

**Eng, A. H., Kawahara, S. and Tanaka, Y.** (1994). Trans-isoprene units in natural rubber. *Rubb.Chem.Technol*. **67**. 159-168.

**Esteve-Núñez, A., Núñez, C. and Lovley, D. R.** (2004). Preferential reduction of FeIII over fumarate by *Geobacter sulfurreducens*. *J Bacteriol*. **186**. 2897-9.

**Fita, I. and Rossmann, M. G.** (1985). The NADPH binding site on beef liver catalase. *Proc Natl Acad Sci U S A*. **82**. 1604-8.

**Foote, N., Peterson, J., Gadsby, P. M., Greenwood, C. and Thomson, A. J.** (1984). A study of the oxidized form of *Pseudomonas aeruginosa* cytochrome c-551 peroxidase with the use of magnetic circular dichroism. *Biochem J*. **223**. 369-78.

**Fournier, M., Zhang, Y., Wildschut, J. D., Dolla, A., Voordouw, J. K., Schriemer, D. C. and Voordouw, G.** (2003). Function of oxygen resistance proteins in the



anaerobic, sulfate-reducing bacterium *Desulfovibrio vulgaris hildenborough*. *J Bacteriol.* **185**. 71-9.

**Fülöp, V., Ridout, C. J., Greenwood, C. and Hajdu, J.** (1995). Crystal structure of the di-haem cytochrome c peroxidase from *Pseudomonas aeruginosa*. *Structure.* **3**. 1225-33.

**Garman, E. and Owen, R. L.** (2006). Cryocrystallography of macromolecules: practice and optimization. *Methods Mol Biol.* **364**. 1-18.

**Gilmour, R., Goodhew, C. F., Pettigrew, G. W., Prazeres, S., Moura, I. and Moura, J. J.** (1993). Spectroscopic characterization of cytochrome c peroxidase from *Paracoccus denitrificans*. *Biochem J.* **294 (Pt 3)**. 745-52.

**Gilmour, R., Goodhew, C. F., Pettigrew, G. W., Prazeres, S., Moura, J. J. and Moura, I.** (1994). The kinetics of the oxidation of cytochrome c by *Paracoccus* cytochrome c peroxidase. *Biochem J.* **300 (Pt 3)**. 907-14.

**Gilmour, R., Prazeres, S., McGinness, D. F., Goodhew, C. F., Moura, J. J., Moura, I. and Pettigrew, G. W.** (1995). The affinity and specificity of Ca(2+)-binding sites of cytochrome-c peroxidase from *Paracoccus denitrificans*. *Eur J Biochem.* **234**. 878-86.

**Goodhew, C. F., Brown, K. R. and Pettigrew, G. W.** (1986). Heme staining in gels, a useful tool in the study of bacterial c-type cytochromes. *BBA.* **852**. 288-294.

**Goodhew, C. F., Wilson, I. B., Hunter, D. J. and Pettigrew, G. W.** (1990). The cellular location and specificity of bacterial cytochrome c peroxidases. *Biochem J.* **271**. 707-12.

**Gordon, E. H., Pike, A. D., Hill, A. E., Cuthbertson, P. M., Chapman, S. K. and Reid, G. A.** (2000). Identification and characterization of a novel cytochrome c(3) from *Shewanella frigidimarina* that is involved in Fe(III) respiration. *Biochem J.* **349**. 153-8.

**Green, D. W., Ingram, V. M. and Perutz, M. F.** (1954). The structure of hemoglobin.IV. Sign determination by the isomorphous replacement method. *Proc.Roy.Soc.A.* **225**. 287-307.

**Hanlon, S. P., Holt, R. A. and McEwan, A. G.** (1992). The 44 kDa c-type cytochrome induced in *Rhodobacter capsulatus* during growth with dimethylsulphoxide as an electron acceptor is cytochrome c peroxidase. *FEMS Microbiol Lett.* **97**. 283-288.

**Heitmann, D. and Einsle, O.** (2005). Structural and biochemical characterization of DHC2, a novel diheme cytochrome c from *Geobacter sulfurreducens*. *Biochemistry.* **44**. 12411-9.

- Hendrickson, W. A., Smith, J. L., Phizackerley, R. P. and Merritt, E. A.** (1988). Crystallographic structure analysis of lamprey hemoglobin from anomalous dispersion of synchrotron radiation. *Proteins*. **4**. 77-88.
- Holm, L. and Sander, C.** (1993). Protein structure comparison by alignment of distance matrices. *J Mol Biol*. **233**. 123-38.
- Honig, B. and Nicholls, A.** (1995). Classical electrostatics in biology and chemistry. *Science*. **268**. 1144-9.
- Huston, W. M., Harhangi, H. R., Leech, A. P., Butler, C. S., Jetten, M. S., Op den Camp, H. J. and Moir, J. W.** (2007). Expression and characterisation of a major c-type cytochrome encoded by gene *kustc0563* from *Kuenenia stuttgartiensis* as a recombinant protein in *Escherichia coli*. *Protein Expr Purif*. **51**. 28-33.
- Ibbi-Nivol, C., Crooke, H., Griffiths, L., Grove, J., Hussain, H., Pommier, J., Mejean, V. and Cole, J. A.** (1994). A reassessment of the range of c-type cytochromes synthesized by *Escherichia coli* K-12. *FEMS Microbiol Lett*. **119**. 89-94.
- Jahn, D., Verkamp, E. and Söll, D.** (1991). Glutamyl transfer RNA: a precursor of heme and chlorophyll biosynthesis. *Trends Biochem. Sci*. **17**. 215-218.
- Jendrossek, D. and Reinhardt, S.** (2003). Sequence analysis of a gene product synthesized by *Xanthomonas* sp. during growth on natural rubber latex. *FEMS Microbiol Lett*. **224**. 61-5.
- Kaim, W. and Schwederski, B.** (2004). Bioanorganische Chemie. Zur Funktion chemischer Elemente in Lebensprozessen. Stuttgart, Teubner.
- Kane, S. R., Beller, H. R., Legler, T. C. and Anderson, R. T.** (2002). Biochemical and genetic evidence of benzylsuccinate synthase in toluene-degrading, ferric iron-reducing *Geobacter metallireducens*. *Biodegradation*. **13**. 149-54.
- Kappler, A. and Straub, K. L.** (2005). Geomicrobiological cycling of iron. *Reviews in Mineralogy and Geochemistry*. **59**. 85-108.
- Khare, T., Esteve-Nunez, A., Nevin, K. P., Zhu, W., Yates, J. R., 3rd, Lovley, D. and Giometti, C. S.** (2006). Differential protein expression in the metal-reducing bacterium *Geobacter sulfurreducens* strain PCA grown with fumarate or ferric citrate. *Proteomics*. **6**. 632-40.
- Kim, B. C., Leang, C., Ding, Y. H., Glaven, R. H., Coppi, M. V. and Lovley, D. R.** (2005). OmcF, a putative c-Type monoheme outer membrane cytochrome required for the expression of other outer membrane cytochromes in *Geobacter sulfurreducens*. *J Bacteriol*. **187**. 4505-13.

- Kissinger, C. R., Gehlhaar, D. K. and Fogel, D. B.** (1999). Rapid automated molecular replacement by evolutionary search. *Acta Crystallogr D Biol Crystallogr.* **55**. 484-91.
- Kleywegt, G. J.** (1996). Use of non-crystallographic symmetry in protein structure refinement. *Acta Cryst.* **D52**. 842-857.
- Kleywegt, G. J. and Read, R. J.** (1997). Not your average density. *Structure.* **5**. 1557-1569.
- Kraemer, S. M., Butler, A., Borer, P. and Cervini-Silva, J.** (2005). Siderophores and the dissolution of iron-bearing minerals in marine systems. *Reviews in Mineralogy and Geochemistry.* **59**. 53-84.
- Kranz, R., Lill, R., Goldman, B., Bonnard, G. and Merchant, S.** (1998). Molecular mechanisms of cytochrome c biogenesis: three distinct systems. *Mol Microbiol.* **29**. 383-96.
- La Fortelle, E. d., Irwin, J. J. and Bricogne, G.** (1997). SHARP: A maximum-likelihood heavy-atom parameter refinement and phasing program for the MIR and MAD methods. *Crystallograoh.Comp.* **7**. 1-9.
- Laemmli, U. K.** (1970). Cleavage of structural proteins during the assembly of the head of bacteriophage T4. *Nature.* **227**. 680-5.
- Laskowski, R. A., MacArthur, M. W., Moss, D. S. and Thornton, J. M.** (1993). Procheck: a program to check the stereochemical quality of protein structures. *J.Appl.Cryst.* **26**. 283-291.
- Leang, C., Adams, L. A., Chin, K. J., Nevin, K. P., Methe, B. A., Webster, J., Sharma, M. L. and Lovley, D. R.** (2005). Adaptation to disruption of the electron transfer pathway for Fe(III) reduction in *Geobacter sulfurreducens*. *J Bacteriol.* **187**. 5918-26.
- Leang, C., Coppi, M. V. and Lovley, D. R.** (2003). OmcB, a c-type polyheme cytochrome, involved in Fe(III) reduction in *Geobacter sulfurreducens*. *J Bacteriol.* **185**. 2096-103.
- Lee, B. and Richards, F. M.** (1971). The interpretation of protein structures: Estimation of static accessibility. *J.Mol.Biol.* **55**. 379-400.
- Lin, W. C., Coppi, M. V. and Lovley, D. R.** (2004). *Geobacter sulfurreducens* can grow with oxygen as a terminal electron acceptor. *Appl Environ Microbiol.* **70**. 2525-8.
- Lloyd, J. R., Leang, C., Hodges Myerson, A. L., Coppi, M. V., Cuifo, S., Methe, B., Sandler, S. J. and Lovley, D. R.** (2003). Biochemical and genetic characterization of

- PpcA, a periplasmic c-type cytochrome in *Geobacter sulfurreducens*. *Biochem J.* **369**. 153-61.
- Londer, Y. Y., Pokkuluri, P. R., Erickson, J., Orshonsky, V. and Schiffer, M.** (2005). Heterologous expression of hexaheme fragments of a multidomain cytochrome from *Geobacter sulfurreducens* representing a novel class of cytochromes c. *Protein Expr Purif.* **39**. 254-60.
- Lovley, D. R.** (1993). Dissimilatory metal reduction. *Annu Rev Microbiol.* **47**. 263-90.
- Lovley, D. R.** (2001). Bioremediation. Anaerobes to the rescue. *Science.* **293**. 1444-6.
- Lovley, D. R.** (2002). Analysis of the genetic potential and gene expression of microbial communities involved in the in situ bioremediation of uranium and harvesting electrical energy from organic matter. *Omics.* **6**. 331-9.
- Lovley, D. R., Giovannoni, S. J., White, D. C., Champine, J. E., Phillips, E. J., Gorby, Y. A. and Goodwin, S.** (1993). *Geobacter metallireducens* gen. nov. sp. nov., a microorganism capable of coupling the complete oxidation of organic compounds to the reduction of iron and other metals. *Arch Microbiol.* **159**. 336-44.
- Lovley, D. R., Holmes, D. E. and Nevin, K. P.** (2004). Dissimilatory Fe(III) and Mn(IV) reduction. *Adv Microb Physiol.* **49**. 219-86.
- Lu, Y.** (2006). Biosynthetic Inorganic Chemistry. *Angew.Chem:Int.Ed.* **45**. 5588-5601.
- Lumppio, H. L., Shenvi, N. V., Summers, A. O., Voordouw, G. and Kurtz, D. M., Jr.** (2001). Rubrerythrin and rubredoxin oxidoreductase in *Desulfovibrio vulgaris*: a novel oxidative stress protection system. *J Bacteriol.* **183**. 101-8.
- Madigan, M. T., Martinko, J. M. and Parker, J.** (2002). Brock. Mikrobiologie. Heidelberg, Berlin, Spektrum Akademischer Verlag.
- Magnusson, L. U., Farewell, A. and Nyström, T.** (2005). ppGpp: a global regulator in *Escherichia coli*. *TRENDS in Microbiology.* **13**. 236-242.
- Matthews, B. W.** (1968). Solvent content of protein crystals. *J Mol Biol.* **33**. 491-7.
- Mehta, T., Coppi, M. V., Childers, S. E. and Lovley, D. R.** (2005). Outer membrane c-type cytochromes required for Fe(III) and Mn(IV) oxide reduction in *Geobacter sulfurreducens*. *Appl Environ Microbiol.* **71**. 8634-41.
- Méthé, B. A., Nelson, K. E., Eisen, J. A., Paulsen, I. T., Nelson, W., Heidelberg, J. F., Wu, D., Wu, M., Ward, N., Beanan, M. J., Dodson, R. J., Madupu, R., Brinkac, L. M., Daugherty, S. C., DeBoy, R. T., Durkin, A. S., Gwinn, M., Kolonay, J. F., Sullivan, S. A., Haft, D. H., Selengut, J., Davidsen, T. M., Zafar, N., White, O., Tran, B., Romero, C., Forberger, H. A., Weidman, J., Khouri, H., Feldblyum, T.**

- V., Utterback, T. R., Van Aken, S. E., Lovley, D. R. and Fraser, C. M. (2003).** Genome of *Geobacter sulfurreducens*: metal reduction in subsurface environments. *Science*. **302**. 1967-9.
- Moore, G. R. and Pettigrew, G. W. (1990).** Cytochromes c. Evolutionary, structural and physicochemical aspects. Berlin, Germany, Springer-Verlag.
- Mullis, K. B. and Faloona, F. A. (1987).** Specific synthesis of DNA in vitro via a polymerase-catalyzed chain reaction. *Methods Enzymol.* **155**. 335-50.
- Murshudov, G. N., Vagin, A. A. and Dodson, E. J. (1997).** Refinement of macromolecular structures by the maximum-likelihood method. *Acta Crystallogr D Biol Crystallogr.* **53**. 240-55.
- Myers, J. M. and Myers, C. R. (2002).** Genetic complementation of an outer membrane cytochrome *omcB* mutant of *Shewanella putrefaciens* MR-1 requires *omcB* plus downstream DNA. *Appl Environ Microbiol.* **68**. 2781-93.
- Navaza, J. (1994).** AMoRe: an automated package for molecular replacement. *Acta Cryst.* **A50**. 157-163.
- Nelson, D. P. and Kiesow, L. A. (1972).** Enthalpy of decomposition of hydrogen peroxide by catalase at 25 degrees C (with molar extinction coefficients of H<sub>2</sub>O<sub>2</sub> solutions in the UV). *Anal Biochem.* **49**. 474-8.
- Newman, D. K. and Kolter, R. (2000).** A role for excreted quinones in extracellular electron transfer. *Nature.* **405**. 94-7.
- Nunez, C., Adams, L., Childers, S. and Lovley, D. R. (2004).** The RpoS sigma factor in the dissimilatory Fe(III)-reducing bacterium *Geobacter sulfurreducens*. *J Bacteriol.* **186**. 5543-6.
- Nunez, C., Esteve-Nunez, A., Giometti, C., Tollaksen, S., Khare, T., Lin, W., Lovley, D. R. and Methe, B. A. (2006).** DNA microarray and proteomic analyses of the RpoS regulon in *Geobacter sulfurreducens*. *J Bacteriol.* **188**. 2792-800.
- Otwinowski, Z. and Minor, W. (1997).** Processing of X-ray Diffraction Data Collected in Oscillation Mode. *Methods in Enzymology.* **276**. 307-326.
- Pauleta, S. R., Cooper, A., Nutley, M., Errington, N., Harding, S., Guerlesquin, F., Goodhew, C. F., Moura, I., Moura, J. J. and Pettigrew, G. W. (2004a).** A copper protein and a cytochrome bind at the same site on bacterial cytochrome c peroxidase. *Biochemistry.* **43**. 14566-76.
- Pauleta, S. R., Guerlesquin, F., Goodhew, C. F., Devreese, B., Van Beeumen, J., Pereira, A. S., Moura, I. and Pettigrew, G. W. (2004b).** *Paracoccus pantotrophus*

pseudoazurin is an electron donor to cytochrome c peroxidase. *Biochemistry*. **43**. 11214-25.

**Pettigrew, G. W., Echaliier, A. and Pauleta, S. R.** (2006). Structure and mechanism in the bacterial dihaem cytochrome c peroxidases. *J Inorg Biochem*. **100**. 551-67.

**Pettigrew, G. W., Prazeres, S., Costa, C., Palma, N., Krippahl, L., Moura, I. and Moura, J. J.** (1999). The structure of an electron transfer complex containing a cytochrome c and a peroxidase. *J Biol Chem*. **274**. 11383-9.

**Pitts, K. E., Dobbin, P. S., Reyes-Ramirez, F., Thomson, A. J., Richardson, D. J. and Seward, H. E.** (2003). Characterization of the *Shewanella oneidensis* MR-1 decaheme cytochrome MtrA: expression in *Escherichia coli* confers the ability to reduce soluble Fe(III) chelates. *J Biol Chem*. **278**. 27758-65.

**Poulos, T. L. and Kraut, J.** (1980). The stereochemistry of peroxidase catalysis. *J Biol Chem*. **255**. 8199-205.

**Prazeres, S., Moura, J. J., Moura, I., Gilmour, R., Goodhew, C. F., Pettigrew, G. W., Ravi, N. and Huynh, B. H.** (1995). Mossbauer characterization of *Paracoccus denitrificans* cytochrome c peroxidase. Further evidence for redox and calcium binding-induced heme-heme interaction. *J Biol Chem*. **270**. 24264-9.

**Ramachandran, G. N., Ramakrishnan, C. and Sasisekharan, V.** (1963). Stereochemistry of polypeptide chain configurations. *J Mol Biol*. **7**. 95-9.

**Reguera, G., McCarthy, K. D., Mehta, T., Nicoll, J. S., Tuominen, M. T. and Lovley, D. R.** (2005). Extracellular electron transfer via microbial nanowires. *Nature*. **435**. 1098-101.

**Roden, E. E. and Lovley, D. R.** (1993). Dissimilatory Fe(III) Reduction by the Marine Microorganism *Desulfuromonas acetoxidans*. *Appl Environ Microbiol*. **59**. 734-742.

**Rossmann, M. G. and Blow, D. M.** (1962). The detection of sub-units within the crystallographic asymmetric unit. *Acta Cryst*. **15**. 24-31.

**Saiki, R. K., Gelfand, D. H., Stoffel, S., Scharf, S. J., Higuchi, R., Horn, G. T., Mullis, K. B. and Erlich, H. A.** (1988). Primer-directed enzymatic amplification of DNA with a thermostable DNA polymerase. *Science*. **239**. 487-91.

**Sanger, F., Nicklen, S. and Coulson, A. R.** (1977). DNA sequencing with chain-terminating inhibitors. *Proc Natl Acad Sci U S A*. **74**. 5463-7.

**Schneider, T. R. and Sheldrick, G. M.** (2002). Substructure solution with SHELXD. *Acta Crystallogr D Biol Crystallogr*. **58**. 1772-9.

**Schulz, H. and Thöny-Meyer, L.** (2000). Interspecies complementation of *Escherichia coli* ccm mutants: CcmE (CycJ) from *Bradyrhizobium japonicum* acts as a heme chaperone during cytochrome c maturation. *J Bacteriol.* **182**. 6831-3.

**Shimizu, H., Schuller, D. J., Lanzilotta, W. N., Sundaramoorthy, M., Arciero, D. M., Hooper, A. B. and Poulos, T. L.** (2001). Crystal structure of *Nitrosomonas europaea* cytochrome c peroxidase and the structural basis for ligand switching in bacterial di-heme peroxidases. *Biochemistry.* **40**. 13483-90.

**Sivaraja, M., Goodin, D. B., Smith, M. and Hoffman, B. M.** (1989). Identification by ENDOR of Trp191 as the free-radical site in cytochrome c peroxidase compound ES. *Science.* **245**. 738-40.

**Skerra, A. and Schmidt, T. G.** (2000). Use of the Strep-Tag and streptavidin for detection and purification of recombinant proteins. *Methods Enzymol.* **326**. 271-304.

**Smith, P. K., Krohn, R. I., Hermanson, G. T., Mallia, A. K., Gartner, F. H., Provenzano, M. D., Fujimoto, E. K., Goeke, N. M., Olson, B. J. and Klenk, D. C.** (1985). Measurement of protein using bicinchoninic acid. *Anal Biochem.* **150**. 76-85.

**Stevens, J. M., Daltrop, O., Allen, J. W. and Ferguson, S. J.** (2004). C-type cytochrome formation: chemical and biological enigmas. *Acc Chem Res.* **37**. 999-1007.

**Storni, L. C., McCoy, A. J. and Read, R. J.** (2004). Likelihood-enhanced fast rotation functions. *Acta Cryst.* **D60**. 432-438.

**Stura, E. A., Satterthwait, A. C., Calvo, J. C., Kaslow, D. C. and Wilson, I. A.** (1994). Reverse screening. *Acta Crystallogr D Biol Crystallogr.* **50**. 448-55.

**Sundaramoorthy, M., Terner, J. and Poulos, T. L.** (1995). The crystal structure of chloroperoxidase: a heme peroxidase--cytochrome P450 functional hybrid. *Structure.* **3**. 1367-77.

**Sundaramoorthy, M., Terner, J. and Poulos, T. L.** (1998). Stereochemistry of the chloroperoxidase active site: crystallographic and molecular-modeling studies. *Chem Biol.* **5**. 461-73.

**Tanaka, Y., Eng, A. H., Ohya, N., Tangpakdee, J., Kawahara, S. and Wititsuwannakul, R.** (1996). Initiation of rubber biosynthesis in *Hevea brasiliensis*: characterization of initiation species by structural analysis. *Phytochemistry.* **41**. 1501-1505.

**Thompson, J. D., Higgins, D. G. and Gibson, T. J.** (1994). CLUSTAL W: improving the sensitivity of progressive multiple sequence alignment through sequence weighting, position-specific gap penalties and weight matrix choice. *Nucleic Acids Res.* **22**. 4673-80.

- Thöny-Meyer, L.** (1997). Biogenesis of respiratory cytochromes in bacteria. *Microbiol Mol Biol Rev.* **61.** 337-76.
- Thöny-Meyer, L.** (2002). Cytochrome c maturation: a complex pathway for a simple task? *Biochem Soc Trans.* **30.** 633-8.
- Thöny-Meyer, L., Fischer, F., Kunzler, P., Ritz, D. and Hennecke, H.** (1995). Escherichia coli genes required for cytochrome c maturation. *J Bacteriol.* **177.** 4321-6.
- Timoteo, C. G., Tavares, P., Goodhew, C. F., Duarte, L. C., Jumel, K., Girio, F. M., Harding, S., Pettigrew, G. W. and Moura, I.** (2003). Ca<sup>2+</sup> and the bacterial peroxidases: the cytochrome c peroxidase from Pseudomonas stutzeri. *J Biol Inorg Chem.* **8.** 29-37.
- Tsuchii, A. and Takeda, K.** (1990). Rubber-Degrading Enzyme from a Bacterial Culture. *Appl Environ Microbiol.* **56.** 269-274.
- Turner, S., Reid, E., Smith, H. and Cole, J.** (2003). A novel cytochrome c peroxidase from Neisseria gonorrhoeae: a lipoprotein from a Gram-negative bacterium. *Biochem J.* **373.** 865-73.
- Vagin, A. and Teplyakov, A.** (1997). MOLREP: an automated program for molecular replacement. *J. Appl. Cryst.* **30.** 1022-1025.
- Villalain, J., Moura, I., Liu, M. C., Payne, W. J., LeGall, J., Xavier, A. V. and Moura, J. J.** (1984). NMR and electron-paramagnetic-resonance studies of a dihaem cytochrome from Pseudomonas stutzeri (ATCC 11607) (cytochrome c peroxidase). *Eur J Biochem.* **141.** 305-12.
- Wang, Y., Graichen, M. E., Liu, A., Pearson, A. R., Wilmot, C. M. and Davidson, V. L.** (2003). MauG, a novel diheme protein required for tryptophan tryptophylquinone biogenesis. *Biochemistry.* **42.** 7318-25.
- Weber, K. A., Achenbach, L. A. and Coates, J. D.** (2006). Microorganisms pumping iron: anaerobic microbial iron oxidation and reduction. *Nat Rev Microbiol.* **4.** 752-64.
- Weiss, M. and Hilgenfeld, R.** (1997). On the use of the merging R factor as a quality indicator for X-ray data. *J. Appl. Cryst.* **30.** 203-205.
- Wendrich, T. M., Beckering, C. L. and Marahiel, M. A.** (2000). Characterization of the relA/spoT gene from Bacillus stearothermophilus. *FEMS Microbiol Lett.* **190.** 195-201.
- Wendrich, T. M. and Marahiel, M. A.** (1997). Cloning and characterization of a relA/spoT homologue from Bacillus subtilis. *Mol Microbiol.* **26.** 65-79.
- Wosten, M. M.** (1998). Eubacterial sigma-factors. *FEMS Microbiol Rev.* **22.** 127-50.



---

**Yanyushin, M. F., del Rosario, M. C., Brune, D. C. and Blankenship, R. E.** (2005). New class of bacterial membrane oxidoreductases. *Biochemistry*. **44**. 10037-45.

**Zahn, J. A., Arciero, D. M., Hooper, A. B., Coats, J. R. and DiSpirito, A. A.** (1997). Cytochrome c peroxidase from *Methylococcus capsulatus* Bath. *Arch Microbiol.* **168**. 362-72.

## 10 Curriculum vitae

### Maren Hoffmann

Date of birth: 21.03.1978  
Place of birth: Göttingen  
Birth name: Prieß  
Marital status: married  
Citizenship: German

### Education:

1997 Abitur, Gymnasium am Silberkamp, Peine

1997-2003 Studies of Biology and Mathematics (Lehramt an Gymnasien) at the Georg-August-Universität of Göttingen

2002 Examination thesis in Molecular Plant Physiology; "Untersuchungen zur Stärkemobilisierung bei Arabidopsis (Wildtyp und NR-Mutante) in Abhängigkeit von verschiedenen Signalen", (Prof. Dr. Rudolf Tischner)

2003-2007 Ph.D. studies at the Georg-August-University of Göttingen, Department of Molecular Structural Biology